Development of a Reliable Electrostatic Multijet Printhead for Three Dimensional Printing

by

Christopher James Shu

S.B. Mechanical Engineering, Massachusetts Institute of Technology
(1993)

SUBMITTED TO THE DEPARTMENT OF
MECHANICAL ENGINEERING IN PARTIAL
FULFILLMENT OF THE REQUIREMENTS
FOR THE DEGREE OF

MASTER OF SCIENCE

at the

MASSACHUSETTS INSTITUTE OF TECHNOLOGY

September 1995

Signature of Author_
Department of Mechanical Engineering
May 18, 1995

Certified by_____
Professor Emanuel Sachs
Thesis Supervisor

Accepted by_____
Professor Ain A. Sonin, Chairman
Graduate Committee, Department of Mechanical Engineering

Development of a Reliable Electrostatic Multijet Printhead for Three Dimensional Printing

by

Christopher James Shutts

Submitted to the Department of Mechanical Engineering
on May 10, 1995 in partial fulfillment of the
requirements for the Degree of Master of Science

ABSTRACT

Three Dimensional Printing (3DP) is a rapid prototyping technology with the ability to fabricate functional parts one layer at a time, directly from CAD files. Powder is spread in a thin layer, and then a printhead selectively joins the powder with a binder. This printed section forms a cross section of the part. After several successive layers, the part is completed and removed from the powderbed for post processing. Currently parts can be made directly from metal, ceramic or metal-ceramic mixtures.

An accurate, reliable, and fast printhead is the bedrock of a successful 3DP machine. A multiple nozzle continuous jet electrostatic printhead was developed for use on the current MIT Alpha 3DP machine. This technology involves exciting a fluid jet with a piezo, causing it to break up into uniform droplets. These droplets are selectively charged and deflected by a strong electric field. Design goals for this device included reliability, high build rate, and accuracy. This printhead also incorporates proportional deflection for increased part resolution. In addition, an entire fluid support system was constructed to supply the printhead with many fluids continuously. Multiple fluids are recirculated and reused to prevent wasted binder or cleaner solutions.

A methodology was also developed to aid in future efforts to construct useful print heads for 3DP applications. A detailed process is outlined as a guideline for development of a variety of different printheads. A detailed qualitative description of jet breakup is also presented for furthering future printhead and binder development efforts.

To date, a effort to construct a multiple nozzle printhead has been successful. Currently if the printhead is running well, catcher buildup is the limiting reliability factor. Both ceramic and metal parts have been printed with a longest run to date of 8 hours without intervention. Still some work needs to be done to reach surface finish quality and reliability of the original single jet printhead. The Alpha machine cycle time has in the mean been greatly reduced. The largest part (6" x 12" x 12") possible on the MIT 3DP machine could be printed in approximately 30 hours using eight jets.

Thesis Supervisor: Emanuel Sachs

Title: Associate Professor of Mechanical Engineering

Acknowledgments

I would like to acknowledge the support under the National Science Foundation Strategic Manufacturing Initiative (contract number 9215728-DDM), ARPA program on Solid Freeform Fabrication, and the members of the Three Dimensional Printing Industrial Consortium.

I would like to thank the ONR-NDSEG fellowship program for allowing me ultimate freedom in graduate school to work on any project without financial constraints. I definitely picked the best project and group of people to work with at MIT.

This thesis is dedicated to my mother and father, Marie and Jim Shutts, the greatest parents around.

My best friend, Carolyn Rockwell, made me feel better on many occasions when the pressure was intense. Thank you for your help.

Erik Abernathy for his hours of humorous proofreading of this document. No person should ever be subjected to the mental abuse he endured for 113 pages.

LMP has been a wonderful place to work for the past two years. There are some people I would very much like to mention for their help, insight, and great company.

Ely has been challenging to work with. I hope he has benefited as much as I have from this thesis work. Hopefully we will be doing business together in the future.

Jim Bredt is the technical foundation for Three Dimensional Printing. Much of this work is based on his efforts. As with about a dozen other master's theses, Jim's input was essential. Thanks Jim, I hope to someday repay you.

Fred Cote is the force behind progress in machine design and construction at LMP and many other labs around MIT. His efforts and friendship are very much appreciated.

Gerry Wentworth is one of the most skilled (and fun) people I've ever worked with. I very much looked forward to the long days with Gerry on the 7VC trying to get the deflection electrodes machined. Thanks for letting me borrow that tape, jerky.

Dave Brancazio's technical and managerial talents are impressive. Dave holds the project together, directed toward a common goal, when every student just wants to get their own thesis work completed. He is an excellent troubleshooter and a design wizard. That's for your help, Dave.

Jim Serdy has been an enormous asset in printhead development for 3DP. His patience and craftsmanship should be commended. He has helped me on numerous occasions with some very difficult problems. My work would not have progressed without Jim.

Steve Michael's should be commended for his ability to tell five jokes every night, irrespective of how many nights there are in a week. Steve has been a fun person to share an office with and also a great friend.

Many other people should be mentioned- Jain Charnnarong for helping with the bracket shell, Alain Curodeau for letting me invade his induced charging turf, Seth Close for some killer fluids handling equipment, Tim Anderson for both functional and disfunctional electronic equipment, Tiina Hameenanttila for some excellent fabrication assistance, and Mike Rynerson for design advice and righteous ProEngineer wizardry.

Ed Wylonis, Gail Thornton, Earl Sun, Steve Michaels, and Tara Arthur for some wicked good times both in and out the United States.

And all the other students on the 3DP project good luck and thanks for your help.

Table of Contents

List of Figures

Chapter 1: Introduction

1.1 Motivation

Three Dimensional Printing is a process for rapid prototyping or flexible production of parts or tooling. This process creates functional parts directly from CAD models in a variety of materials, including metals and ceramics. A major factor in the success of this process meeting the needs of shorter product development and quicker tooling construction is the functionality of the 3DP machine itself.

A useful 3DP machine must deliver and spread powder as well as selectively join it to form a part based on CAD information. The printhead, the heart of the 3DP machine, applies binder quickly, accurately, and reliably. A major advantage of 3DP over other rapid prototyping technologies is the ability to more accurately build parts with scale able increases in rate. To prove this superiority, development of a multiple (vs. single) nozzle printhead was essential.

Specifically, this motivation was the genesis of many anticipated future needs in the 3DP process development. It was essential to print large (6"x6"x12") parts in hours. High build rate had to be achieved without sacrificing machine accuracy, reliability, or flexibility. Another facet of this motivation was to develop a procedure for the future design of printheads specifically for 3DP applications. This thesis describes a detailed methodology for building future electrostatic printheads for 3DP uses as well as development of the current 3DP multijet printhead.

1.2 Three Dimensional Printing - The Current Work

Three Dimensional Printing is a manufacturing process for the production of complex three-dimensional parts directly from a computer model of the part, without tooling. Three Dimensional Printing creates parts by a layered printing process. The information for each layer is obtained by applying a slicing algorithm to a computer model of the part. Parts are created inside a piston containing a powder bed. The piston is dropped several thousandths of an inch and a new layer of powder is spread across the top. The new layer is selectively joined where the part is to be formed by "ink-jet printing" binder into the powder. This is done by raster-scanning a modulating printhead over the powder bed (Figure 1.1).

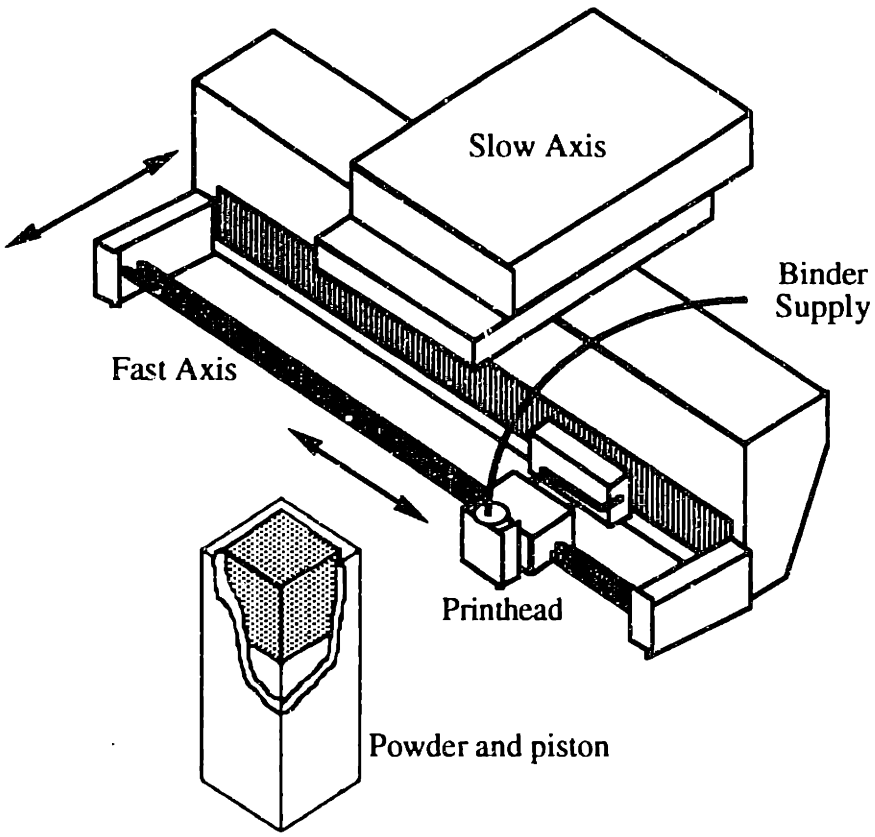

Figure 1-1: Three Dimensional Printing machine.

The printhead holds a nozzle which dispenses pressurized binder and uses a piezoelectric element to break the stream into a regular series of droplets. It then selectively deflects droplets into a "catcher" using electrostatic deflection. Deflected droplets are collected and later recycled; undeflected droplets are printed into the part being formed.

The piston is lowered and a new layer of powder is spread out and selectively joined. The layering process is repeated until the part is completely printed (Figure 1.2). Following a heat treatment, the unbound powder is removed, leaving the fabricated part. A printed part is shown in Figures 1-3 and 1-4.

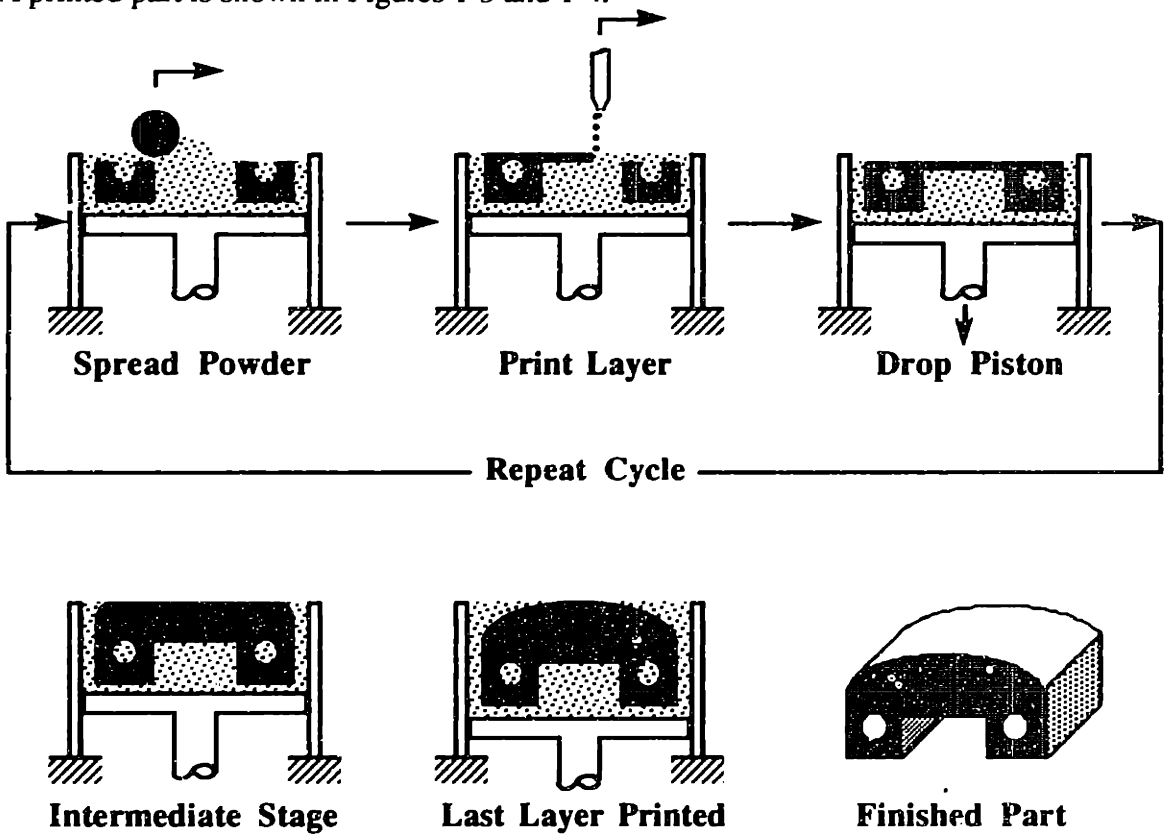

Figure 1.2: Sequence of operations in the Three Dimensional Printing process.

Figure 1-3: A ceramic part created using Three Dimensional Printing.

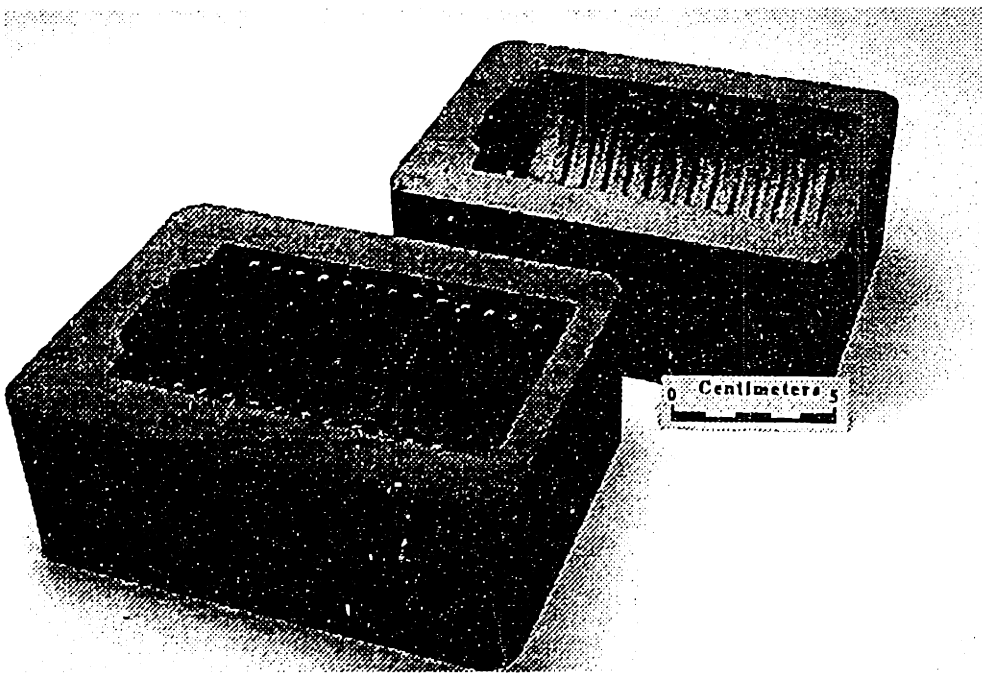

Figure 1-4: A metal part created using Three Dimensional Printing.

Three Dimensional Printing can be used to fabricate parts from a wide variety of materials, including ceramic, metal, metal-ceramic composite and polymeric materials. The objective of 3DP's work is to produce parts that will be used directly as prototype parts (both functional and aesthetic), and to produce parts that will be used directly as tooling.

1.3 Multijet Development

This thesis documents the development of a multijet printhead for use on the MIT Alpha 3DP machine. The physics of the printhead were well established in previous work at MIT (William's Masters' thesis 1990 and Brancazio Masters' thesis 1991) and the commercial inkjet printer industry. The focus of this project was to combine as much of this knowledge as possible with additional development work to produce a reliable, accurate, high speed printhead.

An existing commercial printhead could not be used for several reasons. Existing printheads generally run at higher jet velocities and flow rates. Commercial printheads have longer droplet flight paths, making them in most circumstances not precise enough for 3DP applications. Jetted fluids in 3DP printheads may also adversely affect some wetted materials in commercial devices. Finally, this new printhead had to be light weight to allow high accelerations for the machine's fast axis.

The focus of this work was to build the entire printhead to be as light and compact as possible. With the exception of the droplet generator, every component was specially designed for 3DP applications. Three commercial droplet generators were each tested with water, colloidal silica binder, and water glycol mixtures. Droplet breakup behavior and jet position 'wander' were studied. None of these units were suitable for use in their current condition. Minor modifications were made to the most promising droplet generator to allow continuous reliable operation. Droplet positioning electrodes were designed and constructed from lightweight plated plastic. A droplet catcher was also constructed after extensive testing. These assemblies were then carefully packaged and installed on the MIT Alpha 3DP machine.

Chapter 2: Types Of Print heads

2.1 Types of Ink Jet Printheads

Continuous-jet and drop-on-demand (DOD) print heads currently make up two major market segments of ink jet printing. Drop-on-demand printheads are more common in desktop computer printers. A typical DOD printhead will run 40 to 100 jets with ink flow rates of 1.5 to 3 cc/min for all the jets. These print heads typically rely on a small fluid chamber and a piezo excited to push a small amount of fluid from an orifice to form an ink droplet. Three Dimensional Printing requires higher flow rates than possible from current DOD technology. Because the fluid jet in a DOD head is not continuous, it is prone to clogging with 3DP binders. For these reasons, development work has been centered on electrostatically deflected, continuous-jet print heads.

2.2 Continuous-Jet

Current continuous-jet print heads have many applications in the printing industry. These printers are used for scribing serial numbers in manufacturing plants, labeling poultry in food service, silk screening, printing wall paper, and photograph quality original prints. Flow rates range from 0.2 cc/min per jet to 7cc/min. Droplet production rates range from 50 kHz to 1MHz. This versatile technology poses many technical challenges in the development of robust, reliable, and accurate print heads.

In continuous-jet printing, a pressurized fluid is jetted through a restrictive orifice. This jet is stimulated with a piezo to break it up into uniform droplets. This breakup occurs in a narrow gap or ring raised to a voltage. This gap or ring inductively charges the droplets prior to break-off. The charged droplets then fly through a strong electric field formed by two high voltage parallel plates. While in the deflection cell, charged droplets are accelerated perpendicular to their flight path, causing deflection. Uncharged droplets fly through unaffected. Thus, by simply applying a voltage to the charging cell, the stream position can be continuously varied. This control over droplet position can be used to catch droplets when printing is not desired, or to carefully create images on the print plane. The printhead can be thought of as a voltage to 'jet position' transducer. Uncharged droplets are caught (as opposed to Figure 2-1 below) while charged droplets are printed. Typically the substrate is moved while the printhead is stationary. Print heads run both vertically and horizontally.

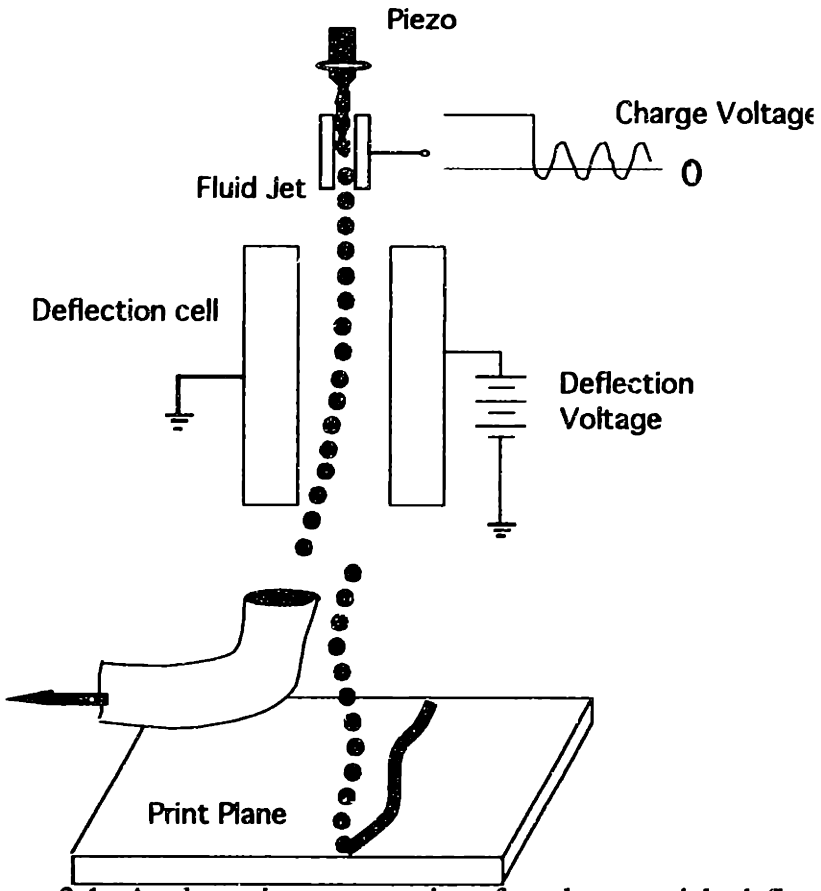

Figure 2-1 : A schematic representation of an electrostaticly deflected continuous-jet printhead.

Unfortunately, the design requirements of the printhead for 3DP were such that an entire commercial unit could not be purchased and implemented. A multiple nozzle print head for the Alpha machine had to have low mass, approximately a 1" flight path, proportional deflection, low (0.9-1.2cc/min) flowrate, compatibility with a variety of binders, and robustness to high accelerations. In addition, the printhead had to be reliable and easy to service under the fast axis of the machine. The 3DP printhead also had to have a higher resolution and higher accuracy than commercial designs. After an extensive search of the printing industry, a complete printhead to meet these needs could not be found. The subject of this thesis is the construction of this printhead as well as a general design philosophy for building future print heads.

Chapter 3: General Printhead Design

3.1 Relating Functional Requirements to Design Specifications

To fully satisfy every intended use of the printhead, it is important to first define its functional requirements. These requirements are based on the designer's perceived needs of the printhead. Macroscopically, these needs can be broken down into droplet positioning, print quality, reliability, maintainability, and multiple material requirements. Each of these functional requirements can then be further broken down into more specific needs.

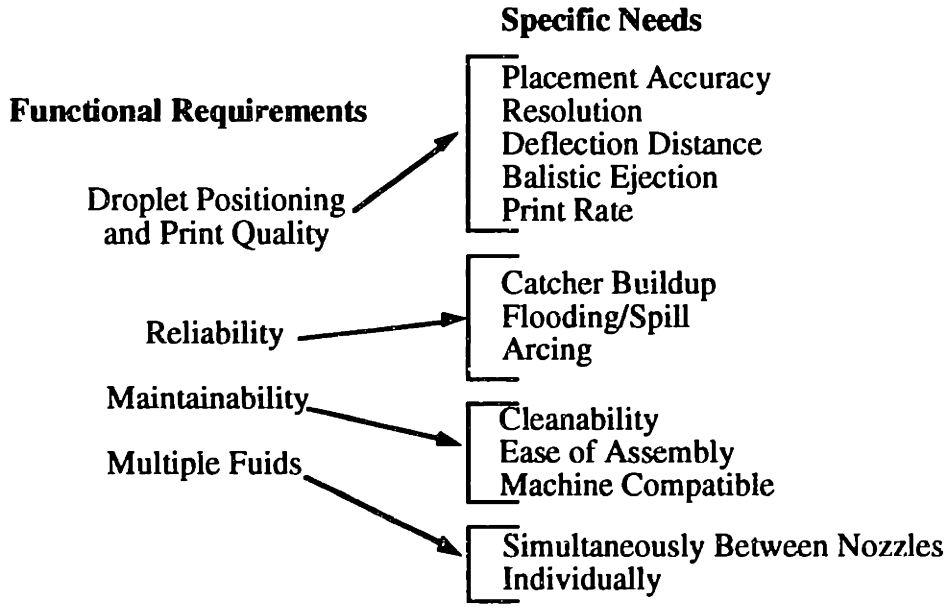

Figure 3-1: Functional Requirements and Specific Needs for a Printhead.

It is essential to transiate these needs into engineering specifications. These specifications can simply be thought of as performance goals for the hardware. Using the engineering specifications, the printhead geometry can be designed. Figure 3-3 uses a house of quality (Clausing p62) approach to relate functional requirements to printhead geometry.

Specific Needs	Specifications
Placement Accuracy	microns
Resolution	drops/mm
Deflection Distance	mm
Balistic Ejection	line depth mm
Print Rate	layers/hour
Catcher Buildup	mg/hour
Flooding/Spill	failure/hour
Arcing	failure/hour
Cleanability	time to clean
Ease of Assembly	assembly time
Machine Compatible	mass (kg), size(mm^3)
Simultaneously	yes/no
Individually	yes/no

Figure 3-2: Needs and Performance Specifications.

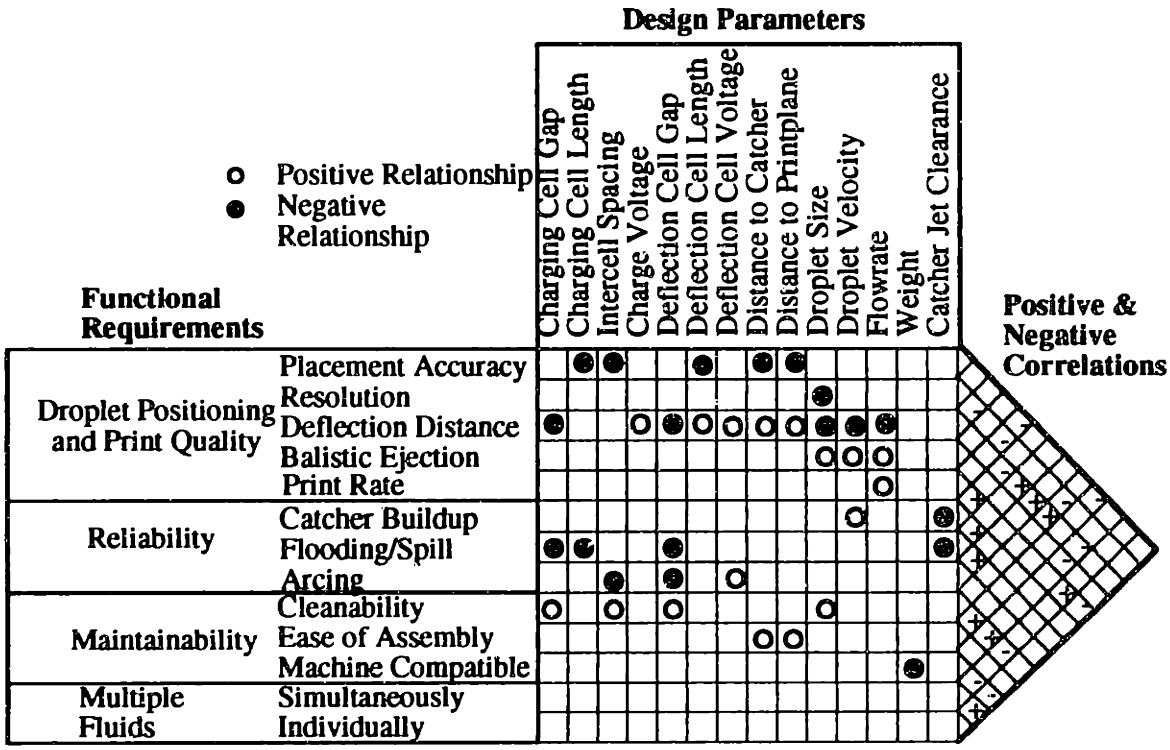

Figure 3-3: Design goals related to printhead geometry.

This matrix style approach is not only useful to relate design parameters to functional requirements, but also to recognize valuable tradeoffs between functional requirements early in the design. This information is conveyed in the triangular portion at the right of Figure 3-3. The positives and negatives are used to show if increasing a functional

requirement increases a neighboring requirement. These increases are considered quantitative regardless of whether the change is detrimental to printhead performance. For example, increasing deflection distance decreases catcher buildup. This correlation would receive a negative symbol although reducing catcher buildup is beneficial.

The square section of Figure 3-3 is used for positive and negative correlations between the functional requirements and the design parameters. Deflection distance is an interesting functional requirement to examine. Virtually every design parameter has an effect on the droplet deflection distance in an electrostatic printhead. The body of this thesis explains the positive and negative correlations between design parameters and functional requirements and how to design using them. This matrix may be worth reviewing after the main discussion of this thesis is read. Some typical numbers for design parameters are listed below for 3DP printheads.

3DP Printhead Specifications

Placement Accuracy	+/- 20 microns
Resolution	40 drops/mm
Deflection Distance	1-1.5 mm
Print Rate	100 cc/hr
Droplet size	75 microns
Droplet Velocity	10-15 m/s
Flight Path Length	24-30 mm
Orifice Diameter	35-60 microns
Droplet Frequency	50-80 kHz

3.2 Printhead Subassemblies

The components within a printhead can be organized into five subassemblies. Breaking the entire system down simplifies the presentation of the design process. It is very important when constructing each assembly to keep in the mind positive and negative relationships shown in the center of Figure 3-3.

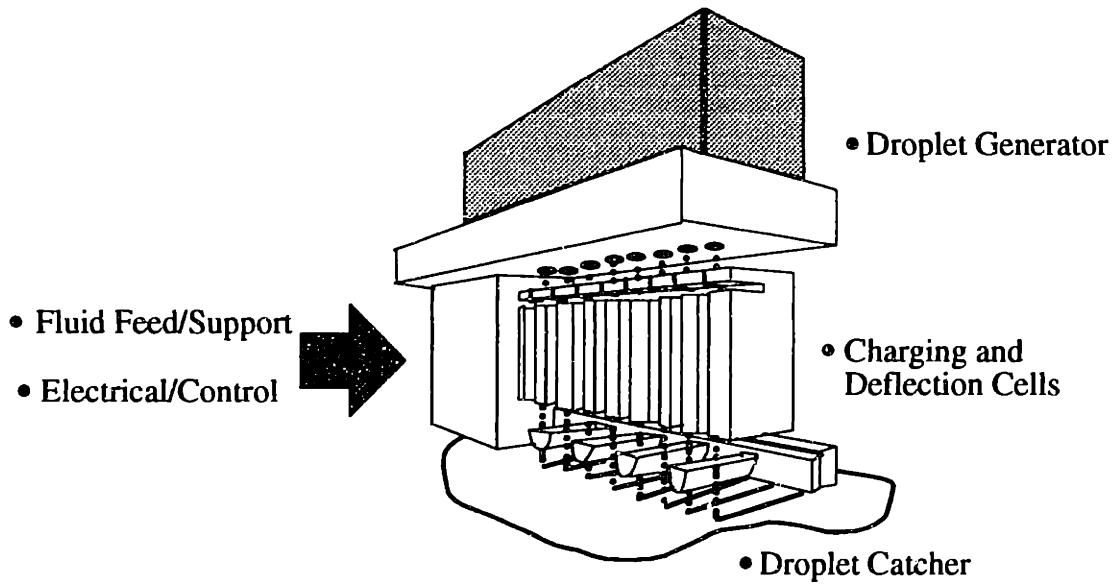

Figure 3-4: Printhead Subassemblies.

The following is a brief description of each subsystem:

Droplet Generation- Generator must produce uniform consistent breakup with minimum phase drift and jet position wander at the required flow rate. Orifice must be robust to wear and compatible with the jetted fluid. Droplet generator must also be easy to disassemble and clean for maintenance. Reliable droplet generation is the most important part of any successful printhead.

Charging and Deflection Electrodes- Electrodes must be robust to cleaning, prevent arcing, flooding, and disturbing the jet. Charging and deflection cells must be accurately placed around the droplet stream while it is jetting to prevent flooding.

Catcher- Droplets must be caught and cleared easily without buildup.

Fluid System Support- Fluid system must be able to supply well filtered fluids to the printhead as well as recirculate them for reuse. The fluid system must provide a stable pressure to the printhead regardless of fast axis accelerations. A means for unclogging jets to minimize down time and facilitate startup is a necessity. The entire fluid system must be compatible with all jetted fluids.

Electrical/Control- This must control the charge and high voltage as well as fault identification and protection.

The flow chart shown below illustrates a reasonable timing of events in the design process. This flow chart also shows the organization of the rest of this document. Arrows to the left reiterate inter-subsystem influences.

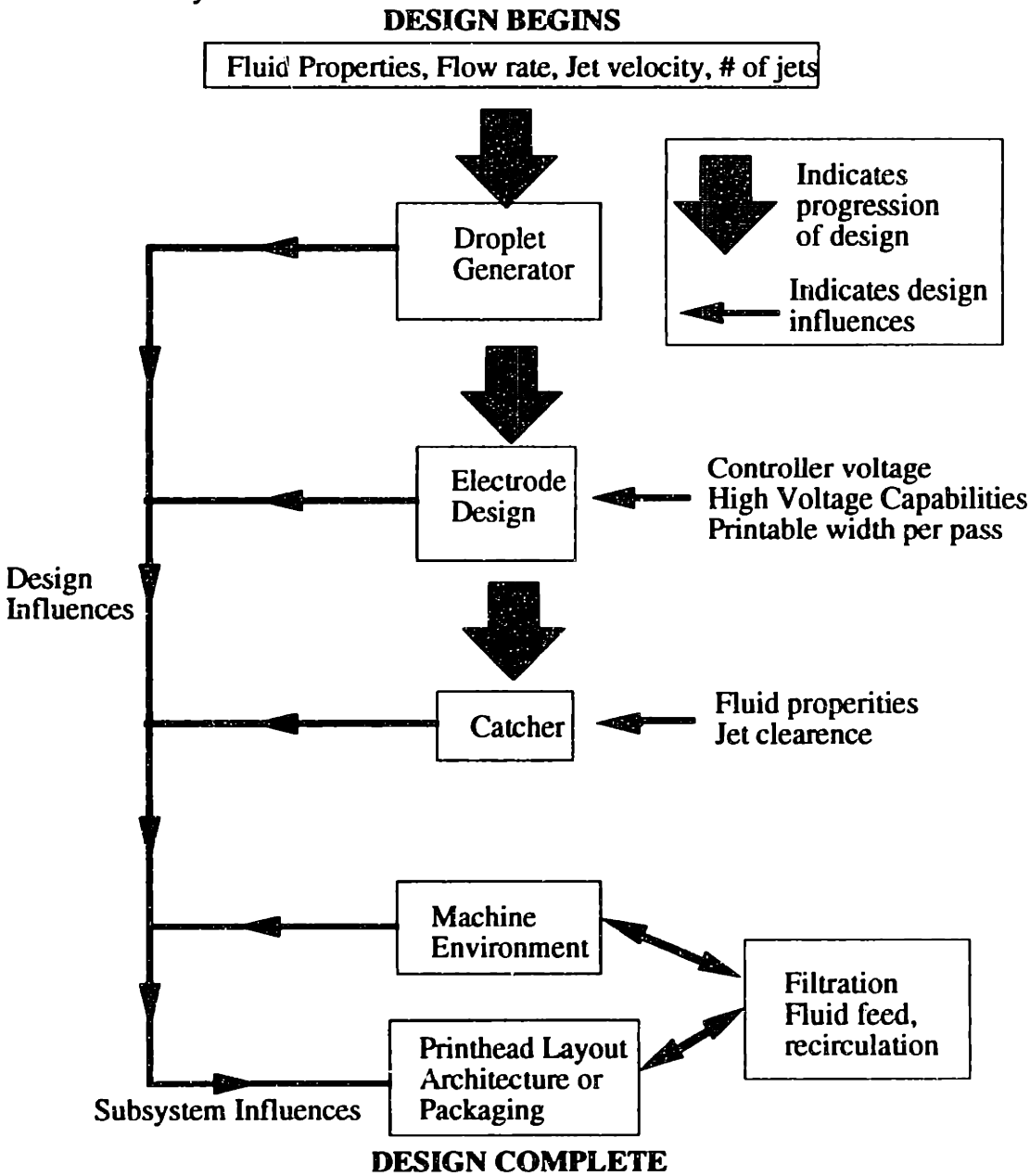

Figure 3-5: Printhead design flowchart/procedure.

Chapter 4: Uniform Droplet Breakup and Jet Stability

4.1 Break-up Frequency

A reliable droplet generator is crucial to a dependable printhead. Droplet generators are simple in principle, but extremely difficult to build in practice. This is an area of intensive research in the ink jet industry and the heart of many trade secrets involved in printhead design and construction. The best way to achieve uniform droplet breakoff is to use an existing commercial droplet generator.

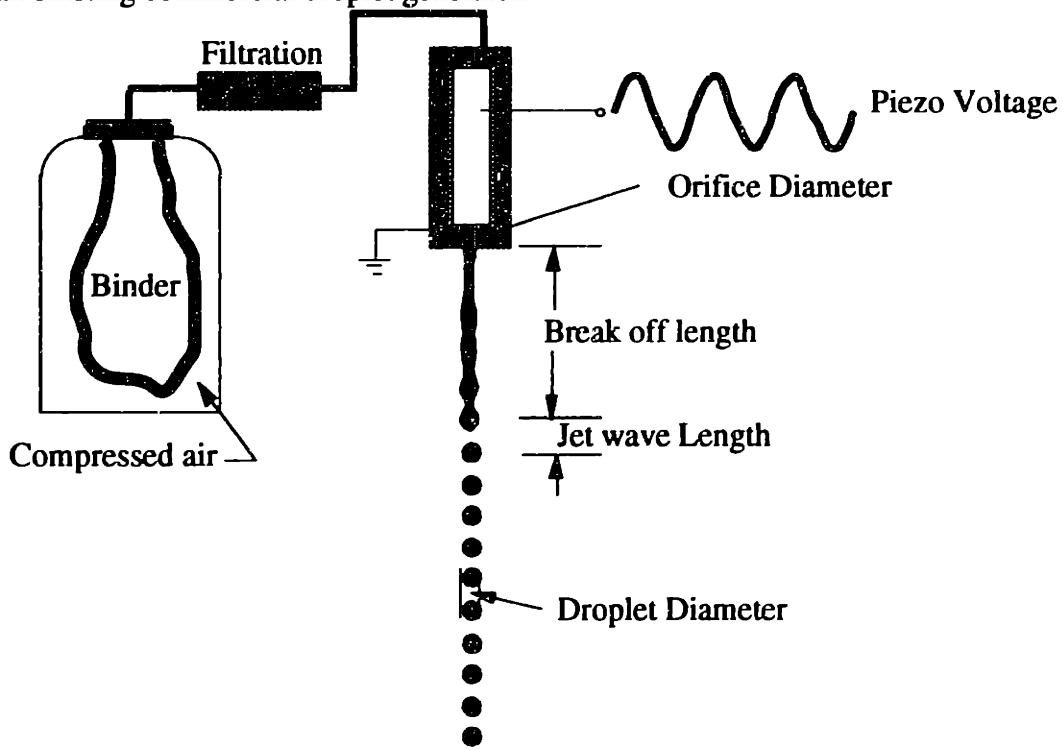

Figure 4-1: Uniform jet breakup.

Fluid jets have a natural frequency of breakup. This frequency, referred to as the Rayleigh number or frequency is dependent on jet velocity, v, and the exiting orifice diameter, d. These parameters are related as follows:

$$f = \frac{v}{4.51(d)} \qquad 4.1.1$$

It is important to note the true meaning of excitation of a fluid jet at its Rayleigh frequency, f_R. Because a cylindrical fluid jet is inherently unstable, it will naturally break up into droplets. This natural breakup is the result of infinitesimal disturbances that grow exponentially within the jet. As disturbances grow, they eventually lead to droplet

breakup. The Rayleigh frequency is the frequency at which the disturbances grow the fastest. Thus for clean breakup at a dominant frequency, it pays to run at this frequency. Remarkably, the Rayleigh frequency for a jet is independent of fluid properties and completely dependent on its mechanical characteristics. Substituting $\lambda=V/f$ into Equation 4.1.1, simplifies to:

$$\lambda = 4.51(d) \qquad 4.1.2$$

Thus at a jet's Rayleigh frequency the ratio of droplet spacing to orifice diameter is 4.51. This is an extremely important run parameter for all commercial droplet generators. When a fluid jet is running at its Rayleigh frequency, the droplet diameter is related to the orifice diameter in the following manner:

$$d_{drop} = 1.89(d_{orifice}) \qquad 4.1.3$$

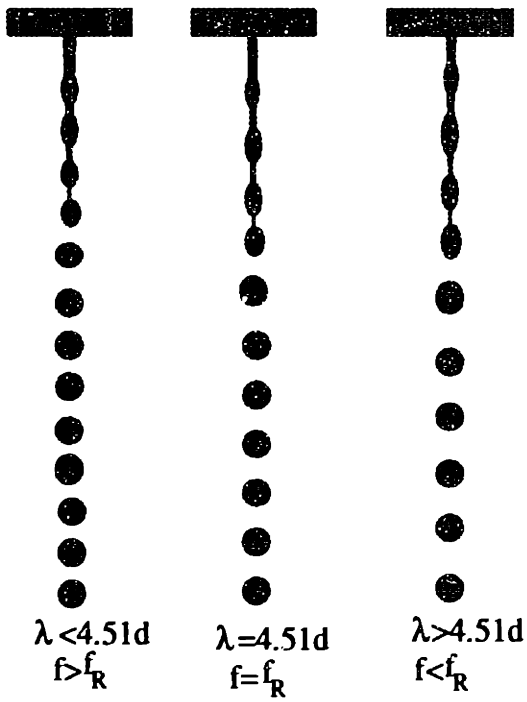

Figure 4-2: Droplet spacing with respect to changes in breakoff frequency.

Figure 4-2 shows three equivalent jets breaking up at different frequencies. Jet 1, running above the Rayleigh frequency, is characteristically unstable, with exiting droplets closer than 4.51 orifice diameters. Not only is uniform jet breakup harder to achieve, but induced charge effects are severely magnified. Because the electric field produced by a droplet spacing as $1/\lambda^2$ (λ is spacing between drops in flight) between droplets, induced charge effects are very significant for droplet generation higher than the jet's droplet frequency. Prior to the installation of the multijet head and the alpha machine, the printhead

was a single jet Diconix resonator running at 1.2cc/min at 77kHz. Because the resonator ran at a frequency higher than the Rayleigh frequency, the droplets were 20% closer together (160 μm droplet spacing verses 207 μm at Rayleigh) at breakoff, seriously affecting the induced charge between droplets at breakoff.

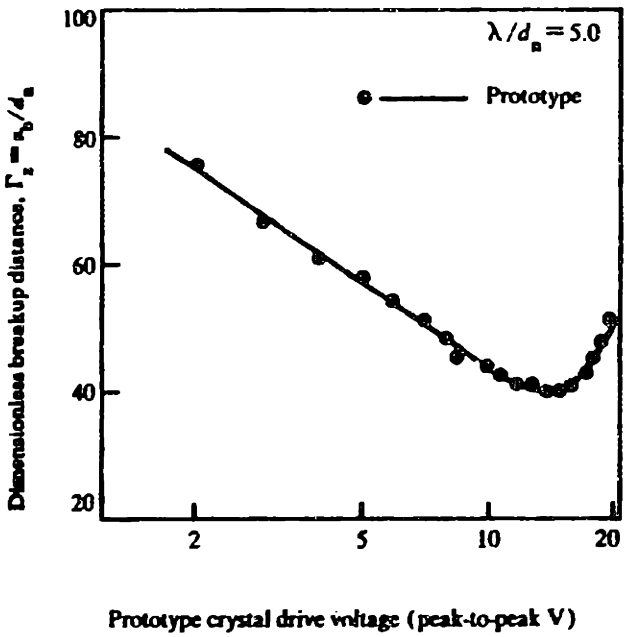

Figure 4-3: Break off length as a function of Piezo drive. Γ is the breakup distance divided by the orifice diameter. (Curry and Portig, IBM Journal, p13)

The breakoff length of the jet can be varied by changing the stimulation amplitude. The breakoff steadily decreases as the input stimulation amplitude is increased until reaching a minimum. Beyond this minimum, as the piezo voltage increases, the jet is overdriven and consequently the breakoff length increases. Still further increases in amplitude cause severe instability in the jet and vaporization occurs at the exit of the orifice.

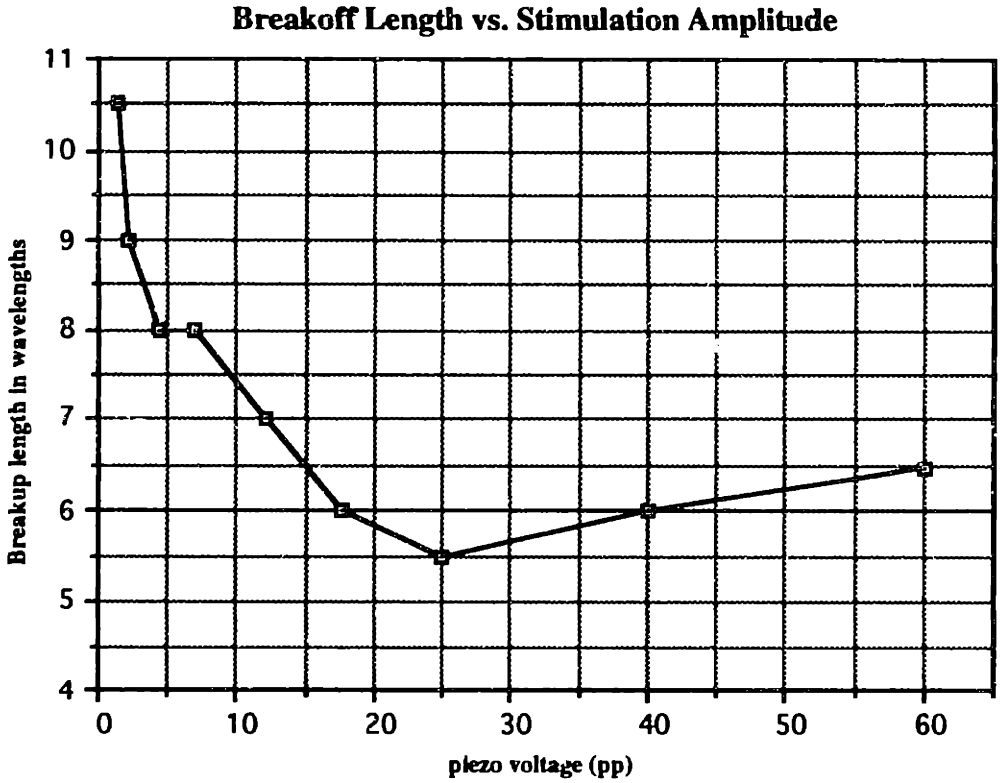

Figure 4-4: Breakoff length vs. peak-to-peak Piezo amplitude. Orifice diameter 35 microns, flowrate .85 cc/min, frequency 64.4 kHz, and jetted material is Acrysol.

4.2 Jet Breakup in Real Life: Satellites

Satellites are small (compared to printed) drops which can form during breakoff. These droplets form from either under or over stimulation of the fluid jet at breakoff. Satellites are composed of the fluid in the thin neck connecting droplets prior to breakoff. If the neck breaks from both droplets at approximately the same time, a satellite will be formed and fly between the two adjacent droplets. The breakoff timing required to cause satellites is such that when one end of the neck breaks, the other must break before surface tension can bring the neck into the neighboring droplet.

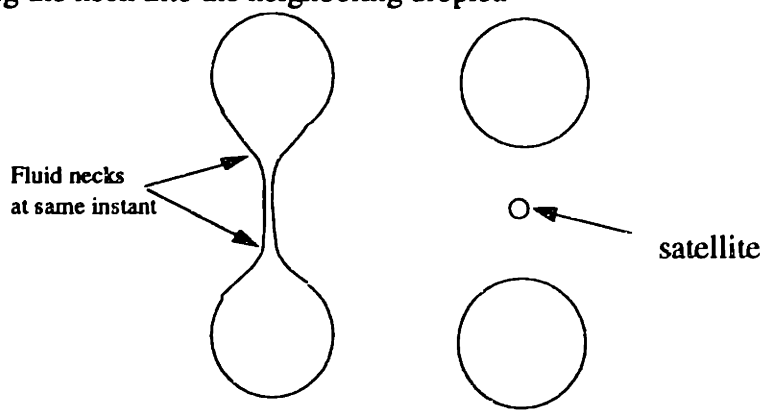

Figure 4-5: Formation of a satellite during jet breakoff.

Satellite formation can occur in three specific regimes. When balanced by both necks breaking at the same instant, satellite droplets will travel long distances, perhaps even to the print plane, without merging into neighboring droplets. The longer the merge time, the greater the chance of the satellites entering the electric field of the deflection cell and flooding the printhead. Satellites can merge to the droplet behind the satellite or forward to the droplet ahead of the satellite. These regimes are referred to as fast and slow satellites. Good satellite control is essential for printhead reliability. Most commercial printhead manufacturers run in a no satellite or forward merging satellite condition.

Figure 4-6: A close-up view of an actual jet breakup with two rearward merging satellites.

A broad range of stimulation regimes, from very low stimulation amplitude up to moderate levels, constitutes a jet with rearward merging satellites. This run point has the virtue of being rather broad in stimulation range. A low but broad piezo voltage range can be chosen and the satellite behavior will not change significantly. This run point is insensitive to drifts in piezo frequency and stimulation amplitude. IRIS Graphics is the only commercial ink jet manufacturer that chooses to run with rearward merging satellites.

Most manufacturer's run at higher stimulation levels, causing fast satellites or none at all. This run point is slightly more sensitive to fluctuations in piezo amplitude, and frequency, if the system is highly resonant. Due to higher stimulation levels required, careful design of the droplet generator is essential. This run point has many advantages, leading to efficient, reliable operation. Figure 4-7 below is based on observations with colloidal silica and Acrysol binders, and is well documented by Pimbley pp 24-5.

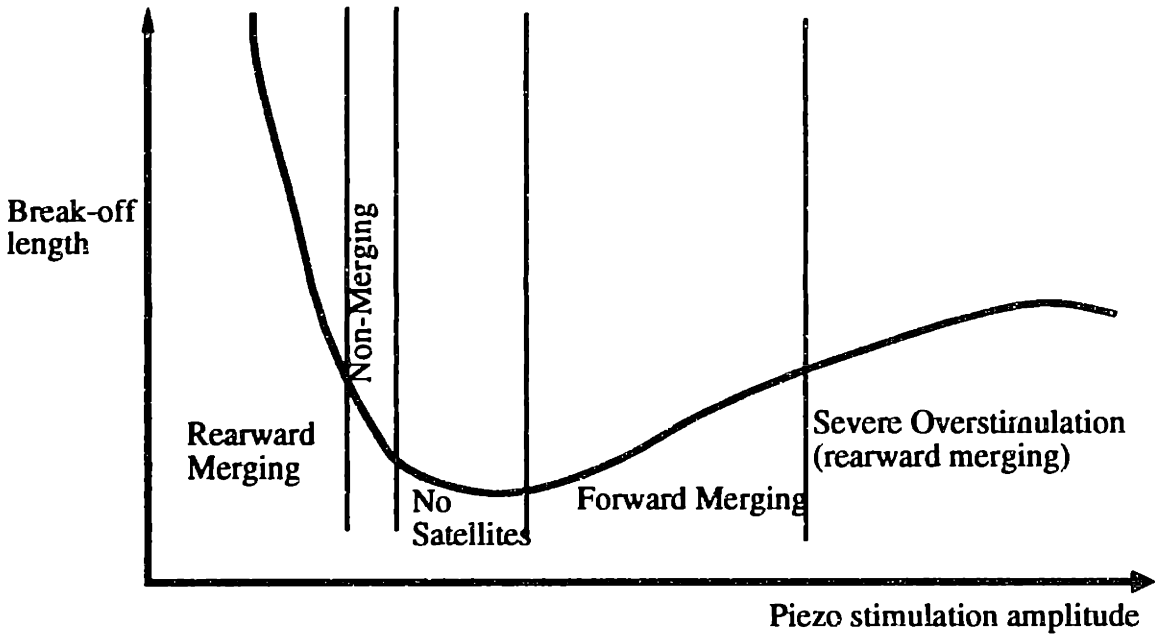

Figure 4-7: Changes in breakoff length correlated with satellite regimes (Pimbley p24, Figure 5).

Forward merging satellites are preferred for several reasons. Because fast satellites are created at shorter breakoff lengths where the fluid necks joining droplets have a larger diameter, they are greater in size than slow satellites and therefore have a lower charge to mass ratio. For this reason, they behave more like actual droplets and are less likely to collide with the deflection plates. Charging errors that are non-existent with forward merging satellites can result from rearward merging satellites. Forward merging satellites are produced and charged at the same instant as the droplet with which they merge. When the satellite merges, the net charge on the entire droplet corresponds closely with the intended charge on the droplet. With rearward merging satellites, the satellite merges to the droplet produced one piezo period later, causing a small error in the charge to mass ratio of the final droplet if a change in charge voltage occurred between breakoffs. The fluid neck during breakoff is smaller for slow satellites. This thin neck acts as a resistor slowing charging by resisting current flow through the jet. This effect is usually insignificant, but for resistive fluids could present dynamic charging errors. A final important benefit of forward merging satellites is phase drift stability. This topic is explained in detail in the following section. Figures 4-7 and 4-8 show satellite behavior as a function of breakoff length and jet stimulation.

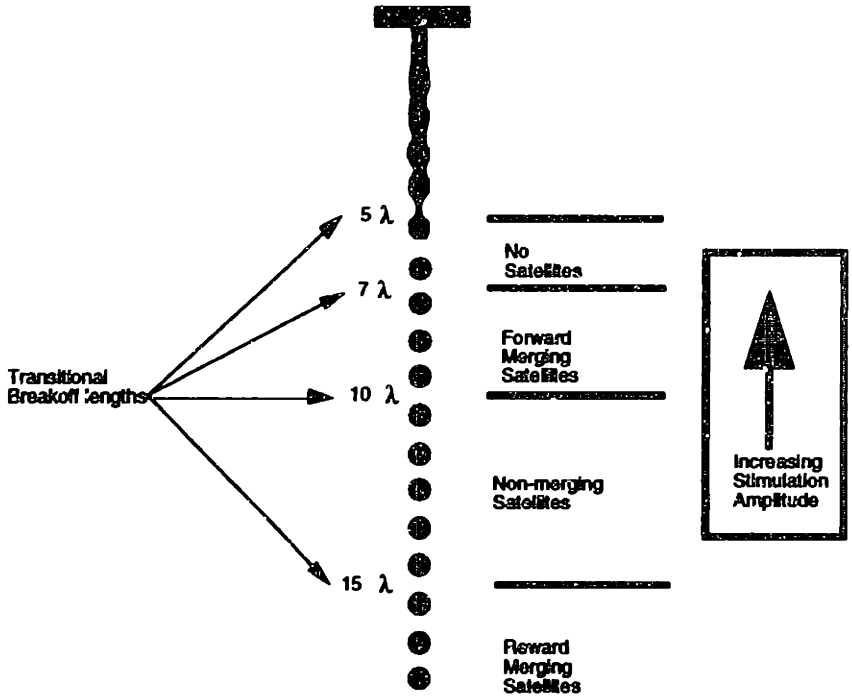

Figure 4-8: Satellite formation as a function of breakoff in nodal lengths. Numbers are typical, and not exact for all droplet generators (Pimpley p29).

4.3 Breakoff Phase Drift and Stability

Breakoff phase refers to the time delay between the excitation pulse and the time for a droplet to break off from the fluid jet. This time delay is typically measured in degrees of piezo oscillation period. Phase drifts occur due to changes in the disturbance propagation rate from the orifice to the point of breakoff. For this reason if the breakoff length is shorter for a given change in propagation rate the change in propagation time will be less. This propagation time when compared to the piezo period is identical to the breakoff phase. This phase is essential for precise charging of the droplets. Figure 4-9 shows a timing diagram of piezo, breakoff, and charge voltage. The instant of droplet breakoff must be known to prevent the generation of mischarged droplets. Changing charge voltage a few

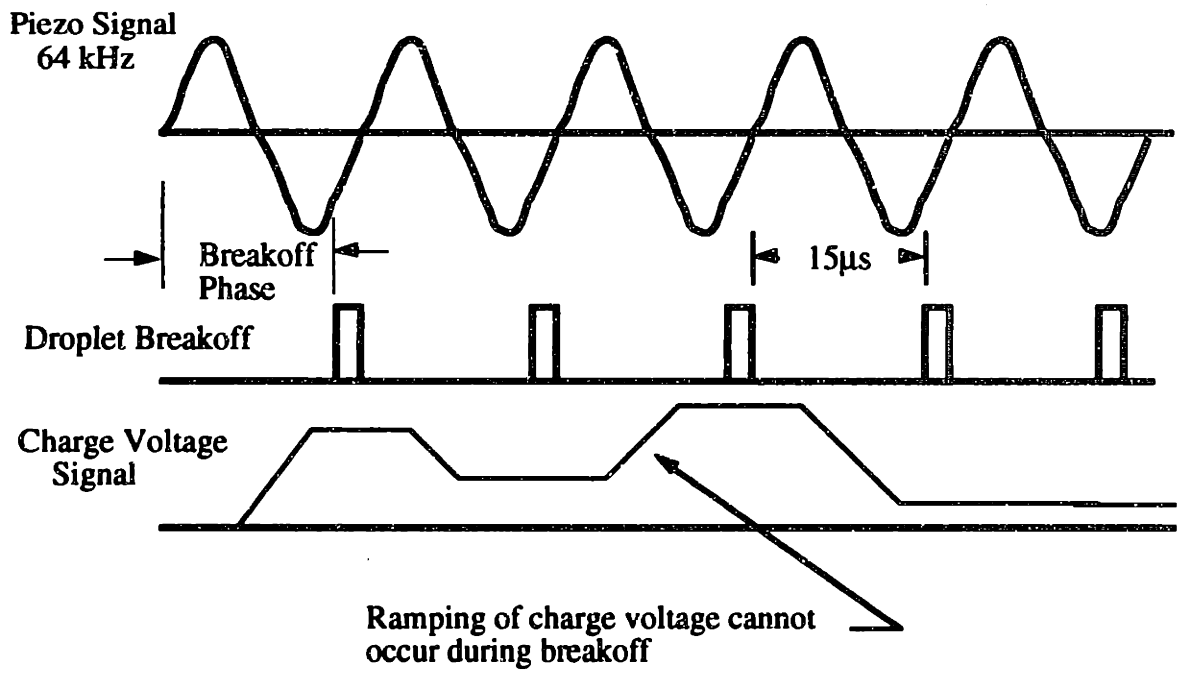

Figure 4-9: Droplet breakoff phase is critical for accurately charged droplets.

hundred volts between droplets with high speed op amps could take as long as 4 µs. The charging cell must have sufficient set up time to establish the proper voltage.

Several scenarios exist for measuring the breakoff phase. Currently on the Alpha machine a triangle wave is sent to the charging cell at half the piezo frequency. This charge sequence produces a stream of droplets of alternating positive and negative charge. A bifurcated stream is the result, until the phase of the triangle wave is adjusted to produce a single jet. When a single jet is produced, the timing of zero crossing of the triangle wave is correlated with that of the piezo signal and a phase is determined. Figure 4-10 summarizes this process. Commercial Inkjet systems measure phase as frequently as two to three times a second.

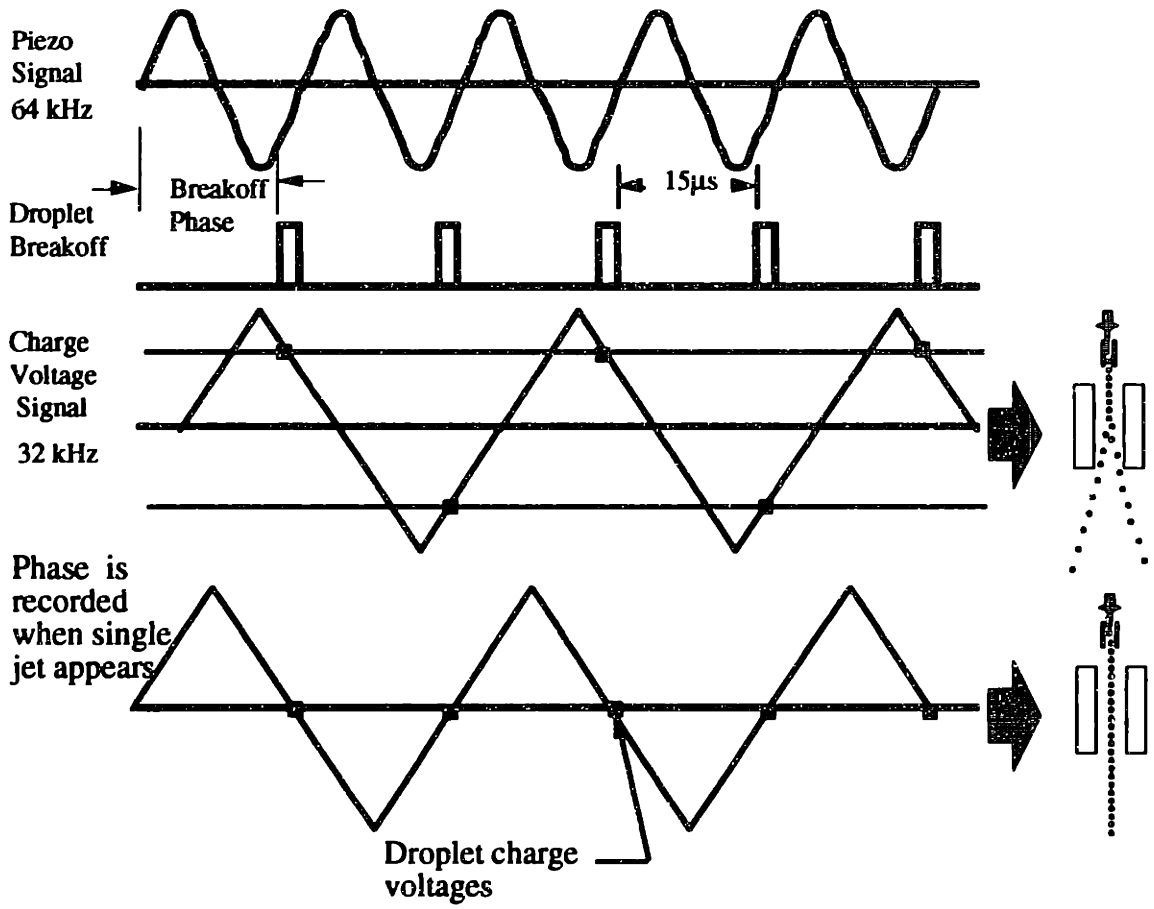

Figure 4-10: Setting the synchronization on the Alpha 3D printer.

It is difficult to determine a quantity for acceptable breakoff phase drift in degrees/hour. If the synchronization measurement is automated, it could be performed frequently making large phase drifts acceptable. Op amp rise time is not the only timing restriction during a piezo period. The current controller has a DAC on the output to the charging cell which requires 1µs for conversion. Also the fluid neck connecting the jet to the droplet breaking off has a time constant associated with the resistance of the fluid neck and the capacitance between the jet and the charging cell walls. The resistance can be calculated using the resistuivity of binder (approxitely 10 ohm-cm) and the size of the fluid neck joining the droplet being charged. Assuming the neck is 1/5 a droplet diameter and the droplet spacing is 4.51 times orifice diameter (the neck is then $3.51d_o$), the resistanec can be approximated as follows:

$$R = \rho\frac{l}{A} = 10\Omega cm\left(\frac{3.51\times 50\mu m}{\pi\left(\frac{50\mu m/5}{2}\right)^2}\right)\times 10000\frac{\mu m}{cm} \approx 200k\Omega \qquad 4.3.1$$

The time constant for this can then be calculated:

$$\tau = RC = (200k\Omega)(1pF) = 0.2\mu s \qquad 4.3.2$$

The total rise time for this first order system (3τ=95%) is then approximately 0.6μs. It can therfore be assumed that the time required for the droplet to fully charge from an ideal step input to the charge cell to a given voltage, is less than 1μs.

Synchronization measurement is not currently automated on the Alpha machine, so a phase drift during a part build must not exceed a certain amount. Figure 4-11 shows the approximate amount of operating room for breakoff drift. Given there may be some error in measuring the breakoff phase, the safe operating window is slightly less than 7μs, and probably around 5.5μs. For a 10 hour run this translates into about 10 degrees/hour or

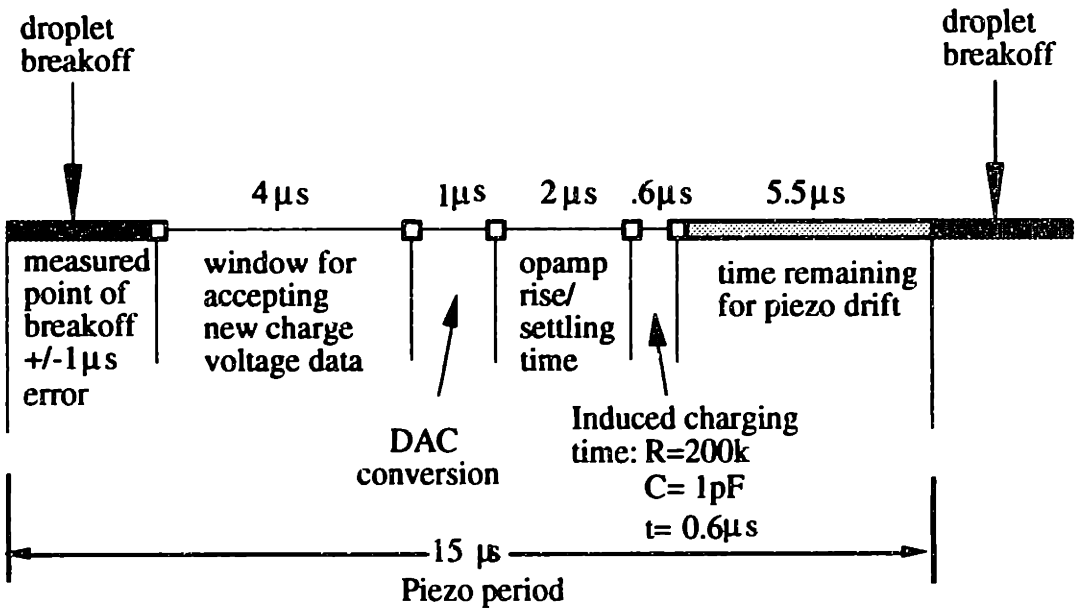

Figure 4-11: Timing of a droplet charging cycle showing room for phase drift.

about 0.5 μs/hour to prevent resynchronization during a run. If all the jets in the Domino droplet generator are clean, phase drift is small, and a particular jet will be stable to within 10-20 degrees for days at a time. On the Alpha machine the 15 μs piezo period is broken up into 16 sections, each slightly less than 1 μs. The test shown in Figure 4-10 determines which of these sections breakoff will occur. Once this phase is established, a safe operating window is established 180 degrees away from the 1μs breakoff window. Ramping of charge voltage is only allowed in the 4 μs wide safe operating window .

4.4 Effects of Fluid Properties on Jet Breakoff Performance

Fluid properties do effect jet dynamics, but not the patterns of satellite behavior. Changes in viscosity and surface tension will simply change the operating window with respect to a particular satellite regime. Thus, fluid properties play a significant role in jet reliability. Typical commercial inks range in viscosity from 2-6 cps and in surface tension from 54-65 dynes/cm. In addition, there is no 'anti satellite' fluid additive, but an anti satellite run point whose width depends on fluid properties.

A measurement parameter when characterizing satellite behavior is satellite interaction time (Pimbley p.24). This parameter is the elapsed time between the first and second fluid neck separations. The longer this interval, the greater momentum transfer to the satellite, causing it to collide faster into a neighboring droplet. Net momentum transfer is zero when a nonmerging satellite is formed. Higher viscosity fluids have longer interaction times lending to a greater robustness to satellite production (Pimbley p.24). Unfortunately at very high viscosities, fluid feed pressures can prohibitively high.

4.5 Jet Position Stability

For printhead alignment and high print quality, static jet position stability over long periods of time is essential. Alignment in multijet printheads is very critical. If changes in jet position are excessive, alignment will not be guaranteed and jets will fail to catch or print properly. Unlike single jet systems, small changes in alignment will be detrimental to multijet operation. Proper orifice geometry leads to long term jet stability as well as minimal external orifice buildup. Jet stability will be dependent on air in the droplet generator, orifice geometry, buildup on the orifice, and wear of the orifice.

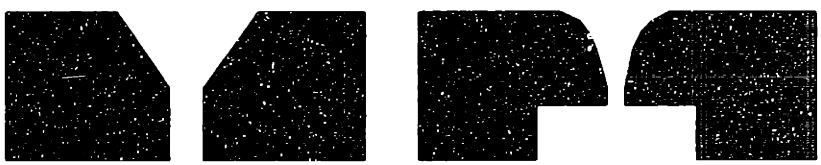

Domino Orifice
Material: Sapphire

Scitex Orifice
Material: Nickel

Figure 4-12: Two orifice geometries used by commercial ink jet manufacturers.

When jetting silica binder long term orifice buildup occurs, causing changes in jet position. A drawing of orifice buildup is shown in Figure 4-14. Solving the issue of orifice buildup is essential for accurate low maintenance printhead operation. Two simple tests can be performed to test for orifice buildup. If build up is present, slight changes in flowrate will

change jet position significantly. Also, large changes in piezo drive may result in changes in jet position. Partially clogged jets will, in general, require more modulation to achieve proper breakoff. When the Alpha machine is not printing, an alkaline solution of ammonia pH 11.5 is jetted to soften and remove orifice buildup. Soligen also runs a similar printhead cleaner at night to solve buildup problems. A major drawback of this solution is complications in fluid system operation. This will be discussed in detail is chapter 9. Figure 4-13 below shows two fluid jets and their relative position at the print plane. Each jet is measured in two directions; X and Y, which are 90 degrees apart. Appendix E contains typical jet position and flowrate fluctuation data over long periods of time.

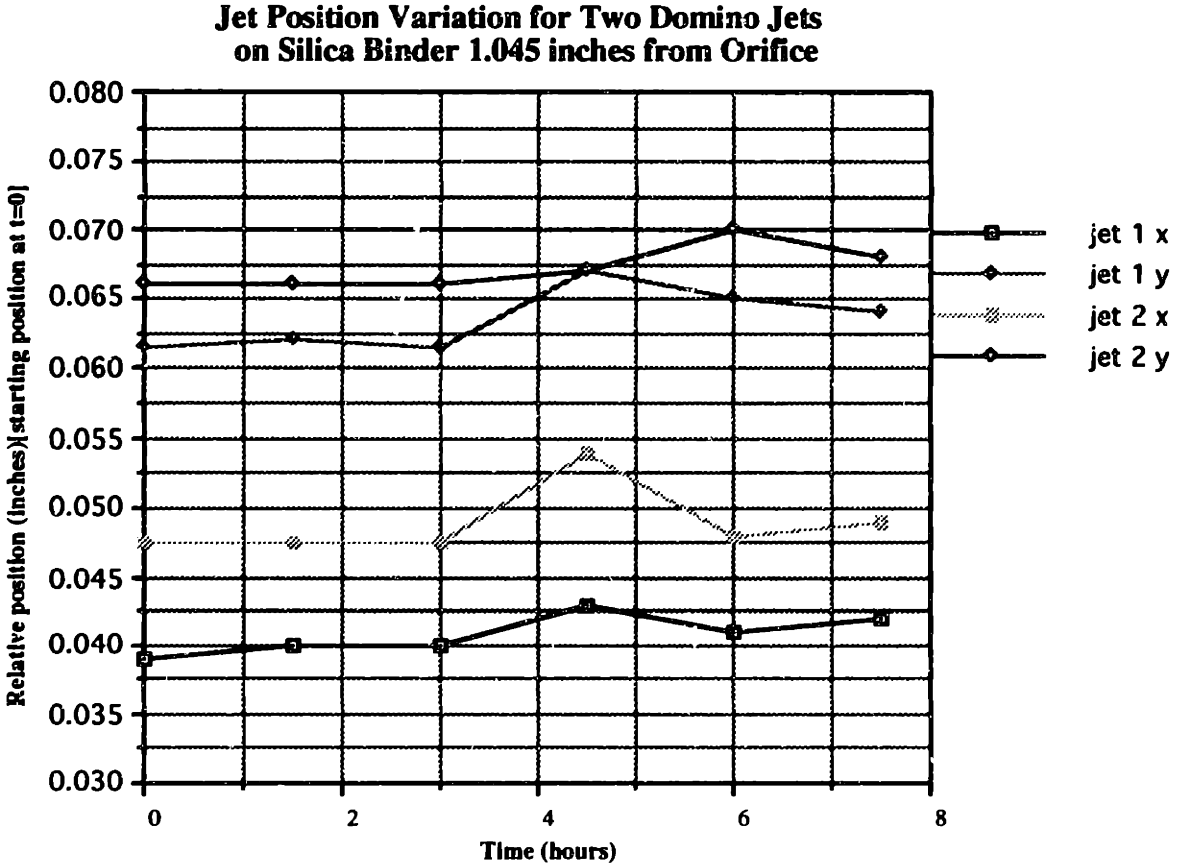

Figure 4-13: Jet position data for two of eight jets running silica binder.

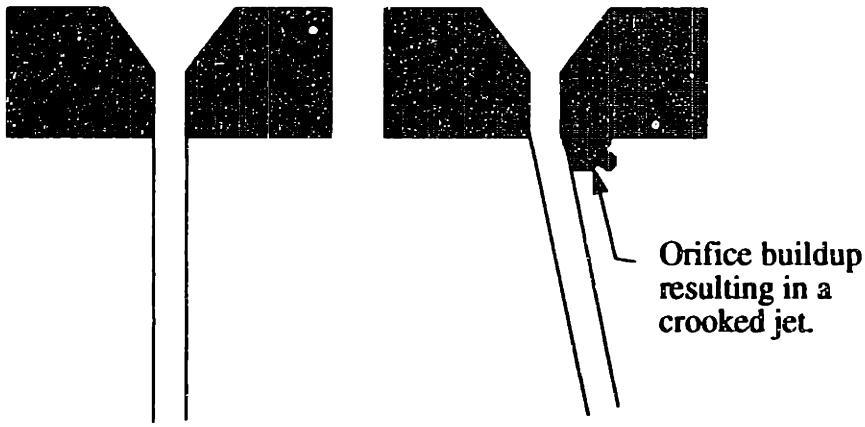

Figure 4-14: Orifice buildup causing jet movement.

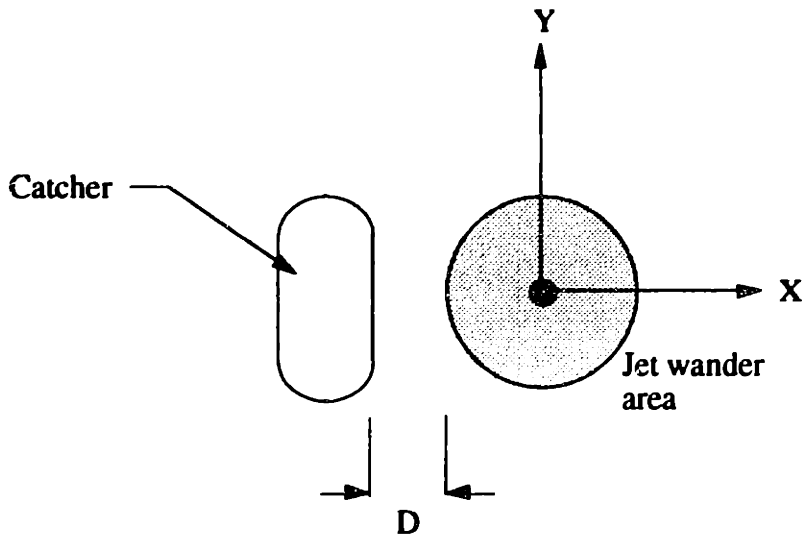

Figure 4-15: Top view of a fluid jet and printhead catcher. Crosshatched circle shows typical jet wander with respect to catcher position.

It is critical to know how much jet wander is tolerable to sustain reliable printhead operation. The amount of tolerable jet wander is a function of printhead clearances and maximum deflection required for catching. Normal jet wander is a few thousands of an inch at the print plane for 3DP. This is easily tolerable for the current printhead. If a jet wanders over time more than this, part quality will be severely affected and would not be acceptable, even if the printhead could tolerate these large jumps in position. For proportionally deflectable printheads, jet wander area is overshadowed by the amount of maximum desired proportional deflection. Jet clearances to the catcher and deflection electrodes should be designed to withstand all possible jet positions- into catch, statically shifted, or proportionally deflected. Typically proportional deflection and catch positions dominate static shift, and therefore should be used to determine electrode configurations (see section 5.1.2).

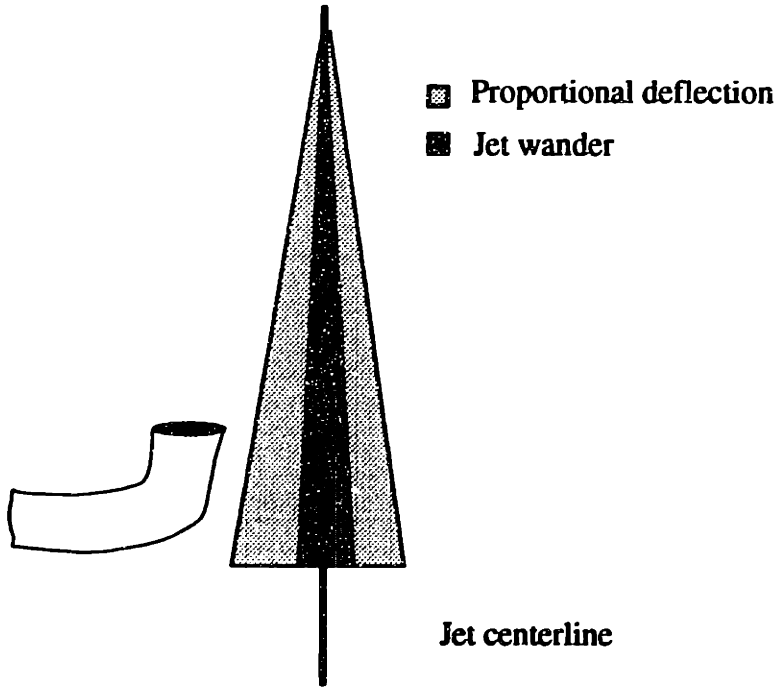

Figure 4-16: Proportional deflection window typically overshadows static jet wander.

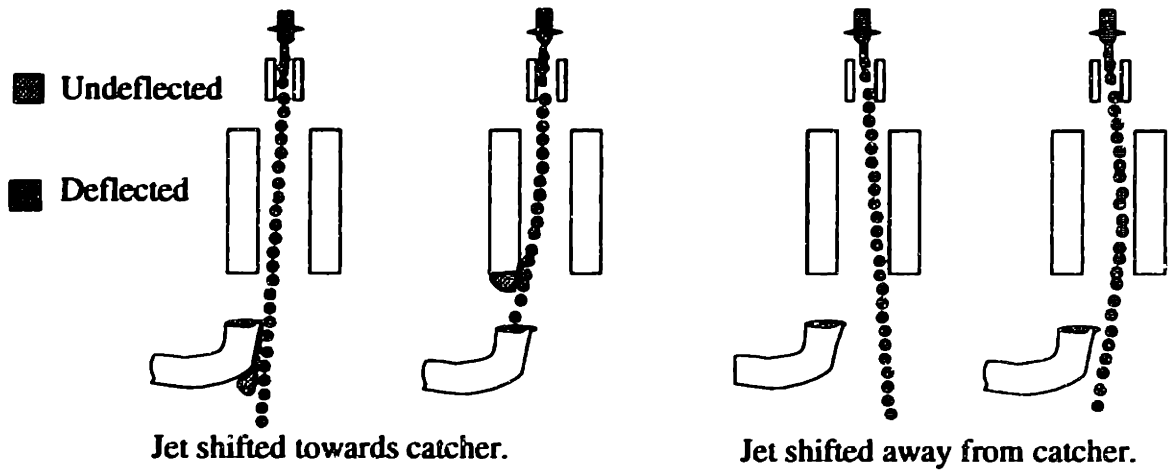

Figure 4-17: Statically deflected jet hindering Printhead performance.
Effects are an uncatchable jet or fluid buildup.

A trade-off exists between printhead performance and reliability. Longer flight paths allow greater catcher clearances, but reduces print accuracy. A critical dimension D shown in Figure 4-15 is important in reducing catcher build from the jet brushing along the catcher edge. Given a finite deflection for a given jet, this distance D must be sufficient to reduce buildup, but also allow the jet to reach the catcher. Calculations and good design parameters for these dimensions are outlined in Chapter 5.4.

4.6 Droplet Generator Qualification for Alpha Multijet

Three multijet droplet generators were rigorously tested for use as the first multijet printhead on the Alpha 3D printer. A brief summary of these tests is described below.

The Toxot: Manufacturer Imaje Incorporated

The Toxot droplet generator is an eight jet unit with two piezo towers. Jet diameter is 50 microns, intended flowrate is 2 cc/min and resonant frequency is 83.33 kHz. Fluid entry is from the back of the head and piezo hookups are on top of the unit. The orifice plate is made of nickel and connects with six 1mm bolts and sealed with a reusable Teflon gasket.

The Toxot is a beautifully designed unit, particularly from a maintenance standpoint. Although it is an extremely compact design, it is very easy to service and clean. Figure 4-18 shows a cutaway of the Toxot design. All eight breakoffs are designed to occur within one wavelength. This was true at the intended Toxot flowrates, but unfortunately not at lower flowrates required for 3DP.

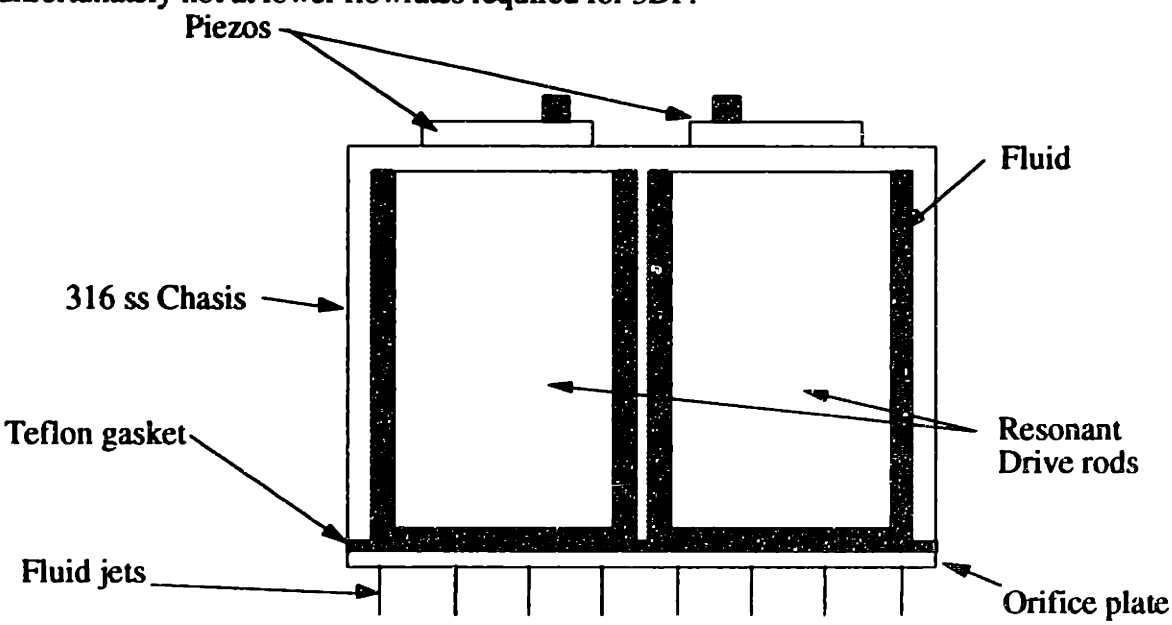

Figure 4-18: A schematic view of the Toxot.

The Toxot breakoff stability was a serious problem. Jets 1,4,5, and 8 had significantly longer breakoffs, presumably due to edge effects form the stainless steel cavity. These effects were severely magnified when the unit was run at lower flow rates. Jet position was very stable, and the Toxot was very easy to operate. It was a difficult decision to

abandon this droplet generator. Long term wear of the nickel orifice plate was also a consideration with potentially abrasive jetted fluids.

128 Jet (used by Soligen): Manufacturer Scitex

A second, desperate attempt to find a suitable droplet generator was the Scitex 128 (4 guard jets) jet unit. Scitex uses a resonant cavity approach to produce uniform droplet breakup. The entire fluid cavity vibrates at a resonant frequency. This vibration causes a small change in volume, resulting in extremely uniform droplet breakup from jet to jet. Scitex is known for very uniform break up between hundreds of jets at a time. Unfortunately this resonator had many drawbacks.

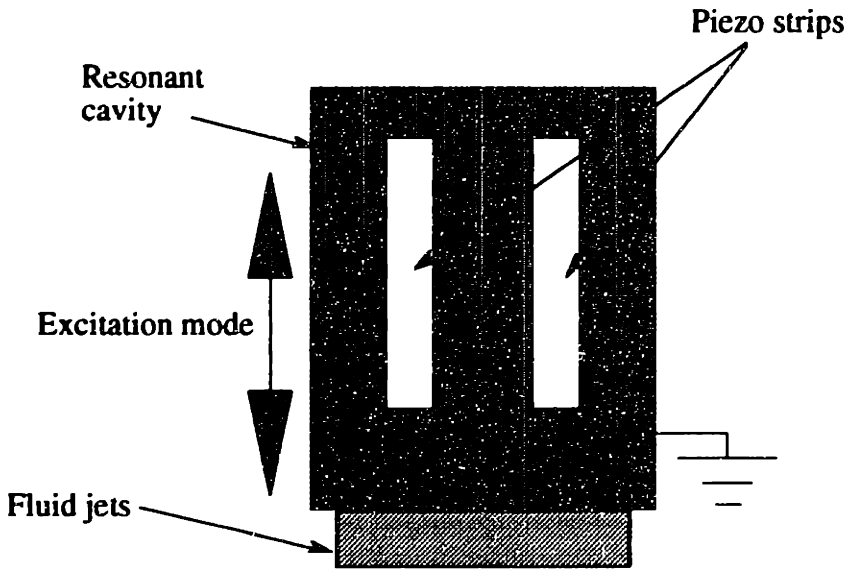

Figure 4-19: Schematic view of the Scitex droplet generator.

First, the orifice plate had to be modified to allow only eight jets to flow from it. This involved carefully plugging 124 jets without disturbing the flow characteristics of the remaining eight jets. The final procedure involved pulling a vacuum under the orifice plate and carefully placing 80 micron PMMA balls over the holes desired to be plugged. The vacuum held the balls in place as the procedure was painfully performed under a microscope. The orifice plate was then slowly heated, allowing the balls to melt and fuse the orifices shut. After many attempts, crooked streams resulted for the remaining eight jets. The system could not be ultra-sonicated to clean the orifice plate without removing pieces of PMMA.

The Scitex printhead had many other drawbacks. The orifice plate was nickel and had a very finite lifetime. Soligen currently runs the droplet generator for 200-300 hours

before replacement. Normal operation with Scitex inks yield better results at about 1000 hours. Finally, the orifice plate was glued to the resonator, making removal and replacement very difficult.

Jet Array: Manufacturer Domino Amjet

The final droplet generator chosen was the Jet Array manufactured by Domino. This aged design is very much like eight separate droplet generators fused together into a monolithic stainless steel block. This droplet generator has many great features useful for 3D printing.

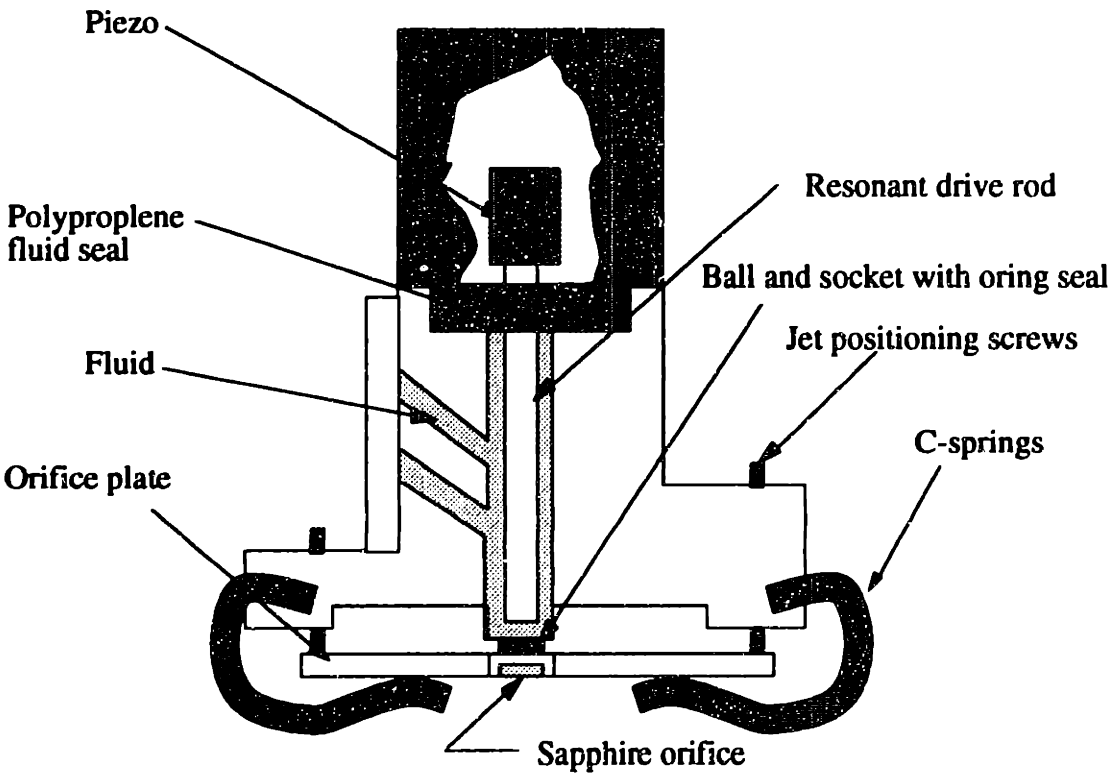

Figure 4-20: An end view of the Jet Array showing the mechanics required for one jet.

The Jet Array has eight separate piezos, allowing each jet to be tuned independently, with the exception of mechanical cross talk. The stainless steel-sapphire orifice plates are individually replaceable. These rugged orifices last a long time regardless of abrasives in the jetted fluids. Each of these replaceable orifice plates can be individually aimed, allowing continuous, precise jet alignment. This ability to adjust jets individually has two distinct disadvantages. First, it is difficult to align the entire printhead due to lack of a vertical reference position. This problem can be eliminated by locating the catcher with dowel pins insuring a good jet aiming reference. Secondly, a partially crooked jet may be

adjusted back into the jet plane causing problems later on if the clog shifts or becomes dislodged. It is difficult to tell if a jet is partially clogged, or simply needs adjustment.

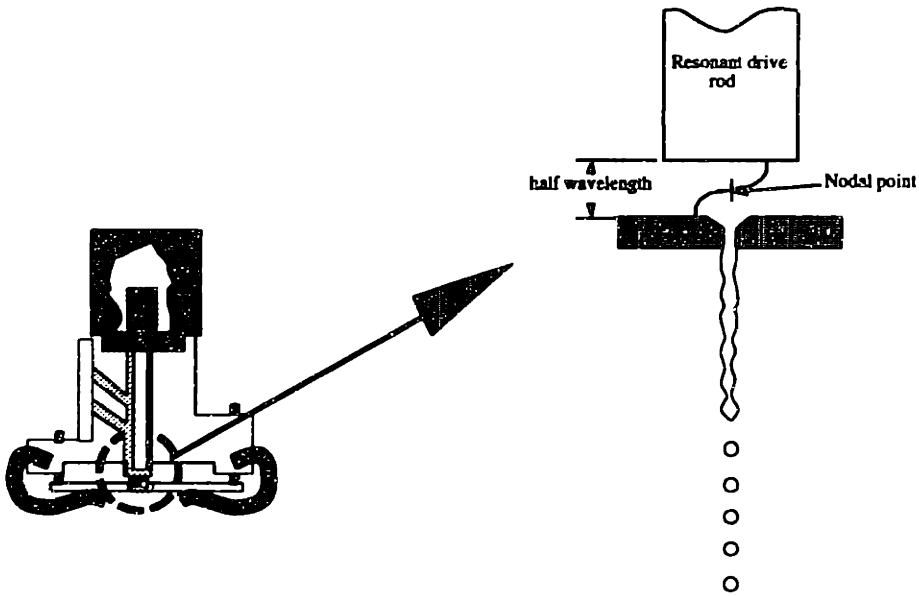

Figure 4-21: Position of the drive rod is critical for peak performance.

Before the Jet array could be used, a few modifications were required. First, the drive rod resonance was at 64 kHz, much higher than the 55 kHz Rayleigh frequency of a 10m/s 50 micron 3DP jet. Operation was attempted off resonance closer to the jet Rayleigh frequency with marginal success. To solve this problem the orifices were replaced with 35 micron jewels to raise the Rayleigh frequency to the drive rod resonance. A major drawback is higher jet velocities, causing ballistic powder ejection, and high fluid working pressures. Current maximum flow rate with these orifices is 1cc/min per jet.

Further tuning of the droplet generator would require a repositioning of the drive rod with respect to the orifice position. As presently designed, the unfixed end of the drive rod is half a wave length away from the orifice (given the sound speed of Domino's inks and the droplet generator running at 64kHz). This induces a standing wave with a nodal point half the distance between the drive rod and the orifice, efficiently transferring modulation to the jet as it exits from the orifice. It is important to establish this length to transmit maximum energy to the orifice plate and to reduce phase drift. Due to differences in sound speed of various fluids, this spacing has not been tuned for different binder uses. Because a 35 micron jet requires much less energy to breakup than a 75 micron jet, inefficiencies due to the drive rod out of position are unimportant. One drawback from not tuning these drive rods is the possibility of increased phase drift.

Other modifications were made to the Jet Array besides jet breakup tuning. The original orifice seals were inadequate. The material of choice from Domino is a elastomer called Flourosint. This seal is favorable because of its stiff modulous, allowing high modulation transfer to the fluid jet. A new design within Domino, but under scrutiny, is a small Viton o-ring seal. This design, although more compliant, is more resistant to damage from silica binder. Because 3DP jets are so much smaller than OEM Domino jets, this loss in modulation is not important. Currently, drive piezos run at 20-30% of their intended voltage rating. At this voltage, the droplet generator runs at resonance, driven from a crystal oscillator, with one or no forward merging satellites.

Other slight modifications includes machining .050" off the c-springs to fit a larger charging cell between the jet and the end of the spring, reducing the size of the load rod

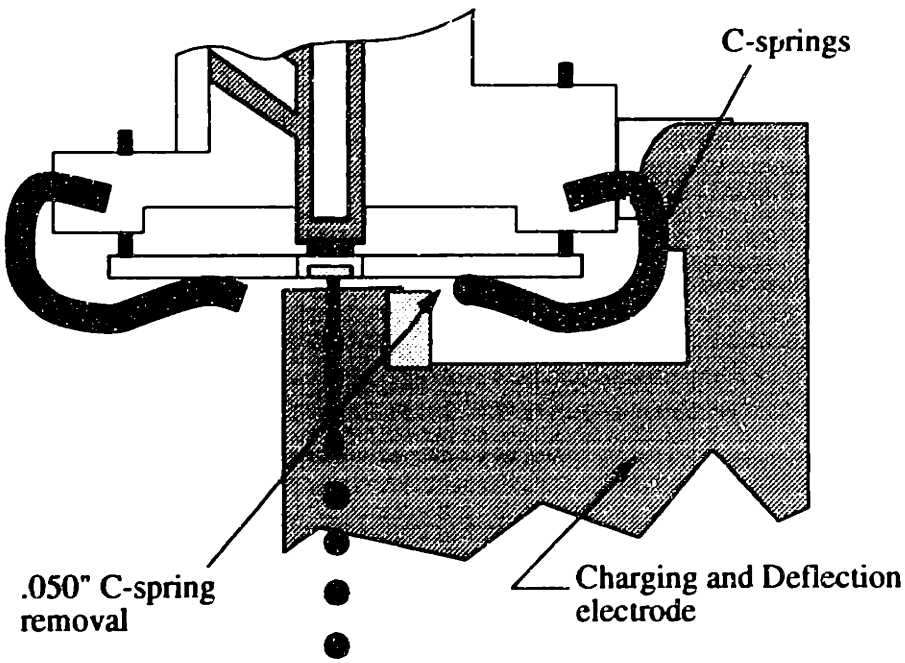

Figure 4-22: C-spring removal for charge cell clearance.

strip Delrin cover, and shortening and changing the connector used for the piezo signals. Lastly, because of problems with galling, accelerated by a caustic printing environment, all stainless steel bolts were coated with lithium grease. A better long term solution would be silver plating of the bolts to preserve cleanliness.

4.7 Procuring a Droplet Generator: A summary

It is important to review the process of qualifying a droplet generator. Design inputs for this procedure are typically flow rate and jet velocity. Using these parameters, one can then calculate the jet breakup frequency. If an existing system is chosen with a fixed mechanical resonance, this will specify the drive frequency, and the orifice diameter must be chosen to meet the system' s flowrate requirements. If droplet velocity is more critical to the system performance, it can be used to directly calculate the required orifice diameter. Sufficient modulation must then be achieved to run with a 5-8λ breakoff with fast or no satellites present. Given this procedure, the droplet generator will be successful if phase drift and jet position requirements are met.

Chapter 5: Droplet Deflection Electrode Design

Once uniform droplet breakup is attained, reliable droplet deflection can be achieved. The goal is to deflect the droplets reliably in as short an overall flight path as possible. Any reduction of the droplet flight path dramatically increases printhead accuracy. However, increasing the flight path allows for greater jet clearances and a more deflectable jet, enhancing reliability. Deflection calculations can be performed to determine printhead flight path geometry based on droplet size and velocity. Maximum charge voltage (catch voltage) is also critical to have determined before calculations can be performed. With these criteria and information in this chapter the following dimensions can be determined:

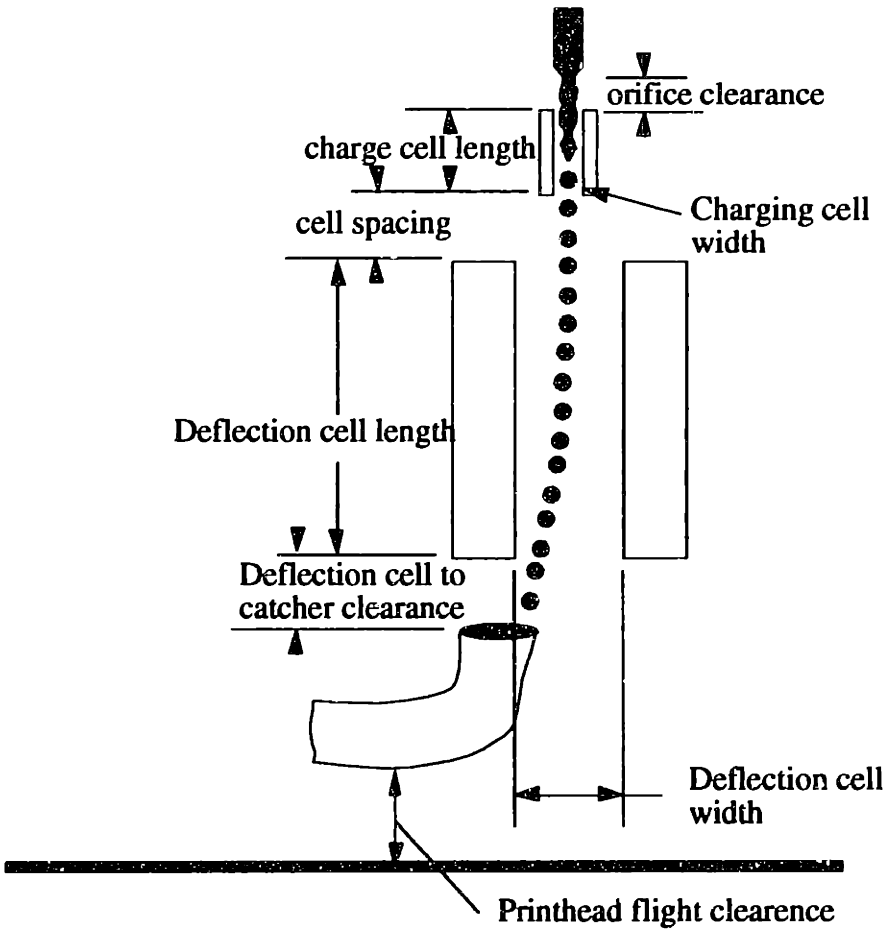

Figure 5-1: Printhead electrode and catcher layout.

5.1 General Layout Guidelines

Before deflection calculations, some general design practices are given which are essential for proper printhead operation.

5.1.1 Charging Cell

For 3D Printing with jet sizes from 35 to 50 microns, a suitable charging cell width is .018-.020". If a larger jet is used, the cell width should be increased to prevent flooding. This demands excellent alignment of the charging cell when placed into the fluid stream. To withstand error from wear and tolerance stacking, this alignment should be adjustable. A wider charging cell will lower the charge to mass ratio of the droplets (for a given charge voltage), significantly reducing deflection. The charging cell should be three times as long as it is wide. This ensures an even electric field for repeatable charge induced on the droplets. If the charging cell is shorter, changes in jet capacitance will result from breakoff length fluctuations in a non-uniform electric field. The jet breakoff should be somewhere in the top third of the charging cell. This ensures a uniform field at breakup and some satellite merge distance before the deflection electric field. The cell depth was chosen to be 4.5mm. This value is less critical, but should also be approximately three times the cell width. Figure 5-2 shows the dramatic effect of varying cell width, and therefore jet capacitance, assuming a perfectly centered jet in the charging cell. If the jet is slightly off center, the charge to mass ratio of the droplets will be significantly increased. This effect will also cause static charging errors, producing jet deflection without deflection voltage. Appendix C derives the effects of an off-center jet on its capacitance. Further derivations of jet capacitance and deflection will be covered in Chapter 5-4.

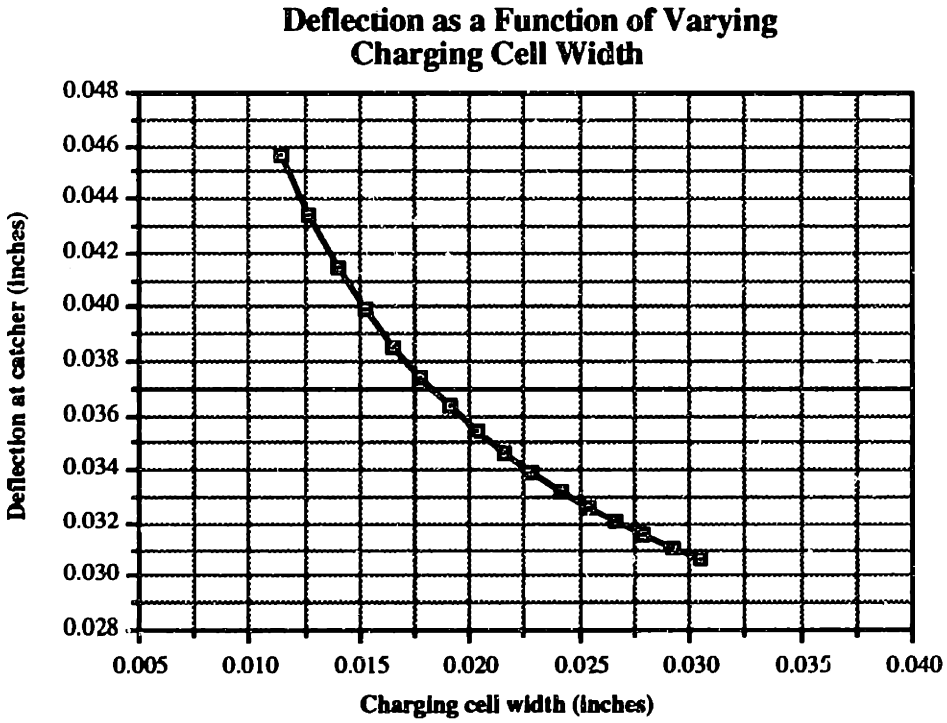

Figure 5-2: Effects of Charging cell width on deflection. Simulation run with Alpha machine parameters Vc=150v; Vd=2200v.

When using nickel orifice plates it is important to positively charge the droplets by applying a negative voltage to the charging cell. If the fluid is negatively charged, the induced flow of electrons is from the orifice plate into the fluid. The resulting electric current is in the opposite direction, out of the fluid into the nickel plate. Positive nickel ions then combine with negative ions in the jetted fluid. The result is accelerated orifice wear from reverse plating of the nickel into the stream of fluid. During positive droplet charging, a current is passed in the opposite direction eliminating this problem.

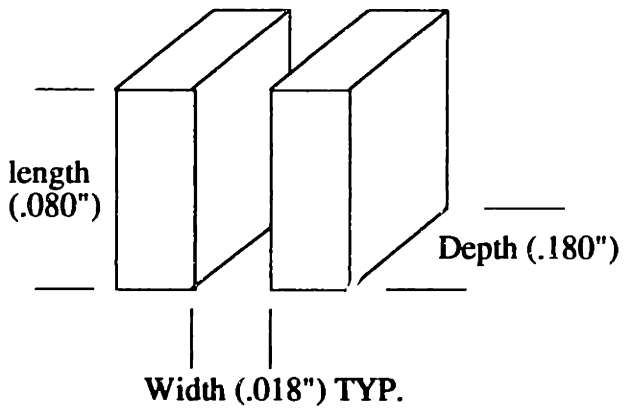

Figure 5-3: A close up of the final Alpha charging cell with dimensions.

5.1.2 Deflection Cell

One of the most problematic areas of any continuous jet printhead is the deflection cell. Arcing is typically the failure mode as a result of fluid buildup. Satellites (non merging for many λ), due to their large charge to mass ratio, always land in the deflection cell. Several points are worth mentioning about the deflection cell to extend the reliability of the printhead.

Radiusing sharp corners of the electrodes is critical. This reduces the focusing of the electric field, and hence arcing. A satisfactory radius for this application is .020". Deflection cells can run at many kilovolts- close to the air permeability break down of 3 x 10^6 volts/meter. This maximum electric field between parallel plates in air is an ideal breakdown, assuming no sharp localizations of field strength. On the Alpha printer the deflection cell runs at a conservative 2.4 KV, or about 53% of spontaneous arcing. Typical figures for breakdown percentages on commercial machines are 50 -60% of maximum breakdown potential. It is essential that all sharp internal corners be rounded to prevent localized concentration in the electric field. Finally, as is commonly done in industry, to reduce voltage potentials between the deflection cells and other printhead components, the

total voltage was produced by applying +/- 1.1 KV (versus 0V and +2.2KV) to the two deflection plates. This further precaution helps prevent the deflection cell from arcing to other printhead components, such as the charging cell.

For further reliability it is helpful to build a relief into the deflection cell wall to allow more jet clearance on the side of the deflection cell closest to the catcher. Under maximum deflection it is important to leave .015" to .020" jet clearance from the high voltage plates. Appendix G shows a sample simulation from an Excel spread sheet of a jet deflecting in a curved deflection cell. The amount of deflection is based on user inputted jet properties, printhead components, and applied voltages. The spread sheet explicitly draws the deflection cell around the jet, aiding in the design of the cell relief. The simulation will work for any deflection cell length and relief geometry.

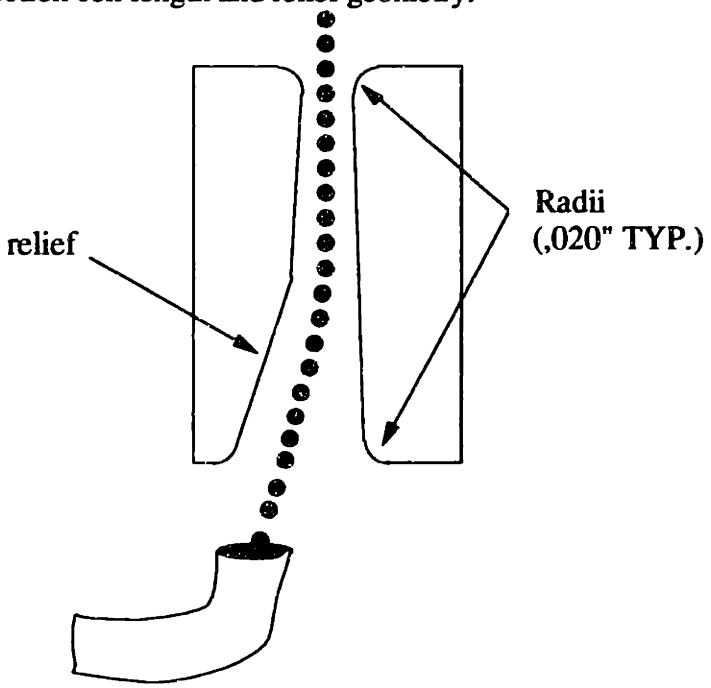

Figure 5-4: A close up view of a deflection cell.

Because of an umbilical longevity problem in bussing high voltage to the printhead, a high voltage power supply rides on the printhead carriage. This allows low voltage signals to travel via the high flex wiring to control the deflection voltage. The high voltage is produced from a specially made DC-DC converter available from EMCO and current limited with series resistors as shown in Appendix B. These power supplies run maximum at 2400 volts. This dictates a cell width of about .060" at the top of the cell plates, to stay within a safe arcing run point. The length of the deflection cell is then dictated by the maximum required deflection. This calculation will be discussed shortly. If required, higher voltage models can be specially made by EMCO. In this case, the deflection cell can

be widened to 50-60% of theoretical breakdown at the higher voltage. A higher deflection voltage would be necessary if the deflection cell gap had to widened to accommodate a very large range of proportional deflection. This would allow more jet clearance while maintaining the same electric field strength. A wider deflection cell produces larger field errors (see Figure 5-5); therefore, the deflection cell width should be kept narrow. If clearance is acceptable, it is advantageous to run at smaller plate spacing with lower deflection voltages.

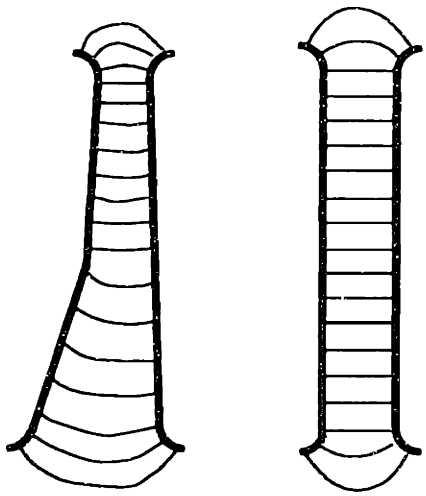

Figure 5-5: Field line disturbances from an angled deflection cell wall. These isopotentials are approximated assuming a perpendicular boundary condition at the cell wall.

Determining the distance between the charging and deflection cells is a compromise involving a few constraints. A large (.100") spacing provides more droplet flight time for satellites to merge before entering the deflection cell. The spacing must also be long enough to prevent arcing between the charging and deflection cells. Minimizing this distance reduces the overall flight distance, and in flight merging between adjacent droplets. If the charge on two consecutive droplets varies significantly in sign (e.g. positive to negative) these droplets will have a significant attraction, causing them to merge in the top of the deflection cell. If the deflection cell is close to the charging cell, these adjacent droplets would be forced apart from the deflection cell electric field prior to merging. Alain Curodeau has found merging with decreased in-flight droplet spacing characteristic of the 3DP Diconix single jet (Chapter 4.1) with an inter cell spacing of .040". Unfortunately a smaller spacing would cause arcing. Perhaps if the in flight droplet distance was increased to 4.51 orifice diameters, closing the inter cell spacing would solve this problem. A compromise was made on the final Alpha multijet by placing the inter cell spacing at .080".

Spacing of the catcher with respect to the bottom of the deflection cell is bounded by two conditions. An increase in this spacing causes a longer flight path and an inefficient design. Once a droplet has left the deflection cell it travels linearly, with deflection growing only proportionally to the flight path. If the spacing is too short, any charged particle or fluid droplet ejected from the catcher will collect on the deflection cell, requiring cleaning after many hours of run time. In the future it may be possible to reduce these effects. Prior to the installation of the EDM catcher on the Alpha machine, electrostatic build up from airborne fluids on the bottom of the deflection cell was a serious problem. The new catcher was designed with an internal slope resulting in a smaller binder contact angle reducing binder foaming. Section 7-3 explains this design thoroughly. The spacing between the deflection cell and catcher should be at least .200" to prevent electrostatic buildup.

5.2 Parameter Summary

To this point charge cell width, deflection cell width, deflection cell voltage, and catcher position from the deflection cells have been determined. Using these parameters with fluid jet breakup parameters and deflection and charge voltages the deflection cell length can be calculated based on the amount of droplet deflection required.

Predetermined variables prior to deflection calculation:

-charge voltage
-charge cell width
-deflection cell width (minimum at top)
-deflection voltage
-distance to catcher

Additional required inputs:

-maximum deflection required to catch
-droplet size, velocity, and breakup frequency

Once the amount of total deflection is calculated the second box in Figure 3-3 will be completed. At that time, the deflection cell length can be calculated, and the electrode design will be complete, but first the amount of deflection must be estimated.

5.3 Estimating Required Amount of Deflection

In theory the catcher could be placed .005" from the jet resulting in only a small amount of deflection required to catch the jet. As mentioned in Chapter 4-6, the printhead must be robust to jet wander without buildup. This requires a sizable distance between the catcher face and the theoretical undisturbed jet centerline. Proportionally deflectable printheads require even more clearance to prevent buildup on the catcher's outside edge. In addition if the jet is aimed away from the catcher by jet wander or a partial blockage, it must still be catchable via electrostatic deflection. Total amount of deflection required in the printhead can thus be broken down to three components: distance to catcher wall, catcher wall thickness, and over deflection into the catcher. Deflection far into catch, beyond the inside wall, is important for two reasons.

If the jet is deflected statically (the fourth case- Figure 4-17) from the catcher wall, it must still be steered into the gutter for normal operation. A second, more subtle, requirement relies on internal catcher buildup.

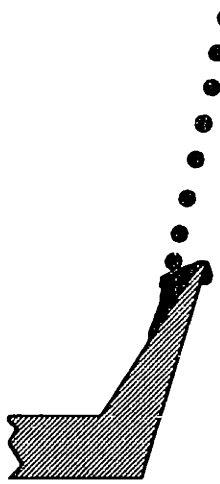

Figure 5-6: Internal catcher buildup causing fluid to collect and fall from the catcher.

With many fluids used for 3D printing internal catcher buildup is a serious problem. In figure 5-4 a catcher is shown dripping fluid because of an internal buildup problem. This seemingly subtle point is a serious issue with fluids such as Acrysol. Deflecting farther into catch does not correct the buildup problem, but allows the printhead to run longer between cleanings. Buildup issues such as this can be solved by adding drying inhibitors to the printed binder.

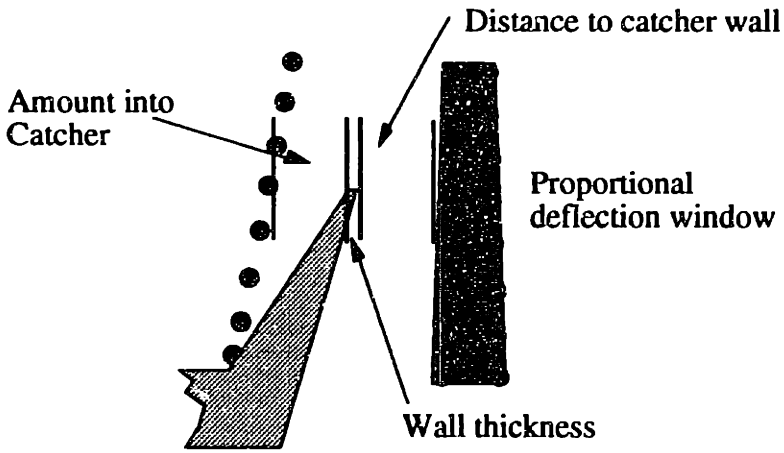

Figure 5-7: Breakdown of deflection distance.

Figure 5-5 shows a typical scenario for managing deflection. Catcher wall thicknesses range from .002-.004". A thinner wall would be difficult to machine, and have questionable resistance to wear from continuous scraping and cleaning. A reasonable out of catch safety margin is typically .010-.015" in addition to expected jet wander measurements or proportional deflection amounts of typically +/-.003-5" at the catcher. This will prevent external catcher buildup. For the case of the Jet array this distance was chosen to be .020". The into catch safety margin was chosen to be .010" in addition to proportional deflection/jet wander problems, arriving at a measurement of .015". From these figures and a catcher wall of .002", the total required deflection is .037" at the catcher level. This is summarized below.

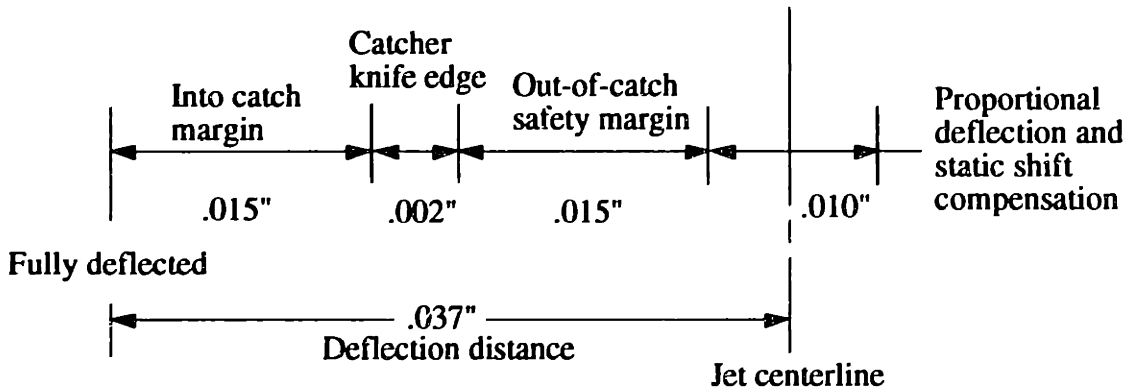

Figure 5-8: A breakdown of total deflection required for the multijet printhead.

5.4 Calculating Deflection

Material in this section is partially the result of significant theory developed by J. Bredt '93, J. Milner '93, P. Williams '90, and D. Brancazio '91 all from MIT. Some new material is presented in conjunction with this previous work. An Excel spread sheet (see Appendix H) has also been developed to aid in the following calculations. This section is meant to describe some theory and experimental measurements, while the spread sheet is intended for estimating the deflection for any printhead design. The spread sheet also contains rigorous documentation increasing its useability.

5.4.1 Droplet Charging

Droplets are inductively charged by capacitive coupling between the fluid jet and the charging cell walls. Modeling the jet as a line of charge, the electric field around it can be calculated as:

$$E = \frac{q'}{2\pi\varepsilon_0 r} \qquad 5.4.1$$

Where q' is the charge per unit length on the jet, and E_O is the permittivity constant 8.85×10^{-12}F/m. The potential difference for a cylindrical capacitor can be found by integrating the electric field from the surface of the jet to the electrode. This potential difference, V, equals:

$$V = \frac{q'}{2\pi\varepsilon_0} \ln\left(\frac{d_{cell}}{d_{jet}}\right) \qquad 5.4.2$$

where d_{cell} and d_{jet} are the diameter of the charge cell and the diameter of the jet, respectively. For any capacitor, the capacitance equals the charge, q, over the potential difference V. The capacitance per length, C', is equal to:

$$C' = \frac{q'}{V} \qquad 5.4.2$$

The capacitance per unit length for a cylindrical capacitor is therefore equal to:

$$C' = \frac{2\pi\varepsilon_0}{\ln\left(\frac{d_{cell}}{d_{jet}}\right)} \qquad 5.4.3$$

This derivation is very close to a parallel plate charging cell. Appendix C outlines the derivation of a more exact approach using the method of images. The results of integrating the electric field (using this method) from the fluid jet to the cell wall results in the following voltage difference.

$$V = \frac{q'}{2\pi\varepsilon_0}\left[.216 + \ln\left(\frac{w}{d_{jet}}\right)\right] \qquad 5.4.4$$

Where w is the cell width The integration yields a series which converges at .216. Now the capacitance of the parallel plate charging cell per unit length can be determined:

$$C = \frac{2\pi\varepsilon_0}{.216 + \ln\left(\frac{w}{d_{jet}}\right)} \qquad 5.4.5$$

These cell capacitance calculations have a few possible sources of error. The jet is assumed to be a cylinder, when in reality it a cylinder breaking into droplets. A second source of error is the detrimental effects of induced charge from previously broken up droplets.

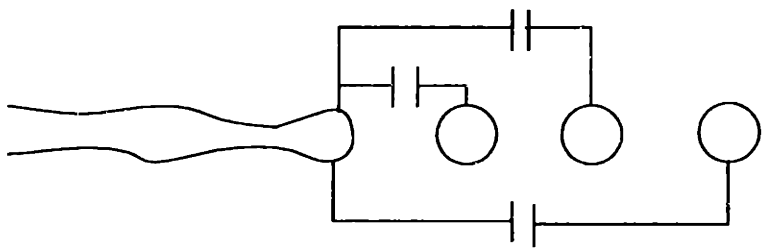

Figure 5-9: Capacitive coupling between droplets.

Equation 5.4.4 over predicts the charge on a droplet by approximately 15.9%, due to the effects of induced droplet charging effects from the three lead droplets. At $\lambda=3.51d_O$, the previous droplet subtracts approximately 11%, the next 4.5% and the third .4% for a total of 15.9% induced charge. These numbers were calculated by Alain Curodeau using a Diconix droplet generator. Since droplets are charged opposite of the charge cell wall, they will induce an opposite charge on the droplet breaking off- reducing it charge. To compensate for these effects a correction factor is used to calculate the adjusted cell capacitance per unit length:

$$C_{Adjust} = \alpha C_{Calculated} \qquad 5.4.6$$

This factor is calculated using the three values mentioned above and scaling these by $1/\lambda^2$ as the droplet spacing changes for different flow rates and frequencies.

The droplet charge is then simply:

$$q_{Drop} = C_{Adjust} V\lambda \qquad 5.4.7$$

Where V is the charge voltage and λ is $V_{jet} / f_{modulation}$.

Figure 5-7 shows measured and calculated droplet charge for a .018" charging cell at several charge voltages. These measurements were made using a current to voltage Opamp transducer (Horowitz and Hill p227). This measured input current was converted to droplet charge using the following equation:

$$\frac{\text{Coulombs}}{\text{Drop}} = \text{Droplet Charge} = \frac{I_{measured}}{\text{Drop Frequency}} \qquad 5.4.8$$

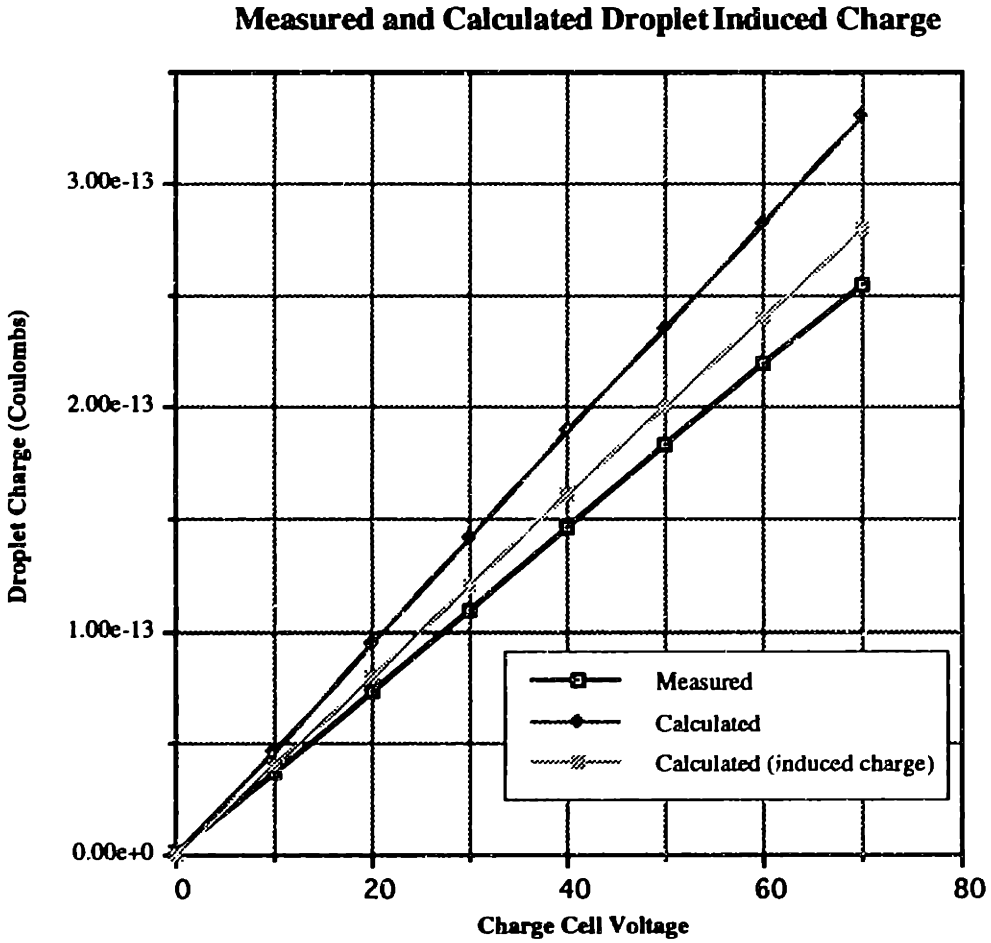

Figure 5-10: Measured and Calculated Droplet Charge. Measurements were made at 64kHz, flowrate .85cc/min, 35 micron orifice, and jetted fluid was Acrysol.

5.4.2 Droplet Deflecting

Once the droplet charge is calculated, determining the amount of deflection at the catcher can now be accomplished. The force exerted on a droplet in the deflection cell is:

$$\vec{F} = \left(\frac{V_d}{D_w}\right)\left(q_{Drop}\right) \qquad 5.4.9$$

Where V_d is the deflection cell voltage and D_w is the deflection cell width.

The droplet acceleration is then:

$$\vec{a}_y = \left(\frac{q_{drop}}{m_{drop}}\right)\left(\frac{V_d}{D_w}\right) \qquad 5.4.10$$

It is important to note that the acceleration occurs in the deflection cell only. Upon exit of the deflection cell, droplets fly in a straight trajectory with horizontal and vertical velocity components.

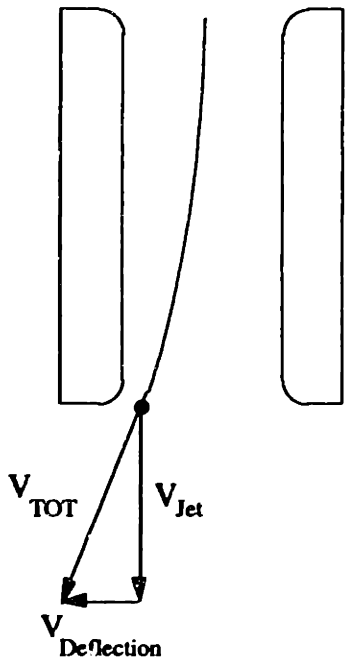

Figure 5-11: Droplet flight trajectory is parabolic in the deflection cell, and straight upon exit.

These calculations do not account for a relieved deflection cell explained in section 5.1.2. Calculations for a relieved cell are performed in an incremental manner on the previously mentioned Excel spread sheet. Simply inputting the cell width at ten points along its length in this spread sheet will approximate the proper deflection. In the case of a tapered deflection cell Equation 5.4.11 is used for each of the 10 sections of varying width along the deflection cell length. For a straight deflection cell the deflection can be calculated as shown on the following page.

$$y_{Deflection} = \frac{a_y}{(V_{jet})^2}\left[\frac{1}{2}(l_d)^2 + (l_d)(l_{cat})\right] \qquad 5.4.11$$

Under normal Alpha operation:

Vd=2000 volts

Vjet=14m/s

ld=.0097 m (straight deflection cell)

ay=2800 m/s^2

Vc=150 volts

lcat=.00508 m

Substituting these values yields deflection at the catcher of 1.25 mm or .047".

Chapter 6: Electrode Construction

Once the electrode configuration has been finalized, building it to exacting specifications is the next challenge. For 3D printing, it was essential that the electrode be easy to clean, durable, consistently accurate, and very lightweight. Commercial designs are composed of metallized ceramic substrates, or a series of carefully aligned stainless steel plates. All of these fabrication techniques result in a heavy design, incompatible with the high acceleration environment of the Alpha machine. For this reason, a new procedure was developed. A brief overview of the final process is summarized in Figure 6-1.

6.1 Electrode Construction Overview

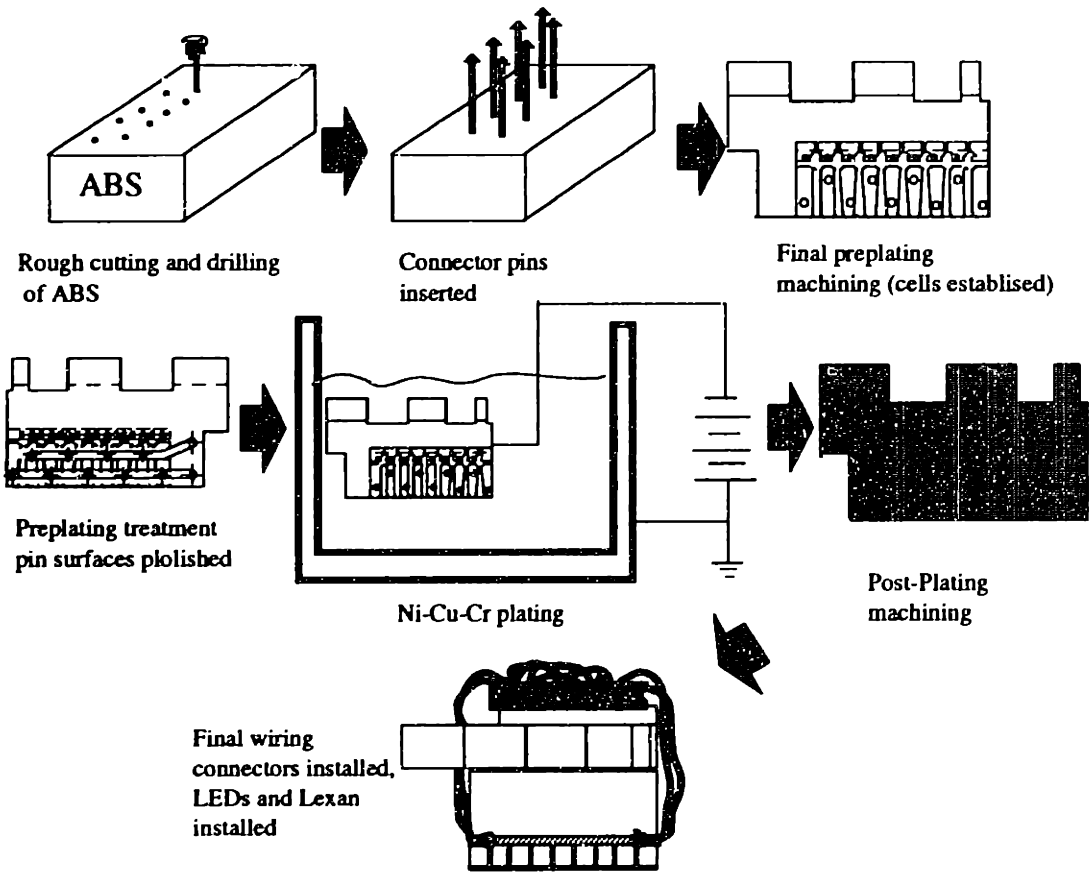

Figure 6-1: A summary of electrode construction.

The heart of the design is a chrome plated, carefully machined ABS block. The plating is used to make both the charging cell plates and the deflection cell plates. These plates are electrically isolated via a delicate post-plating machining process. Stainless steel pins are used to make contact with these electrode plates. The pins travel through the block

and are then wired on the back of the block away from printed fluids. Other important features such as alignment and jet strobing are also incorporated into the assembly. In theory it is possible to incorporate more features, such as phase electrodes, into this lightweight flexible design. Each of the fabrication steps are explained in detail as follows.

6.2 Machining and Pin Connection Details

Initially the ABS blocks are fly cut to the external dimensions. Smooth surface finish is essential. Next the holes are drilled into the ABS block to make the electrical connections. Specific cutting parameters are crucial for a smooth hole. Due to the large aspect ratio, a slow cutting speed coupled with a short dwell time is preferred to prevent heat buildup and melting of the ABS. Coolant is also required. These holes were drilled with auto pecking on a CNC mill. Figure 6-2 shows details of these holes with stainless steel pins inserted. Each of the holes is drilled in two stages. The first stage is a slip fit, used for alignment, and for reducing the stress level in the completed ABS block. The second is a press fit used to securely hold the pin in place during the service life of the electrode. This detail is shown clearly in figure 6-3.

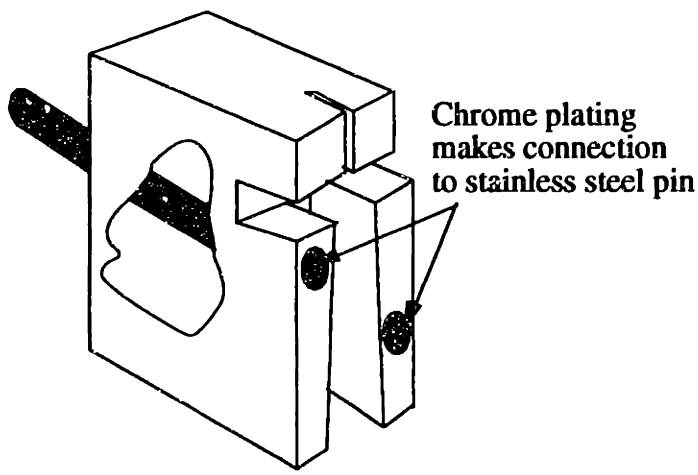

Figure 6-2: Using stainless steel pins to make electrical connections.

All plating was out-sourced to General Superplating. Attempts were made to electroless nickel plate in house with limited success. Electroless nickel plating had reasonable adhesion, but scratched very easily. A stronger material had to be chosen to withstand the sundry of abrasives soon to be jetted through the printhead. The final plating chosen consisted of 5μm of electroless nickel, 10 μm of copper and 10μm of chrome for a total plating thickness of 25μm. This combination is very rugged, and adheres to stainless pins nicely when they are properly prepared.

Proper pin preparation consists or carefully sanding the head of the pin after insertion with progressively finer (up to 600 grit) sand paper. These pins must be ground flat on one end and chamfered on the opposite end for smooth insertion. This technique is crucial for success. After plating, the face of the electrode assembly is completely smooth and resists collection of fluid.

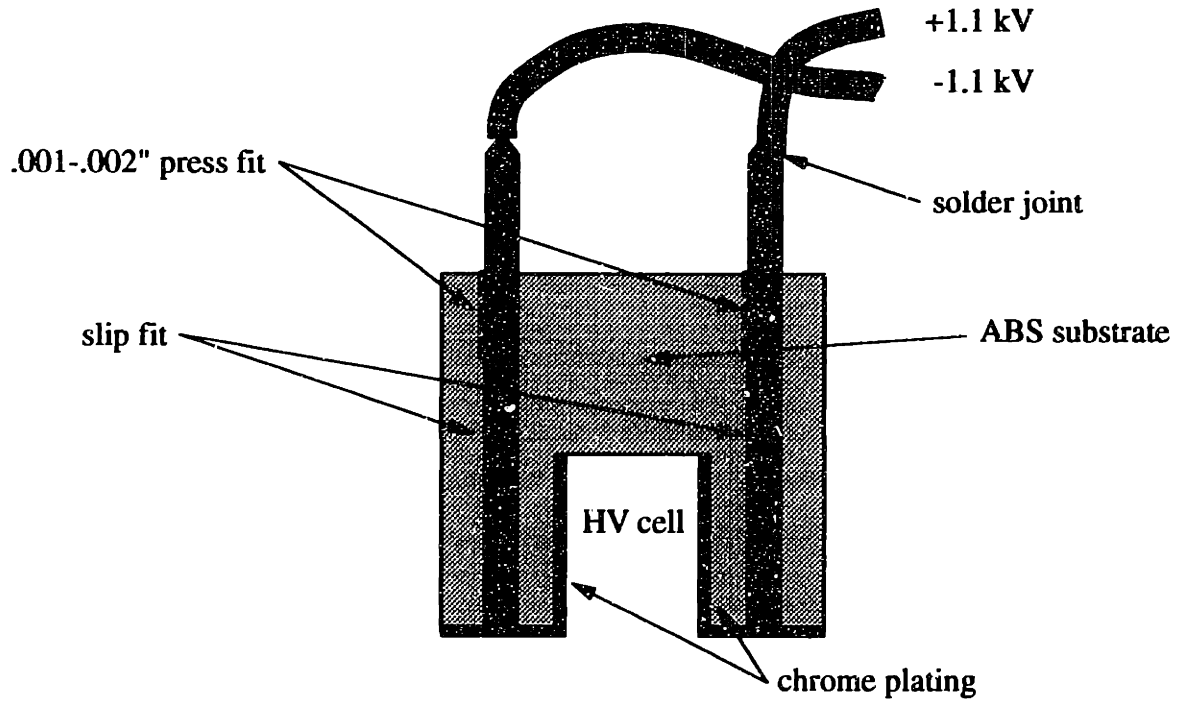

Figure 6-3: Detail of positioning of the stainless steel pins for electrical contacts.

High voltage pins are .0625" in diameter versus .0457" used for the charging cell contacts. The larger pins are used for the high voltage cells to increase the connection surface area. The larger area prevents damage to the plated connection from high voltage arcs. The charge cell pins are prepared and inserted in an identical manner. The high voltage pins are machined in place to ensure a smooth surface for plating on the back of the electrode block. This clean surface is then used to create positive and negative high voltage busses in the back of the electrode assembly. This connection is then completed using a three pin Molex power connector with the center pin unused for improved high voltage

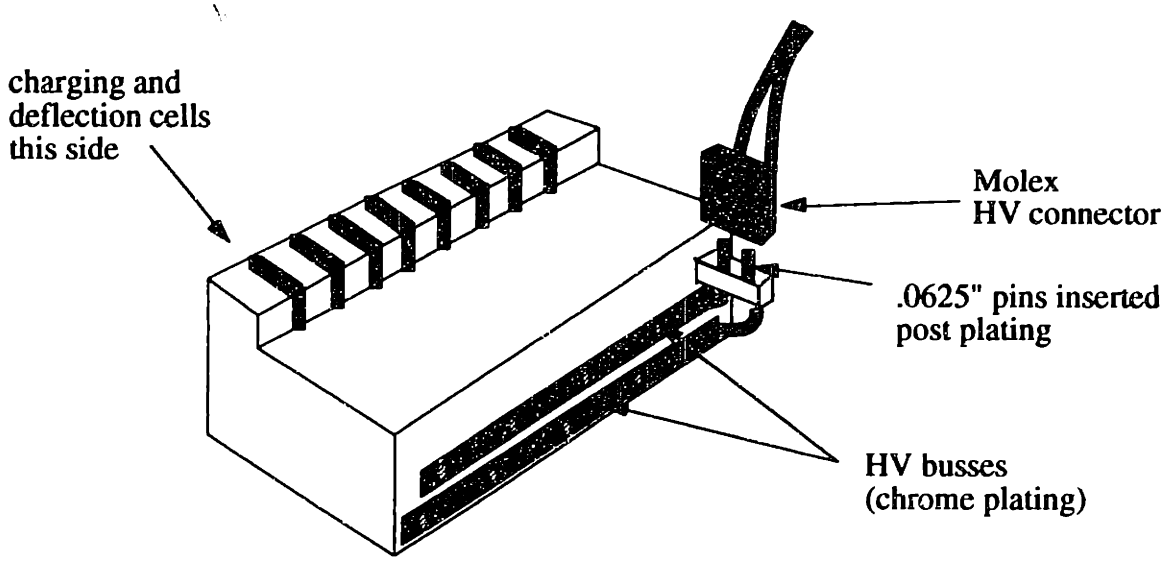

Figure 6-4: High voltage bus detail.

insulation. Figure 6-4 shows this high voltage buss and the Molex high voltage junction. Connection from the Molex to the high voltage interrupt circuit is done with 10kV test lead wire. Connection from the high voltage buss strips to the HV connector is done with stainless steel pins carefully pressed into the drilled ABS block. These are the only pins added after electroplating. The HV connector pins are silver epoxied into plated holes and the entire assembly is then potted for durability with epoxy or RTV.

Preplating machining of the charging cells was performed with specially made cut off saws. To prevent flexing and inaccuracies during machining, an all carbide low profile cut off wheel was used. This wheel was designed to overhang from the tool mandrel .030" beyond that required to cut the charging cell. This arrangement provided excellent charging cell alignment in operation on the Alpha machine.

Placement of the electrode assembly with respect to the droplet generator is critical and must be adjustable. The deflection assembly must also be hinge-able to allow a clean insertion of the electrodes around the fluid streams once they are jetting correctly. Several designs to accomplish this are discussed in Chapter 8.

6.3 Post Plating chrome plating removal

The most difficult task in electrode construction is the removal of the unwanted plating in the charging and deflection cells. Unwanted plating is carefully machined from the ABS with micro endmills. This slightly crude technique eliminates the difficult task of using selectively applied photoresists. Attempts to have good plating adhesion around photoresist areas were unsuccessful.

This delicate post machining process required the use of two modified end mills. Figure 6-5 shows the results. These micro end mills were made from high speed steel and center ground on a lathe to the specifications shown in figure 6-5. A Dremel tool was used with an aluminum oxide cut off wheel. This simulated tool post grinder arrangement with the use of a microscope, allowed for careful modification of each endmill. The inter cell removal endmill simply required a deep cut. As long as the shank of the tool cleared the flukes left on the end mill, it was sufficient for plating removal.

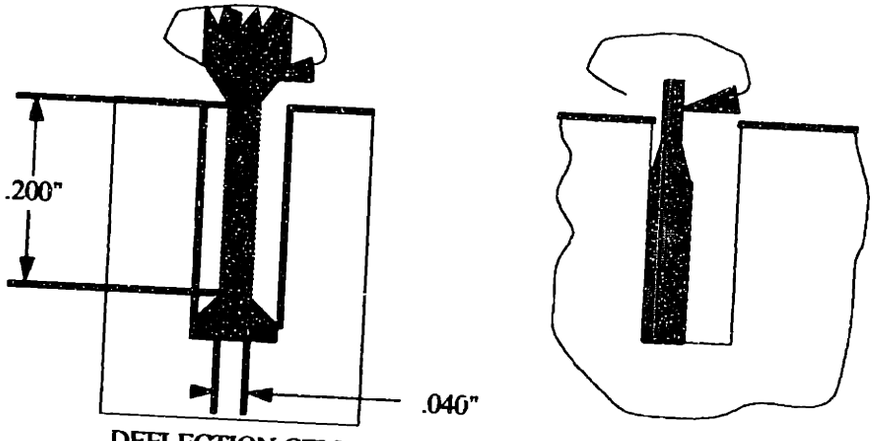

Figure 6-5: Post plating removal of the ABS electrodes.

These modified end mills were extremely fragile and required small depths of cut with a water soluble oil emulsion lubricant to prevent breaking. This machining was typically done by back lighting the endmill for alignment in the deflection cell prior to making each pass of plating removal.

6.4 Back-lighting the Jets for Control of jet breakoff parameters

To assist in printhead reliability it is convenient to back light each stream and monitor its performance with a CCD camera. This feature had to be incorporated into the multiple nozzle printhead. Using an individual LED for each jet was cumbersome and possibly unreliable in the long term. Instead, a light bar was created with two high brightness LEDs placed at the ends of it. When the whole bar illuminates, the jets can be easily viewed. This technique was also crucial due to the space constraints around the orifices on the Domino resonator. Appendix B shows details of LED strobing.

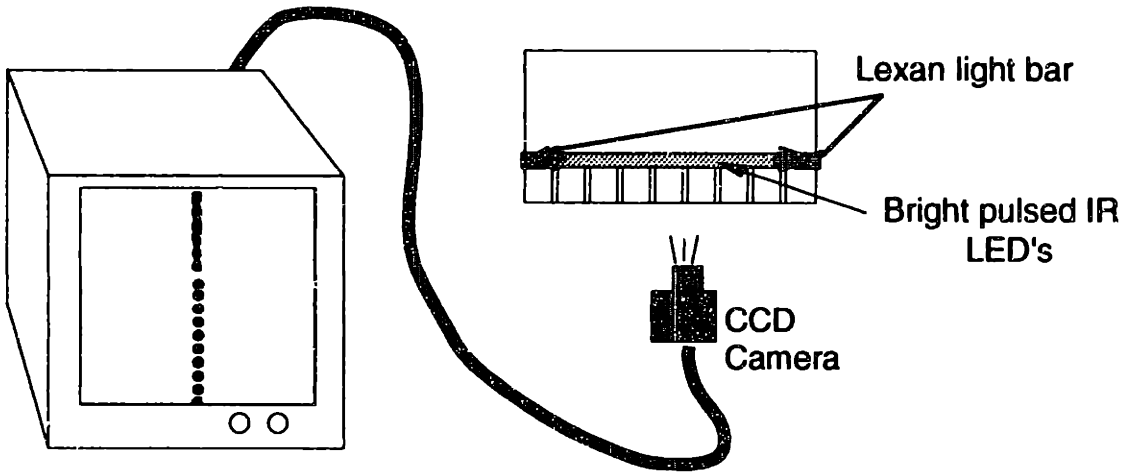

Figure 6-6: The light bar placed behind the charging cell.

Chapter 7: Catching Unprinted Droplets

7-1 Catcher Design Requirements

During normal operation the droplet catcher is the current failure mode determining average run length between printhead failures or intervention. Some binders such as Acrysol will lead to significant catcher buildup, even with the printhead simply sitting in catch. Proper catcher design is essential for long term reliability.

The catcher must be thin when viewed from the fluid jet axis, but be rugged enough to withstand rigorous, repeated scraping during cleaning. The catcher must also be made of a material resistant to a variety of solvents, acids, and bases. Finally it must be easy to disassemble and clean if a vacuum line clogs.

7-2 Commercial Catcher Designs

Two predominant designs exist in industry to catch droplets. Typical deflect to print (section 2-2) configurations use a small tube into which the jet is aimed. For 22 m/s jets with 120 μm droplets the tube is about 1mm inside diameter with a 40 micron wall. This configuration is used for single and multiple nozzle configurations up to eight nozzles. Greater multijet arrays with single sided electrodes use a wetted wall configuration. These deflect to catch models collide the deflected droplets into a wall at a slight angle allowing the ink to drip down into a pumped opening.

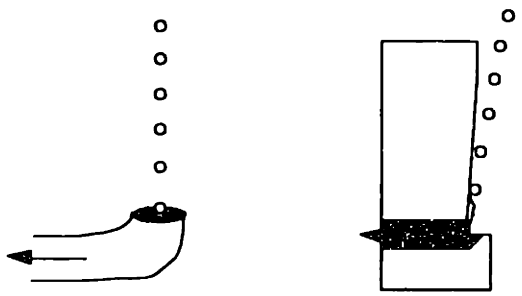

Figure 7-1: Two frequently used catcher styles in industry

It is important that the catcher effectively pump all tubes equally independent of both how many jets are in catch, and how long they have been in catch. Jets not in catch will provide a free air pumping port, while a higher load is seen by the pump at the ports in catch. This imbalance will cause, under specific circumstances, a pumping failure. During startup of must commercial printheads the catcher frequently fails for this reason. Once an even pumping load is established on each port, normal operation may begin.

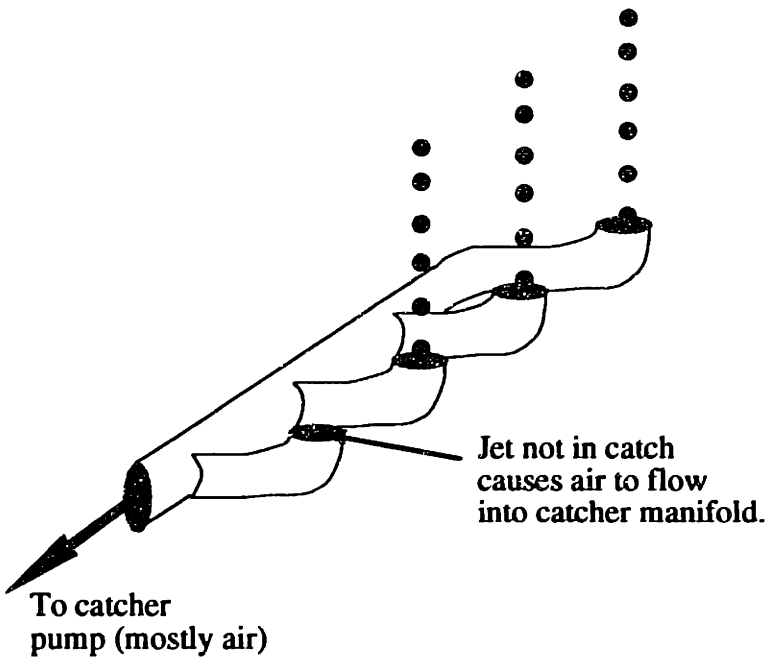

Figure 7-2: Unequal fluid loading between catchers causes pumping problems.

A single manifold catcher is adequate for commercial printing because only selected drops are pulled from the droplet stream. This procedure greatly reduces printing throughput, but is essential to reduce induced charging and merging effects. Thus during a normal printing duty cycle, each catcher has identical pumping resistance, allowing efficient pumping across all ports. In addition, typically the catcher pump runs at 8-10 times the total printhead flow rate. This introduces an enormous amount of air into the system which must be removed. Introducing excess air into the catchers on a 3DP machine running binder will clog the catcher due to accelerated drying of binder. In the near future, separate fluids will be printed simultaneously on the alpha machine, rendering a single manifold catcher useless because of binder mixing. A new catcher design was essential for success on the alpha machine.

7-3 Alpha Catcher Design

For eight jets it was possible to have a separate catcher line for each catcher, but this would be cumbersome to pipe in the fast axis. Four separate lines would be more manageable from a hardware standpoint, while still allowing flexibility for multiple materials. This arrangement would require two adjacent jets to share the same catcher. This method simplifies the electronics because each charging cell can then be run with the

same voltage polarity. Adjacent jets will deflect into each other due to alternating deflection cell electric fields. The final configuration for the eight jet head is shown in Figure 7-3.

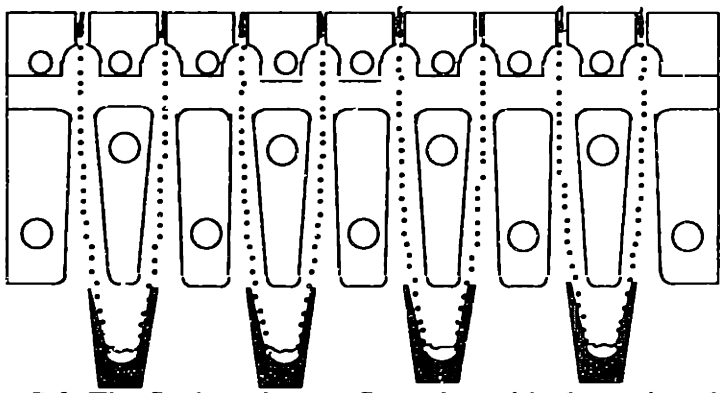

Figure 7-3: The final catcher configuration with alternating electric field in the deflection cells.

A prototype catcher was constructed from aluminum to test the feasibility of the design as well as the machine-ability of creating a knife edge thin wall. A cross section of this design is shown below. It is essential for the jet to strike a slope rather than collide with a surface perpendicular to the jet. If the jet does not collide with a slope, foaming and splashing will result. Foaming also makes removing the printed fluid from the catcher difficult. In addition, if fluid is introduced into the air in mist form, it will collect on the deflection electrodes due to their strong electric field. This relatively slow buildup has long term reliability issues. If the printhead remains in catch for 2-3 hours without moving, electrostatic fluid buildup from airborne fluids will cause arching. In an effort to prevent foaming, an internal slope was cut into the catcher using a micro tapered end mill. The .047" radius was machined with a ball end mill.

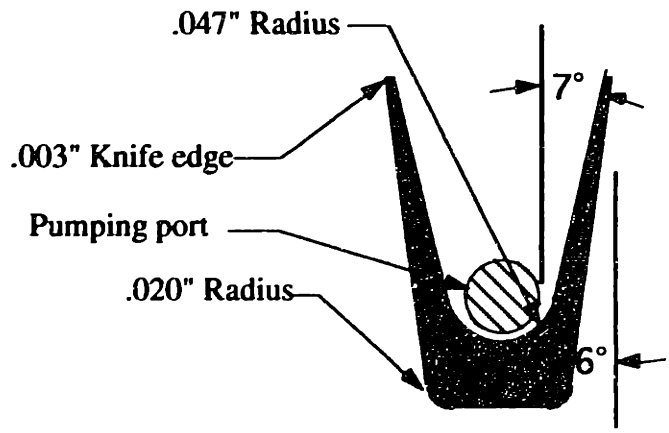

Figure 7-4: A close-up of the prototype catcher pocket.

The external slope of 6 degrees is essential for jet clearance during printing and time of flight measurement. This angle is based on the flight trajectory of the droplets corresponding to the horizontal and vertical velocity components of the droplets. The pumping port is a .0625" hole into which a 14 gauge hypodermic tube is pressed for vacuum connection. Several problems were solved with this prototype catcher. The knife edge was very easy to machine and was decreased to .002" in later designs. The material, 303 ss, chosen for machinability, held up very well to scraping. The entire structure was also very strong, allowing it to hold tight tolerances under repeated abuse from scraping. Unfortunately, this design was not without flaws.

Foaming was a serious issue with this catcher configuration. Due to large amounts of deflection, the droplets frequently missed the inside wall and slammed into the catcher floor, making binder removal very difficult.

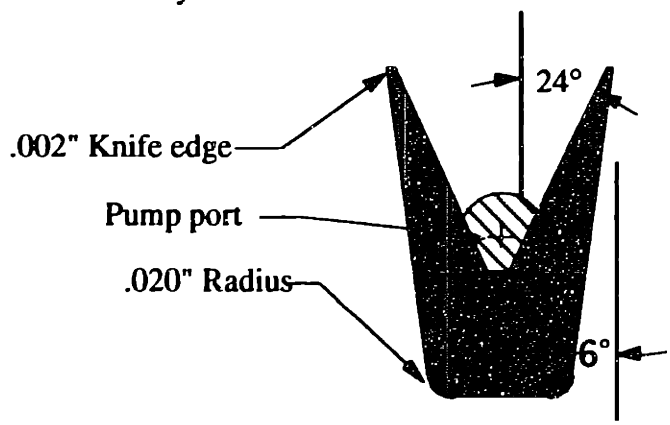

Figure 7-5 : A close-up of the final catcher. The pocket was made using EDM.

Figure 7-5 shows the final design. This catcher had a shallower internal slope, giving the jet position more flexibility by allowing the jets to deflect farther and still collide on the tapered region. This greatly reduced foaming from droplet collision. Pumping was also increased in the final design by decreasing the size of the catcher opening. Finally an anti foaming agent (Antifoam 1500- Dow Corning) was added to the most problematic fluid-colloidal silica. On the final design, the catcher knife edge was reduced to 50 microns. The internal pockets had to be made using an EDM tool.

7-4 Catcher Pumping Methods

7.4.1 Current Design

Each catcher tube must be pumped individually. These pumps must be able to pump a variety of fluids as well as air, be self priming, and have a 100% duty cycle. Catcher pumps used in the ink jet industry include both gear and peristaltic. Gear pumps

are typically too high flow rate for 3DP and might possibly fail from exposure to colloidal silica or abrasive slurries. Peristaltic pumps work well for this application with the exception of reliability. The rotor tubes, under constant flexing, have a finite life span. Soligen currently uses two 3/8" 300rpm peristaltic pumps in parallel to pump on their beta catcher. This configuration typically runs a week between tube replacements. Another possibility would be to use miniature diaphragm pumps as shown in figure 7-6. These pumps have undergone initial testing on the alpha machine, and will hopefully soon replace the peristaltic pumps. However, recently switching to Norprene tubing on the Alpha machine has greatly increased peristaltic pump life.

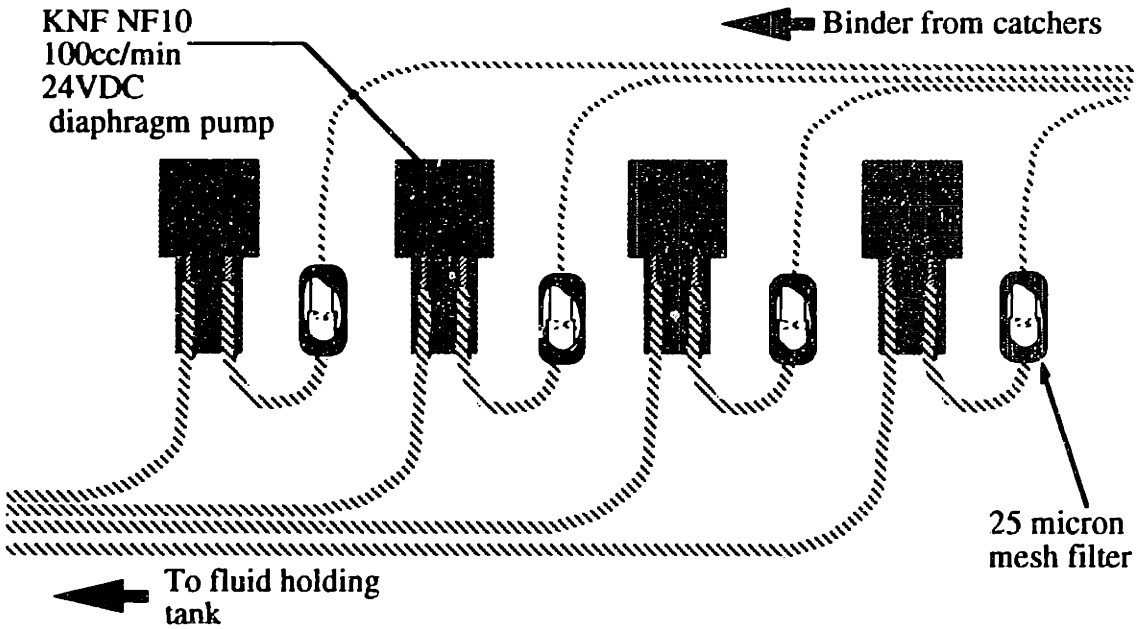

Figure 7-6: Diaphragm pump configuration for catchers.

7.4.2 Reducing Number of Catcher Pumps

Reducing the number of pumps required to pump the catchers would be a great design improvement. Unfortunately because the multijet printhead is a proportionally deflectable, the jets cannot be configured into a wall catcher as shown in Figure 7-1. A wall catcher would allow many jets to be caught and pumped with one pump. The last possibility is then to adopt a manifold style catcher similar to Figure 7-2. This would also be difficult to implement on the Alpha machine. During on-line stream position inspection, jets are out of catch for a few seconds at a time. This out of catch duration would cause a severe imbalance in the system, resulting in a loss of adequate pumping on the catchers.

Chapter 8: Printhead Layout

Once printhead subassembly is completed, the components must be integrated to function together as a single printhead. This is often the most critical part of printhead design. A few issues are important to prevent flooding, insure precise alignment, and facilitate maintenance.

8-1 Droplet Deflection Electrode Positioning.

Droplet Deflection Electrode Positioning is the most difficult aspect of the printhead layout. The electrodes must be removable for cleaning and during startup and shutdown of the printhead. During initial jet startup there is often significant wander, which would cause flooding if the electrodes were fixed. Although some printheads have the ability to startup and jet directly through the electrodes, attempting to recreate this effect on the 3DP machine would be impossible at best.

The position accuracy of the electrodes with an approximately a .018" charging cell is about .001-2" (see Appendix C). A popular technique for achieving this is to hinge the electrodes in a clam shell arrangement. Figure 8-1 shows how this is done on the Imaje Toxot.

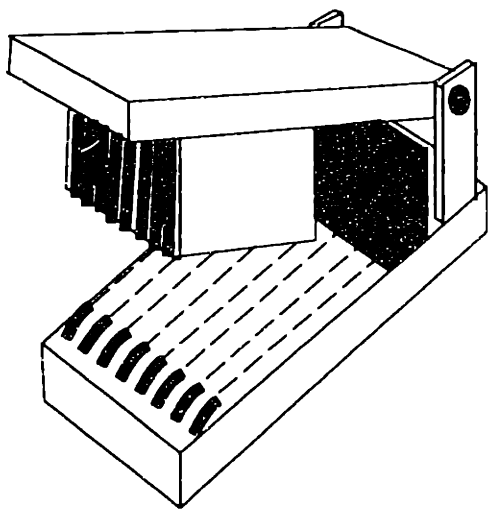

Figure 8-1: A clamshell arrangement for electrode positioning.

The original Alpha single jet design is interesting. Shown in Figure 8-2, this design had the added flexibility of separately removable the charging and deflection electrodes. This layout was the result of unstable, satellite-prone jet development. Consequently, the major drive of the printhead was disassembly to clean after a flood. This printhead was also very adjustable to allow for changes in jet position. Finally, the droplet generator yoke was interchangeable across many resonators. This was an excellent

design for initial printhead development. Frequent shorts, bad connections and jet misalignment plagued the design, making it unsuitable for the multijet. Its clear advantage was easy electrode removal.

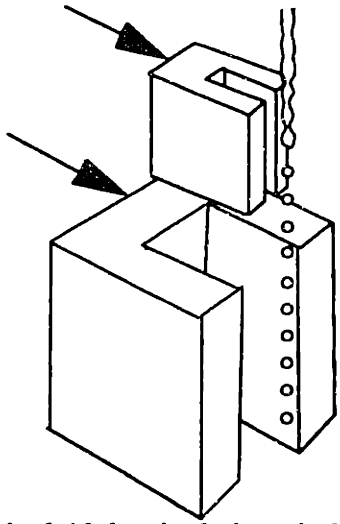

Figure 8-2: Layout for the original Alpha single jet printhead. Design by D. Brancazio. Electrodes can be removed separately.

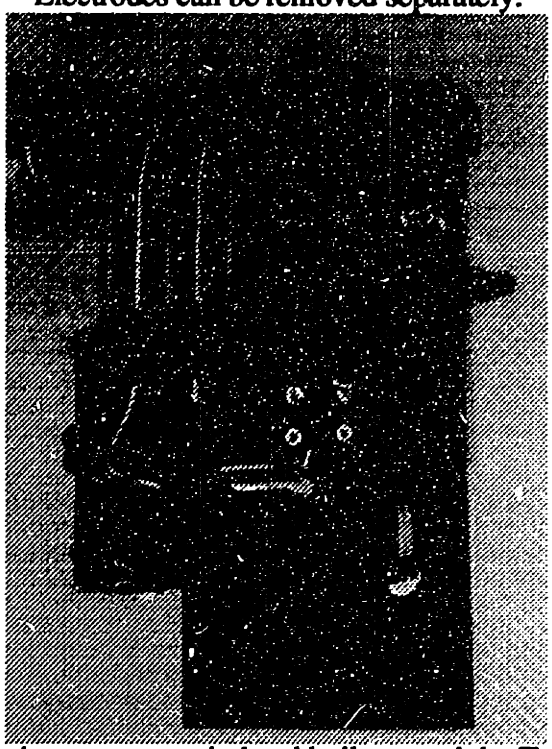

Figure 8-3: An all plastic prototype printhead built around the Toxot droplet generator. This was constructed to test the durability of the chrome plating technology.

Before the entire printhead design was frozen an experimental printhead was constructed with a Toxot droplet generator. This printhead was a classic clamshell arrangement composed entirely of Delrin. The electrodes were chrome plated ABS with

stainless steel pins. Issues such as arcing, cross talk, and deflection were addressed with this design. The entire package was very light weight.

8-2 Final Alpha Design.

Figure 8-4 shows an overview of the Domino design. The electrode assembly, referred to as the DDM, pivots directly on the droplet generator. This ensures precise location with easy adjustment.

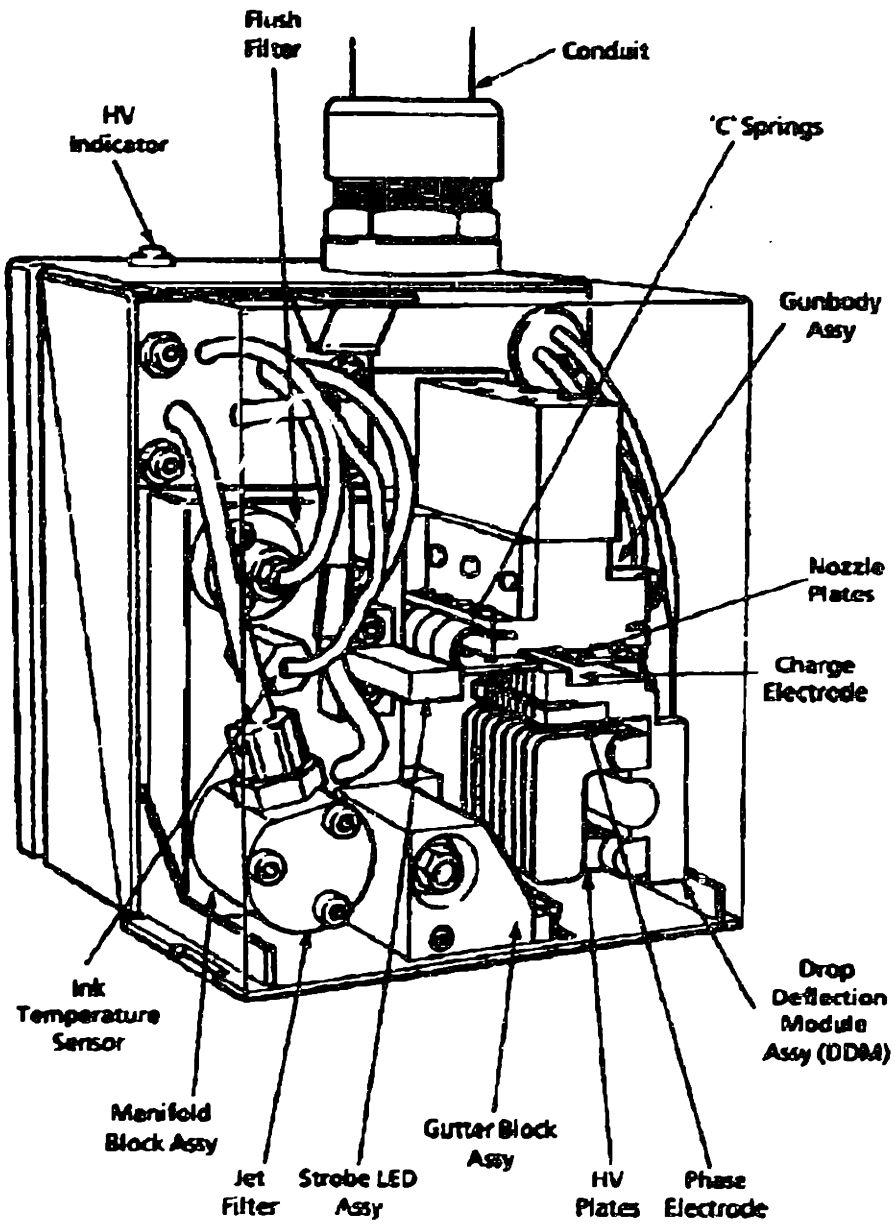

Figure 8-4: The Domino Jet array printhead.

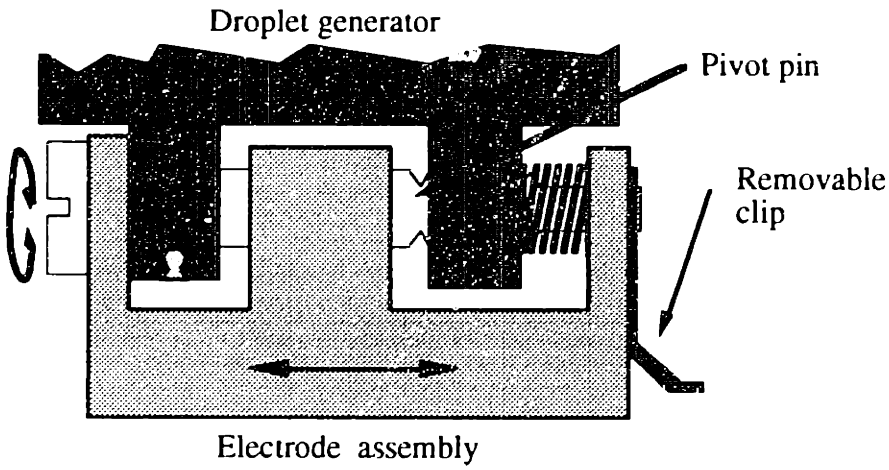

Figure 8-5: Positioning the electrodes on the Alpha multijet head.

One drawback of mounting the DDM in this manner is difficulty of electrode removal. To aid in removal of the electrode door, a special retaining clip was made which can be removed by hand. A spring provides a restoring force against the removable clip. Lateral adjustment is made by twisting the pivot pin with a screwdriver. A set screw is also installed to hold the adjustment as the door swings. Another aid to disassembly is a spring compressor to hold the spring during assembly.

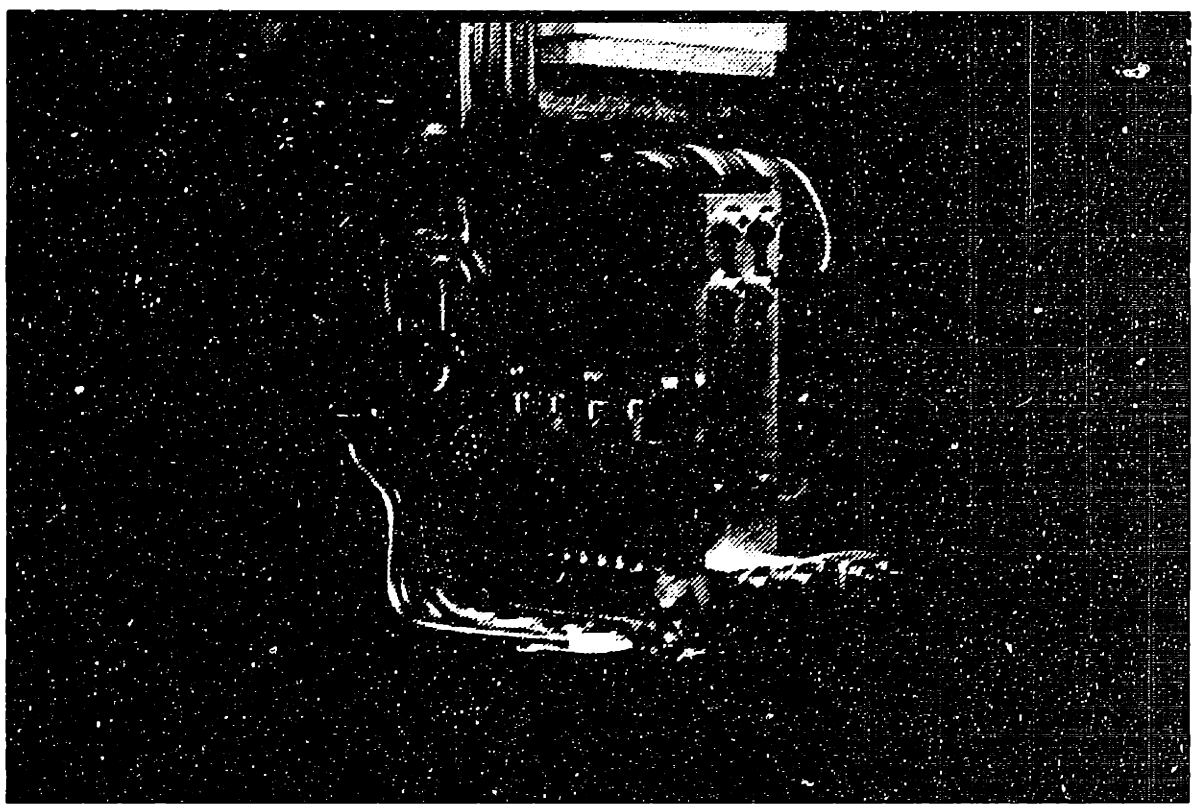

Figure 8-6: The finished Alpha multijet prior to installation.

8.3 Bracket design and Construction

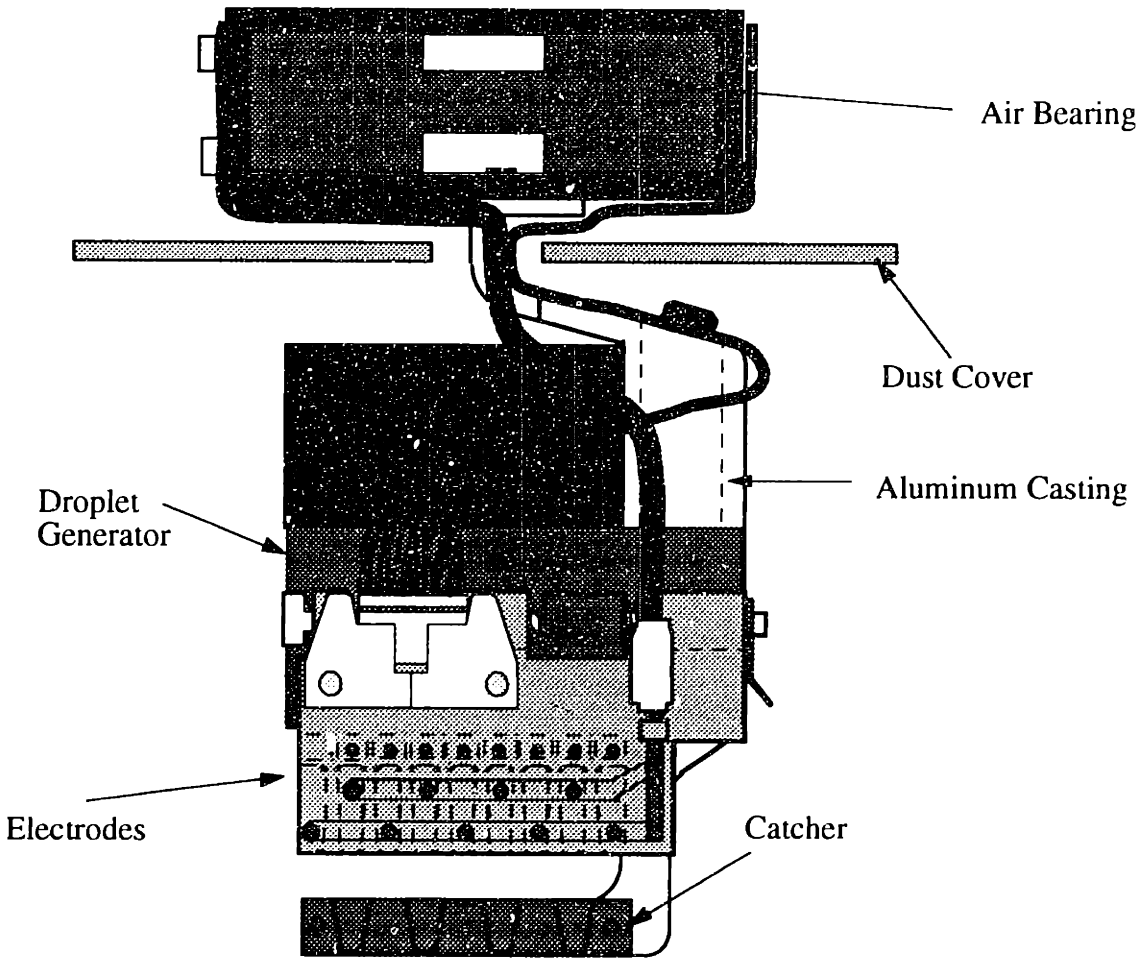

Figure 8-7: The completed printhead layout. The fast axis is oriented into the page.

The droplet generator is cantilevered off an aluminum casting. The droplet catcher bolts on an extension from the bracket at the base. Currently the position of the catcher is adjustable, but in the future it would be desirable to rigidly position it using dowel pins. This is commonly done on commercial printheads.

This complex bracket was created by Three Dimensionally Printing a ceramic mold and having an aluminum casting made at Mass Foundry. Although this casting required some tedious post machining, using the 3DP machine to make parts for itself was an excellent selling tool for the process. Figures 8-8 and 8-9 show the results of this great undertaking. At the time, this ceramic shell was the largest part ever printed on the Alpha machine. The total run length was 30 hours.

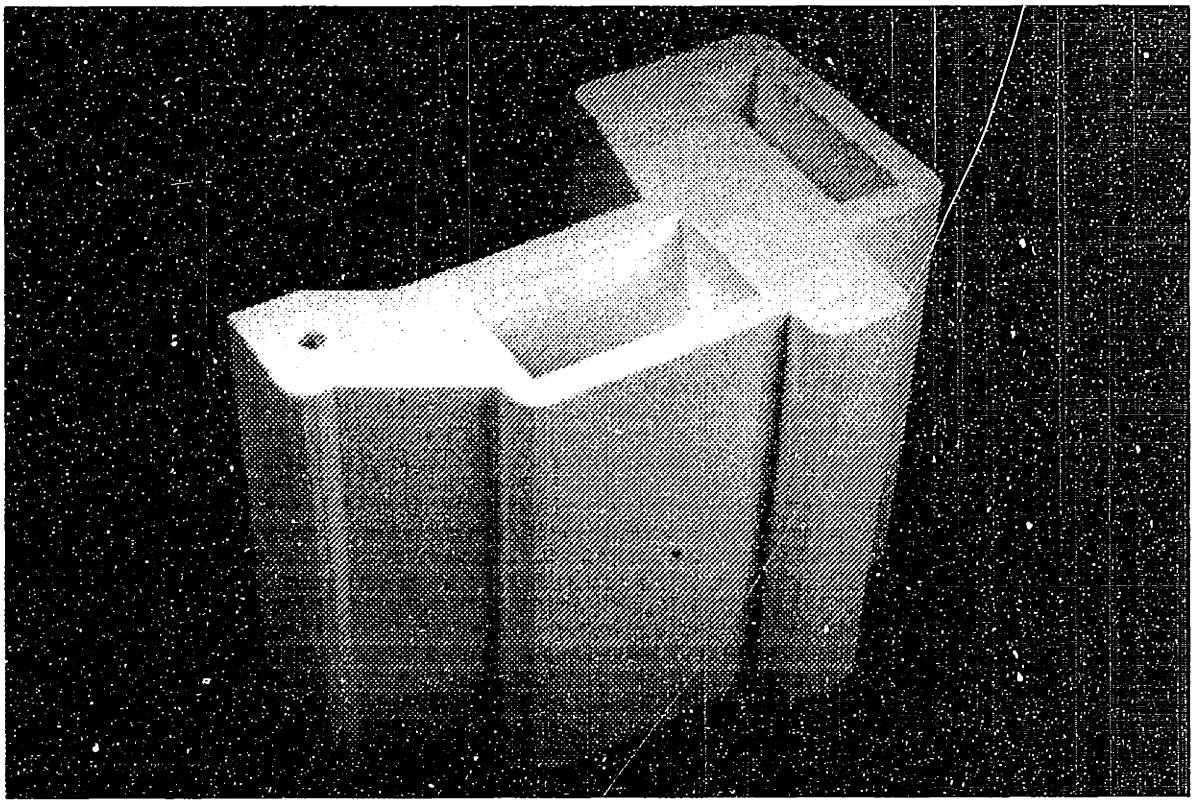

Figure 8-8: The 3DP mold used to cast the aluminum support bracket.

Figure 8-9: The aluminum bracket prior to post machining.

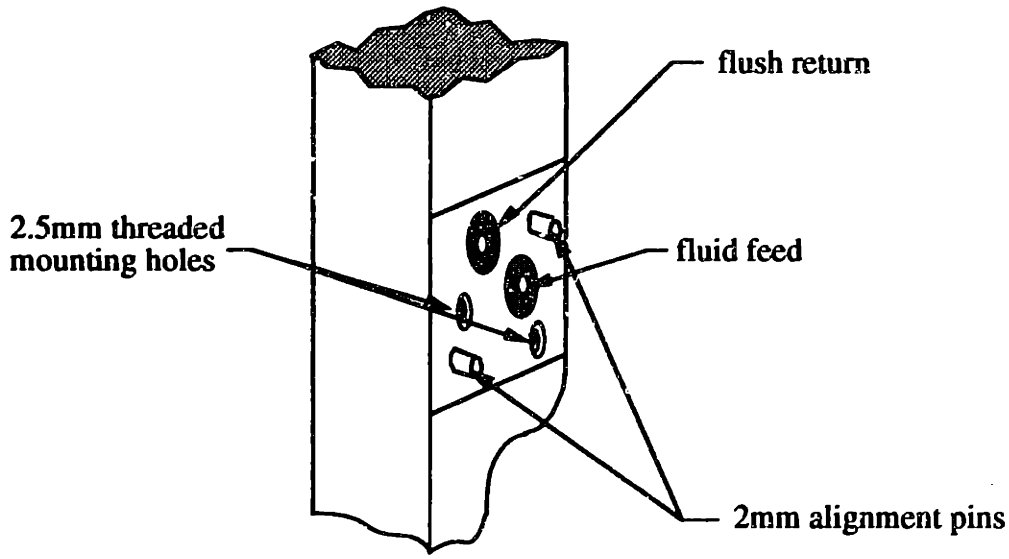

Figure 8-10: A close-up view of the droplet generator mounting scheme.

The droplet generator is mounted with two 2.5mm stainless steel bolts threaded into the aluminum casting. Two 2mm alignment pins precisely locate the droplet generator during reassembly. Fluid feed and bleed connections are made simultaneously. Delrin inserts are pressed into the casting which seal to Viton o-rings in the droplet generator.

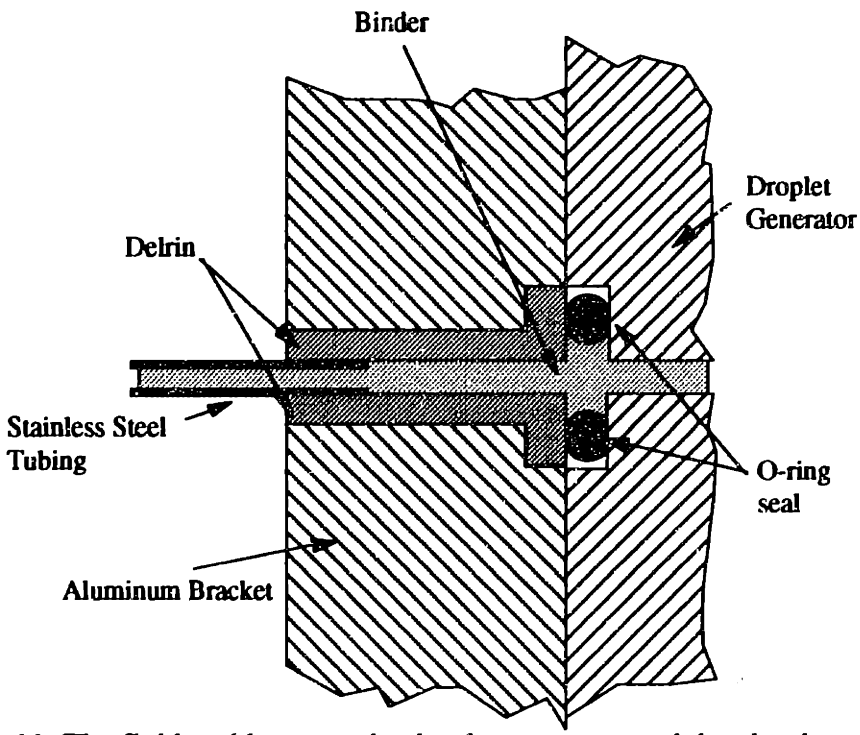

Figure 8-11: The fluid seal between the droplet generator and the aluminum support bracket. The aluminum bracket is not wetted with the jetted fluid.

Chapter 9: Fluid Systems

Fluid systems are an important peripheral for flexible, non-stop, trouble free operation. As mentioned above, it is important to run several fluids on demand as well as switch between them easily. Fluid jets must run continuously to prevent clogging. Fluid recirculation and reuse is therefore essential. This section explains important aspects of reliable fluid operation and how to construct a generic system for any application. The current Alpha machine fluid specifications will also be explored.

9.1 Fluid Pressurization and Recirculation

Initially fluid was supplied to the 3DP printheads using a pressurized canister with a pickup tube. This system was inefficient due to high helium gas consumption. In addition, for the Alpha machine it was desirable to run off a compressed air driver to eliminate constant changing of gas tanks. Helium was used due to its low solubility in binder. Dissolved air in binder accumulates in the droplet generator affecting modulation

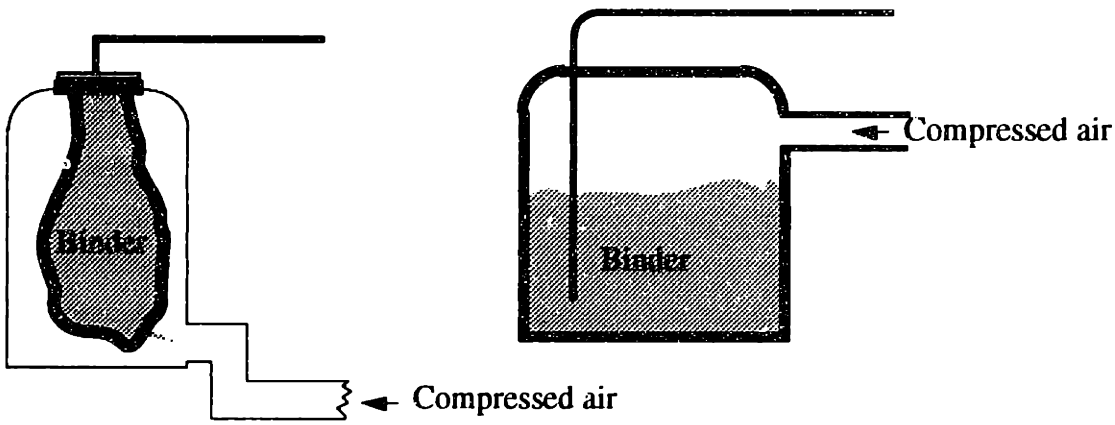

Figure 9-1: Current fluid feed procedure for the Alpha Machine is on the left. This compressed bladder technique is used for all fluids. The older method of pressurized gas direct y in contact with the fluid is shown on the right.

efficiency. In the new system jetted fluid is separated from the compressed air by an EPDM bladder. This entire assembly, intended as fluid capacitors in water based heating systems, is available off the shelf from Wessels Incorporated. They make 2 and 5 gallon containers which can be used for 3DP applications. These pressure tanks can be used with only a few modifications. These changes include installation of an air fitting on the back of the tank, a bleed valve for air removal, a fluid feed line, and a fluid return line.

While the eight jet droplet generator is running at a normal flow rate, average fluid consumption is half a liter of jetted fluid per hour. At this high consumption rate, it is necessary to recirculate all the fluids going to the printhead. A basic layout consists of the printhead draining into a second reservoir which is then pumped back into the pressure source. This reservoir contains 5/8" polypropylene balls floating on the fluid surface to reduce evaporation effects.

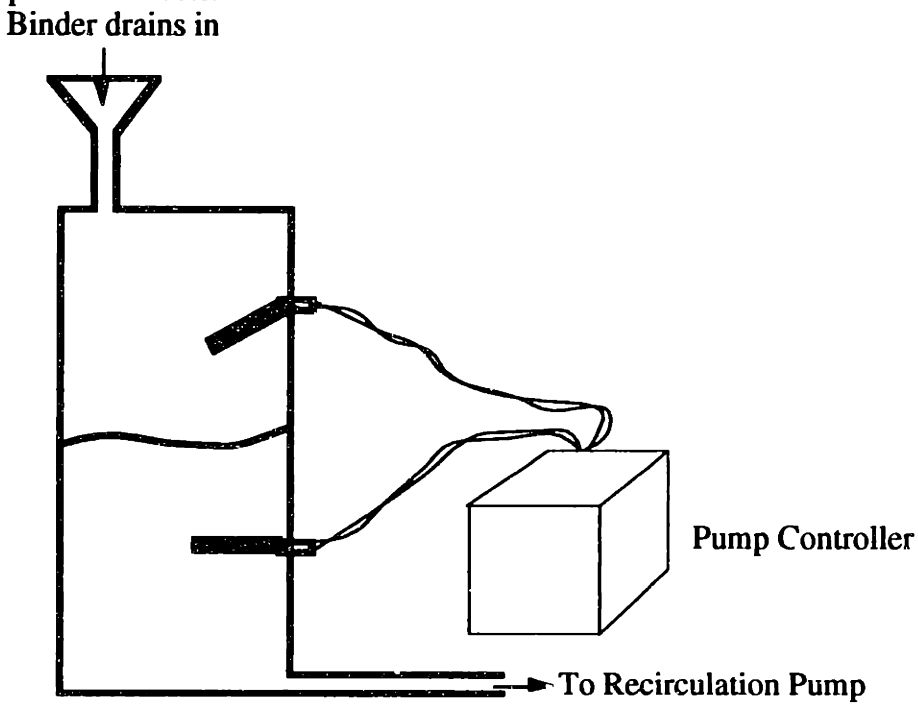

Figure 9-2 : Recirculation pump control. When the upper switch is triggered, the pump drains fluid until the lower switch is triggered. Appendix B shows the circuit schematic for the controller.

Used fluid is stored in a 1-2 gallon reservoir prior to being returned to the pressurized tank. The printhead catcher pump and the inspection system drain both vent into this reservoir. Two polypropylene magnetic reed switches sense the liquid level in the reservoir and adjust its level accordingly during printing. When the reservoir gets full, the pump removes liquid down to the lower switch. It is important to always leave some liquid in the recirculation container to prevent air from being introduced into the system.

Finding a reliable recirculation pump is a serious issue. This pump must be capable of startup under pressure load, holding back pressure, and self priming. Initially a gear pump was used on the water system with limited success. A Gorman Rupp bellows pump was used on the binder side. This pump ran for a few months before developing punctures in the bellow assembly and in one case a failed diaphragm assembly. Finally all the Alpha machine pumps were switched to ShurFlo diaphragm pumps.

This remarkable pump comes in many mechanical specifications and wetted materials. The pump used throughout the machine is a Viton-polypropylene 1.2 GPM model with a 50 psi cut out valve. This workhorse has performed beautifully under all machine conditions without a single failure. In addition, when running, these units are very quiet. To date silica binder, high pH cleaner, and Acrysol have run through these pumps.

As an aside note, an almost equally useful pump family is the NF10 and KNF30 from KNF Neuberger Industries. These low flowrate diaphragm pumps (100 and 300 cc/min) are self priming air/fluid handling pumps with limited pressure capability. These pumps are quiet, efficient and also come in a variety of wetted materials.

9-2 Filtering

Filtering has been an area of enormous progress during the development of the multiple nozzle printhead. This section will discuss details of filtering troublesome binders. Of the current family of 3DP binders the most developed is the colloidal silica system used for printing ceramic shells. This binder contains 17.5% (by volume) 100nm colloidal silica, glycol and mostly water (see J.Bredt Ph.D. thesis 1994). Unfortunately mixing this binder causes substantial micro gelling that will destroy filters with a low surface area. For single jet printing a well clogged capsule filter was still sufficient to get 1.2cc/min flowrate. Unfortunately at higher flow rates a higher surface area filter was essential. Initially filter clogging problems were solved by simply increasing the filter area by a factor of six. The improved filter design is a 10" 222 double o-ring filter seal available from Ametek. This double configuration o-ring design still leaks, however, necessitating the use of a 2.5" sealed Capsule down stream from the 10" bulk filtering. Originally a 5μm and a 1μm filter was used, but later it was found that a single 1μm 10" filter was adequate to handle the loading of silica.

Several other observations should also be noted about filtering behavior of silica binder. After mixing binder for printing, micro gel forms in the solution which causes heavy loading of the filter assemblies. Once this micro-gel is removed, the binder can then be used with smaller filters. In addition, after mixing and prefiltering, the binder is very stable and it is unlikely any additional filter problems will occur. After the micro gel instabilities have been removed, the pressure drop across the filters decreases by about 20% irrespective of accumulated loading on the filter. Filtering off line before placing the binder in the printer, along with 1 and 1.2 μm filtering on the actual 3DP machine is highly recommended. To date this procedure only applies to the silica and possibly slurry binders. Other binders such as Acrysol filter very easily with simply 2.5" Capsule filters.

Micro-jelling binders also cause filters of larger pore size down stream from fine filters to clog. Reagglomeration of jelled particles after they extrude through fine filtration is one possible explanation. The result is a partially clogged filter down stream of bulk (10") filtration. After the fully filtered binder passes through the switching valves its an excellent idea to filter at the printhead to catch particles that have built up within the valves and can clog the printhead. The current preferred filter for this application is a 1" Solex polypropylene/polyethylene filter. This small 'last chance' filter rides on the fast axis carriage. To prevent hydrolysis, materials such as Nylon should be avoided for filtration. Whenever possible all polypropylene or polyethylene filters should be used.

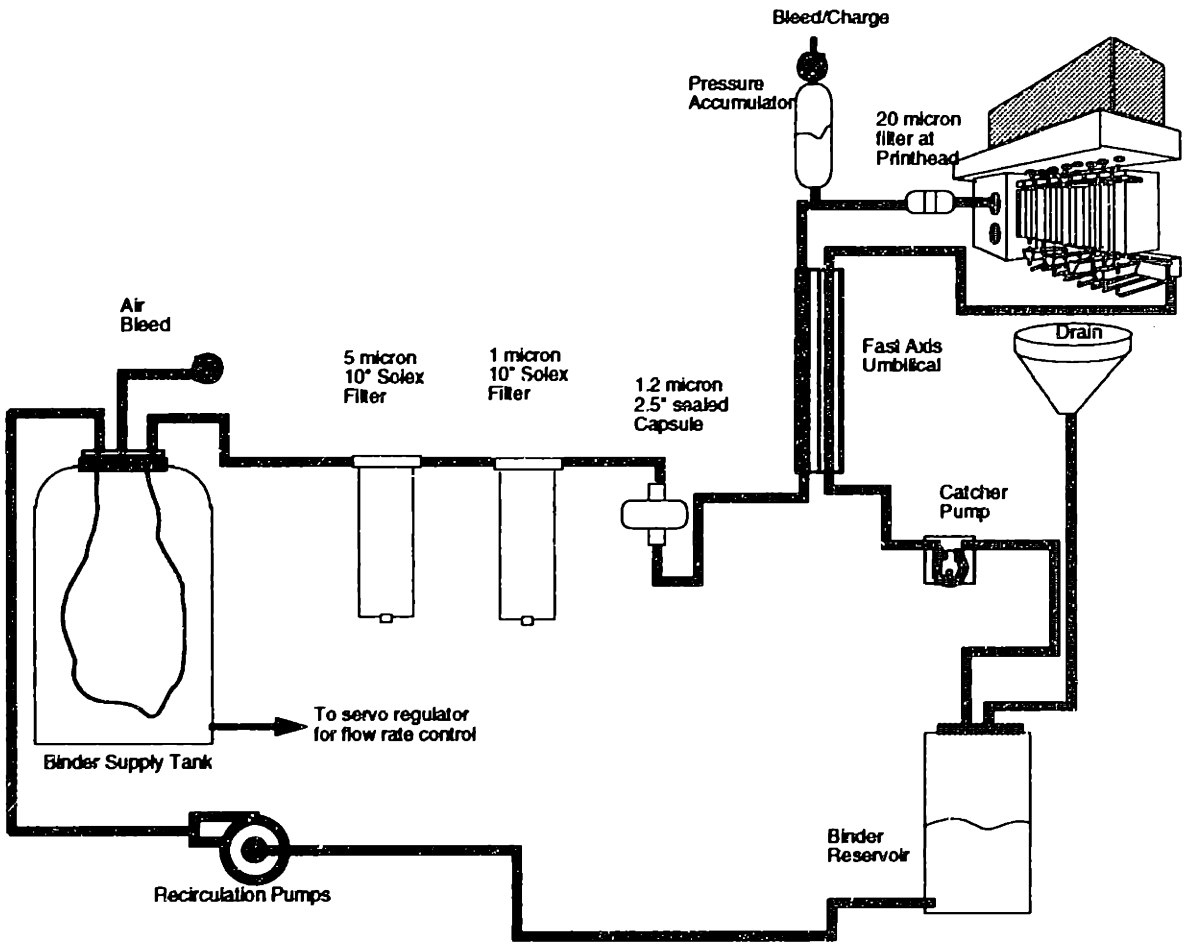

Figure 9-3: The Silica/cleaner fluid system for the Alpha machine. Note the heavy filtration required for typical slurry/colloidal suspension feed systems.

9-3 Fluid Spike Damping

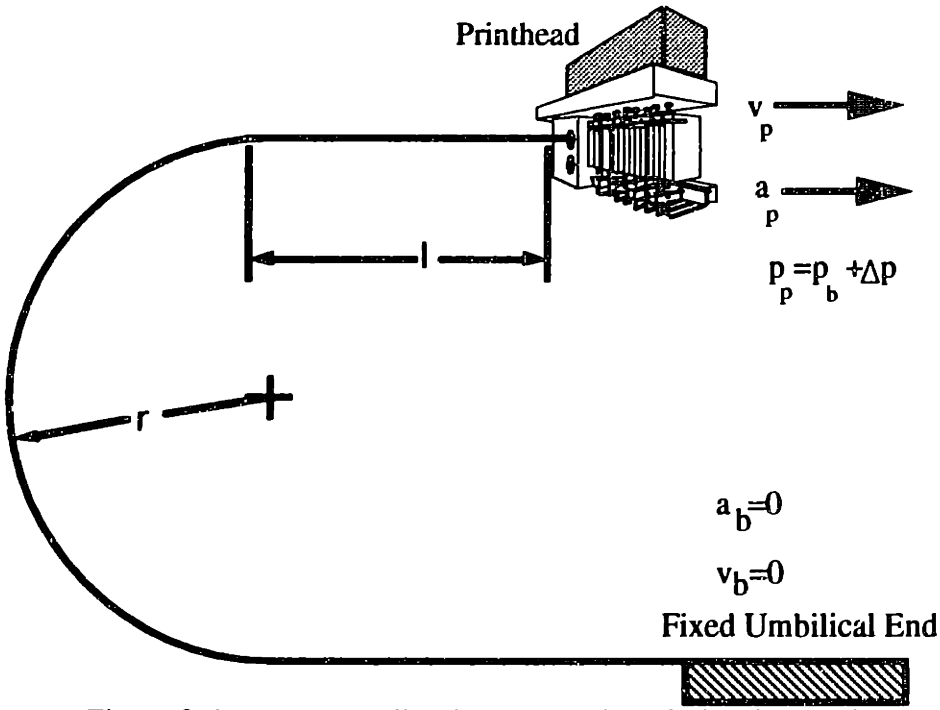

Figure 9-4 : Pressure spikes induced at the printhead caused from its motion along the fast axis.

Due to the high turn around accelerations of the fast axis and the constant rolling and unrolling of the fluid umbilical, pressure spikes are created at the printhead. These spikes have been measured by Soligen to be as great as 1.5 psi. Using momentum theory these fluid spikes can be estimated numerically.

Drawing a control volume as shown if Figure 9-5 below, the momentum flux can be calculated in the following manner:

$$\vec{M} = \int_A \rho \vec{V}\left(\vec{V}_r \cdot \hat{n}\right) dA \qquad 9\text{-}1$$

Where n is the unit normal vector pointing out of the control volume. This momentum equation can be used to calculate pressure as shown in equation 9-2.

$$\frac{d\vec{M}_{sys}}{dt} = \vec{F}_{sys} = \Delta p(A) \qquad 9\text{-}2$$

It is easiest to begin with the constant (during actual printing) velocity case. In this case, a pressure spike is created from rolling/unrolling of the umbilical as it accelerates to the printhead velocity from rest.

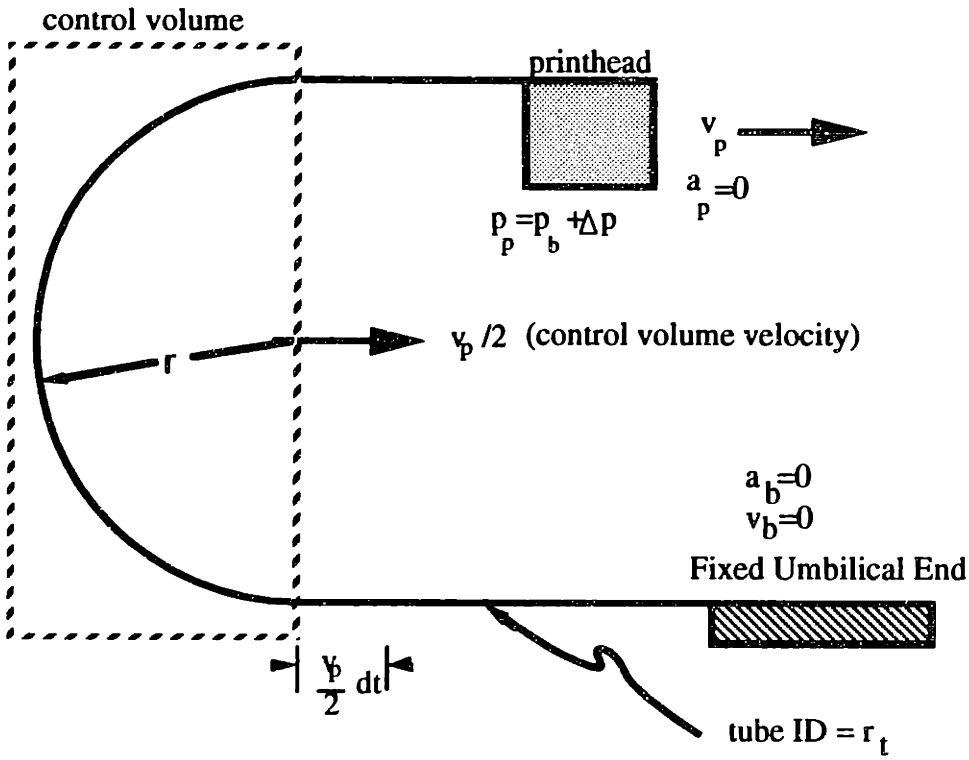

Figure 9-5: Using momentum theory to calculate pressure spikes at the printhead for the zero acceleration case.

Combining equations 9-1 and 9-2 and substituting values, assuming a infinitesimal piece of tubing $(V_p/2)dt$ enters the control volume at $-V_p/2$ velocity and exits at velocity $+V_p/2$ as shown in Figure 9-5, produces the following expression.

$$\frac{d}{dt}\left[\left(\pi\, r_t^2 \rho_l V_p\right)\left(\frac{V_p}{2}dt\right)\right] = dp\left(\pi\, r_t^2\right) \qquad 9\text{-}3$$

Equation 9-3 simplifies (for the zero printhead acceleration case) to:

$$\Delta p = \rho_l\left(\frac{V_p^2}{2}\right) \qquad 9\text{-}4$$

Now when the printhead is accelerating, an additional pressure spike is created from accelerating the straight portion of tubing (length l) and the bend radius half circumference.

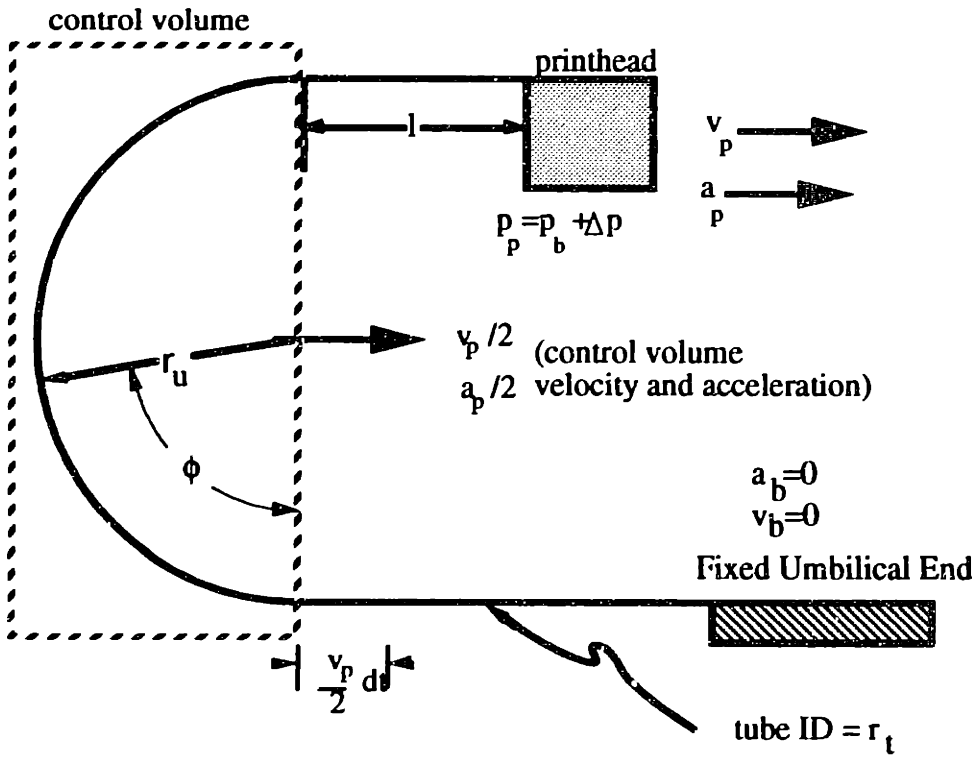

Figure 9-6: Pressure spikes induced at the printhead from turn around acceleration.

For the case when the printhead is accelerating the induced pressure can be broken down into three components.

$$\begin{array}{l}\text{total}\\ \text{induced}\\ \text{pressure}\end{array} = \begin{array}{l}\text{constant velocity}\\ \text{equation 9-4}\end{array} + \begin{array}{l}\text{accelerating}\\ \text{length of tubing}\\ \text{at printhead, l}\end{array} + \begin{array}{l}\text{accelerating portion}\\ \text{of tubing in umbilical}\\ \text{bend radius}\end{array} \qquad 9\text{-}5$$

The second term of equation 9-5 can be obtained,

$$(\rho_l l \pi r_t^2)(a_p) = \Delta p(\pi r_t^2) \qquad 9\text{-}6$$

and simplified to:

$$\Delta p = \rho_l l(a_p) \qquad 9\text{-}7$$

The acceleration in the bend radius changes along its circumference. At the fixed end, the acceleration is zero; however, at the printhead end, the acceleration is a_p. The acceleration along the bend radius can then be expressed in terms of ϕ.

$$a_b = \left(\frac{a_p}{2}\right)(1-\cos\phi);\left[\phi = 0 \rightarrow a_b = 0; \phi = \pi \rightarrow a_b = a_p\right] \qquad 9\text{-}8$$

Integrating this acceleration around the bend radius and applying once again momentum theory the following force balance is obtained:

$$(\rho_l \pi r_t^2)\int_0^{\pi} a_b(\phi) r_u d\phi = (\rho_l \pi r_t^2)\int_0^{\pi}\left(\frac{a_p}{2}\right)(1-\cos\phi) r_u d\phi = \Delta p \pi r_t^2 \qquad 9\text{-}9$$

Evaluating the integral and simplifying it produces the third term in equation 9-5.

$$\left(\rho_l \pi r_t^2\right)\left(\frac{a_p}{2}\right)(\phi - \sin\phi) r_u \Big|_0^{\pi} = \left(\rho_l \pi r_t^2\right)\left(\pi r_u \frac{a_p}{2}\right) = \Delta p \pi r_t^2 \rightarrow \Delta p = \left(\pi r_u \frac{a_p}{2}\right)\rho_l \quad 9\text{-}10$$

Substituting equations 9-4, 9-7, and 9-10 into equation 9-5 yields the following expression for the induced pressure spike at the printhead from its velocity and acceleration.

$$\Delta p = \rho\left[\frac{v_p^{\,2}}{2} + a_p\left(1 + \frac{\pi r_u}{2}\right)\right] \quad 9\text{-}11$$

Equation 9-11 holds only when the printhead is moving right and accelerating to the right. The other three cases are summarized as follows:

Moving right and decelerating:

$$\Delta p = \rho\left[\frac{v_p^{\,2}}{2} - a_p\left(1 + \frac{\pi r_u}{2}\right)\right] \quad 9\text{-}12$$

Moving left and accelerating:

$$\Delta p = \rho\left[-\frac{v_p^{\,2}}{2} - a_p\left(1 + \frac{\pi r_u}{2}\right)\right] \quad 9\text{-}13$$

Moving left and decelerating:

$$\Delta p = \rho\left[-\frac{v_p^{\,2}}{2} + a_p\left(1 + \frac{\pi r_u}{2}\right)\right] \quad 9\text{-}14$$

Figure 9-7 shows a numerical iteration for one round trip pass of the printhead. It is interesting to note the steady state pressure difference created when the printhead travels at a constant velocity.

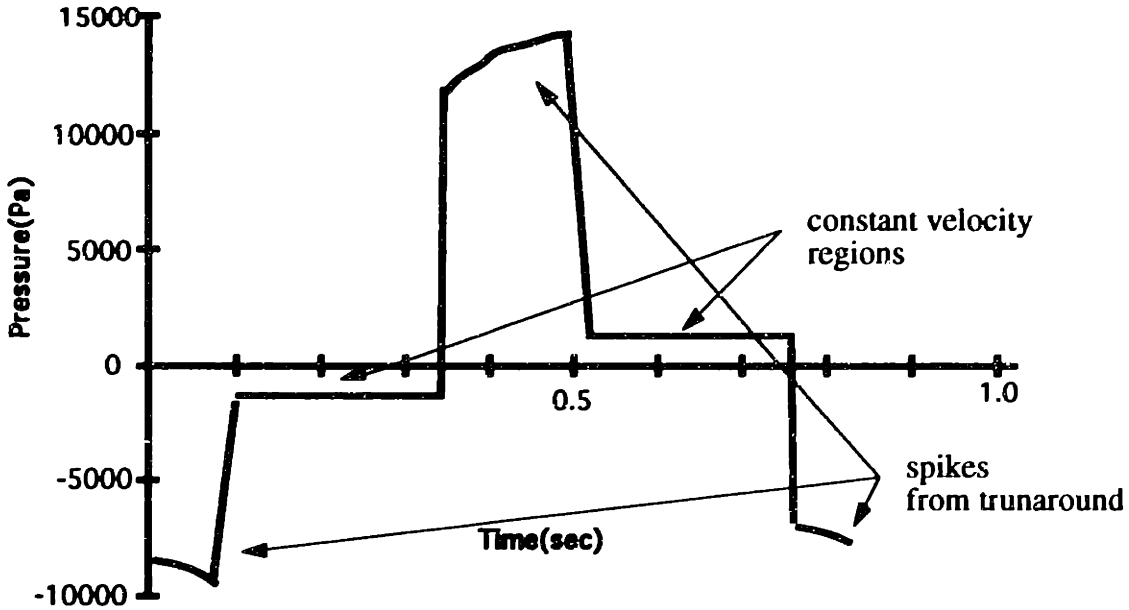

Figure 9-7: Estimating pressure spikes based on momentum theory. The numerical iteration was performed by Prof. Ely Sachs.

When operating at low feed pressures (25psi) these spikes can be a serious problem. They result in a failure mode of buildup in the deflection cell. Commercial inkjet makers using a gear pump fluid feed system with a spring-diaphragm fluid capacitor to damp out pressure spikes at the printhead.

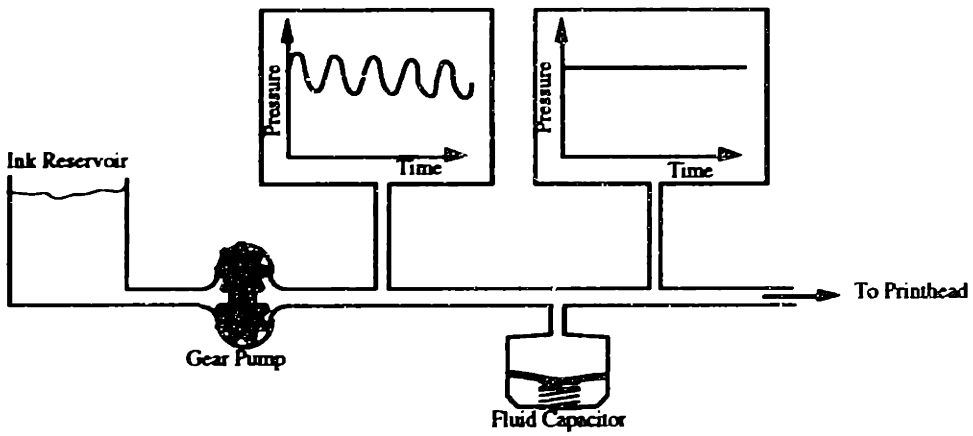

Figure 9-8: A typical spring diaphragm fluid capacitor used to smooth pressure spikes in commercial printheads.

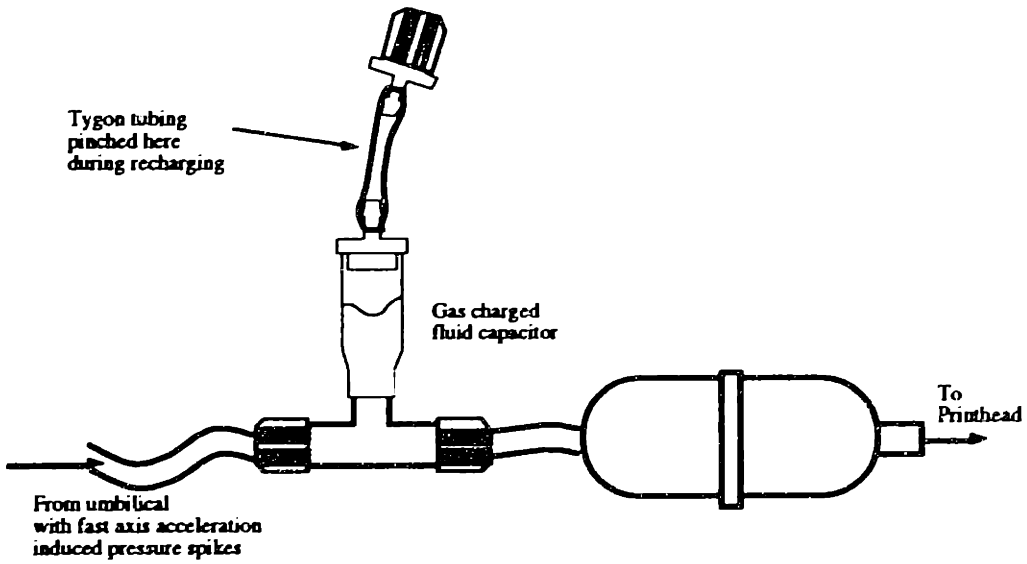

Figure 9-9: The accumulator created to smooth pressure spikes on the Alpha machine.

Due to size and weight considerations on the printhead carriage an air charged accumulator was used to dampen fluid spikes. Ideally this accumulator would be charged with helium to reduce the rate at which the gas spring dissolves into the binder. To further reduce fluid spikes at the droplet generator, during printing the fluid return line should be pinched off. This eliminates two identical pressure waves traveling down the umbilical and

meeting at the printhead doubling the effects calculated in Figure 9-5. At higher feed pressures, 35-45 psi, fluid spikes are less of an issue. Currently with binder pressures of 40 psi on the Alpha machine, effects from pressure spikes have been greatly reduced.

Chapter 10: Summary, Conclusions, and Future Work

10.1 Executive Summary

Three Dimensional Printing is a rapid prototyping process used to fabricate functional parts and tooling directly from CAD models. Parts are created a layer at a time by selectively joining dry powder with binder. The binder is applied with a printhead which charges and deflects droplets for accurate positioning of binder in the cross section of the part. When the jet is desired to be 'shut off' it is deflected into a catcher, or gutter. To enhance 3DP's usefulness in the marketplace, it is necessary to prove its ability to build parts accurately and quickly. Part production rate can be increased by using many nozzles to apply binder. Hence, development of a multiple nozzle printhead was required for advancement of the 3DP process.

The printhead had to have low mass, an approximate 1" flight path, proportional deflection, low (0.9-1.2cc/min) flowrate, compatibility with a variety of binders, and robustness to high accelerations. Commercially available units could not satisfy all of these requirements simultaneously. A completely new design was needed to achieve these unique requirements.

Functional requirements are listed in Figure 10-1 and correlated to the printhead's specific design parameters.

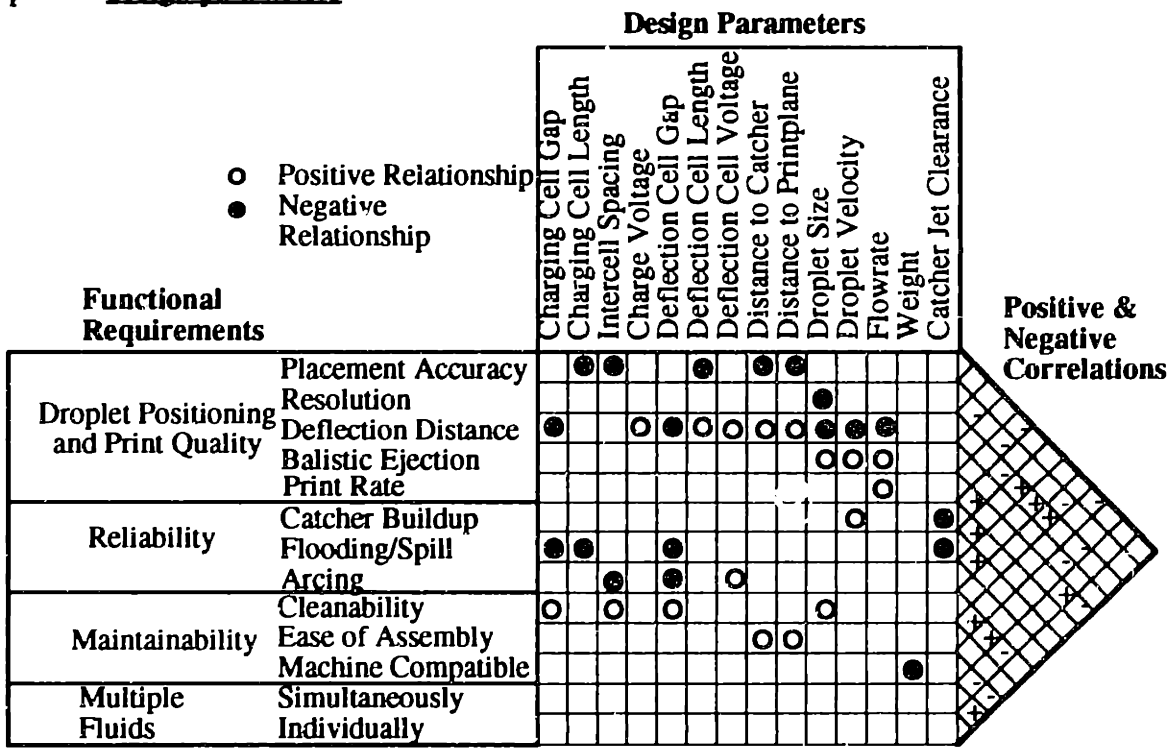

Figure 10-1: Printhead design matrix relating functional requirements to design parameters.

The following is a brief list explaining the positive and negative correlations between the printhead's functional requirements and design parameters.

- Any increase in the length of the droplet flight path is detrimental to droplet **placement accuracy.**
- Printhead **resolution** is inversely proportional to the droplet size. The smaller the droplet the greater the number of droplets that can be placed per inch, thus increasing the resolution of the printhead.
- The single most critical aspect relating to both performance and reliability is **deflection distance**. Decreasing the charge cell gap increases the cell capacitance with the fluid jet and hence, the induced charge on a droplet. This effect dramatically increases the amount of deflection. Induced charge on a droplet increases linearly with applied charge cell voltage. Widening the deflection cell gap decreases its electric field, reducing the droplet's lateral acceleration, and net deflection. If the deflection cell is longer for a given droplet velocity, the drop will experience acceleration for a prolonged period of time, causing deflection distance to increase. At a greater deflection cell voltage, the electric field increases, causing higher acceleration and hence more deflection of charged droplets. Large distances between the deflection cell and the catcher allows the droplet more time to move laterally, increasing its deflection. Proportional deflection distance can be increased by allowing the droplet to fly farther to the print plane after the droplet passes the catcher. Larger droplets have lower surface area to volume ratios. This will decrease its induced charge to mass ratio. The faster a droplet flies, the less time it spends accelerating laterally in the deflection field, reducing its lateral velocity. The result is a strong negative correlation between droplet deflection and velocity. For a fixed orifice diameter, an increase in flow rate reduces deflection due to an increase in droplet velocity. If the orifice diameter is expanded to allow a constant jet velocity at an increased flowrate, deflection will also decrease due to the larger droplet size, as mentioned above.
- **Ballistic powder ejection** increases with both droplet size and velocity. One or both of these droplet characteristics is affected by an increase in flowrate.
- Increasing the flowrate allows the printhead to scan the powder bed faster while maintaining the same amount of binder per unit part volume. The result is a faster **print rate.**

- Higher jet velocities cause splashing of binder in the catcher, which results in buildup. To prevent external **catcher buildup** a minimal amount of undeflected jet clearance is required.
- Electrode **flooding** can be prevented by increasing the jet clearance to several critical components. This is accomplished by widening the charge and deflection cells. A shorter charge cell further reduces the chances of flooding if the jet is crooked.
- **Arcing** can occur in several places within the electrode assembly. This can be prevented by keeping the electric field strength below 60% of spontaneous breakdown in air. This is accomplished by widening the deflection cell and the charge-deflection cell spacing. Reducing the applied voltage also decreases the electric field, and hence arcing.
- The printhead will be **easier to clean** if the spacing between electrodes is large. Wide charge and deflection cells facilitate cleaning. Smaller drops imply a smaller fluid orifice increasing problems with cleaning and clogging.
- The printhead will be easier to **assemble** and **maintain** if the catcher and print plane clearances are substantial.
- A light printhead will be easier to accelerate above the powder bed, making it more **compatible** with 3DP machines.

Interactions between functional requirements are also important to identify potential design conflicts. This information is conveyed in the triangular portion at the right of Figure 10-1 with plus and minus signs. Shortening the flight path to increase placement accuracy reduces the amount of droplet deflection. Resolution will be adversely affected if printhead geometry is enlarged to facilitate cleaning. In addition, a smaller more compact design with a shorter flight path, will make assembly and maintenance more difficult. Multiple jet printing increases build rate, but affects droplet placement accuracy (partly because of stitching between jets) without on-line droplet placement measurement. Small droplets increase resolution, but reduce printhead flow rate and build rate. More jets per droplet catcher, increases catcher buildup. If droplets are not deflected far enough into catch more buildup will occur. Catcher buildup will cause binder spilling, if the deflection distance is reduced. Large amounts of droplet deflection will cause arcing, if droplets graze or collide with the high voltage plates. When the high voltage plates flood, electrical arcing is always present. A printhead with a long flight path and lots of deflection (similar to commercial units), will in general, be more awkward to package on a 3DP machine. Significant powder buildup will occur on the high voltage plates of the printhead if ballistic ejection is significant. Printing multiple fluids simultaneously will require more passes of

the printhead over the powder bed to locally deposit each fluid, adversely affecting print rate. Printing multiple fluids requires more complex fluid handling equipment decreasing 3DP machine compatibility. These engineering constraints strongly influence the design of the printhead.

The design of the eight jet printhead for the MIT machine occurred in a discrete sequential manner. Droplet generator design occurred first to establish droplet size, velocity, and breakup frequency for the deflection calculations. Deflection calculations were then used in the design and construction of the deflection electrodes. The droplet catcher was then configured to function without spilling or buildup using the predetermined droplet deflection. Finally each of these subassemblies was then packaged into a printhead. Figure 3-3 further outlines this timeline for designing 3DP printheads.

Jet position and droplet breakup tests were performed with three commercial droplet generators. Modifications were made to the most promising, the Domino Jet Array, in order to achieve reliable and repeatable droplet formation with 3DP binders.

Guidelines were established for designing the charge cell to produce uniform, substantial droplet charging while preventing floods, arcs, or alignment problems. Providing clearance for the jet during deflection in the deflection cell was discussed, as was rounding the cell wall edges to prevent arcing within the electrode assembly. Calculations were then performed to establish amounts of deflection needed to allow the printhead to meet its proportional deflection and reliability requirements. Additional droplet deflection was required to allow proportional deflection, prevent external catcher buildup, and allow internal catcher buildup without binder spillage. Deflection calculations were used in conjunction with these additional guidelines to freeze the design of the droplet deflection electrode geometry.

Constructing the droplet deflection electrodes to exacting design parameters was the next challenge. To ensure a lightweight design, electrodes were constructed by chrome plating a carefully machined ABS plastic substrate. This plating was then selectively removed to isolate the high voltage plates and individual charging cells. Electrical connections to the plated surfaces were made using stainless steel pins pressed into the ABS block prior to plating. On the electrode side of the block, the chrome plating made the connection to the pins. The wiring to the individual electrodes was placed behind the block on the opposite end of the pins. This procedure completed the construction of the deflection assembly.

Once the droplets were deflected it was important to catch them without spillage or significant dried binder buildup. Different designs were constructed out of stainless steel to

test fabrication feasibility of the thin catcher walls. After initial prototypes were machined, testing began on the printhead. The final design uses one catcher per two jets for a total of four catchers on the eight jet head. This catcher had tapered internal pockets to allow efficient binder removal with minimal buildup. In addition, the final design is robust to the constant scraping required to remove dried binder without loss of the catcher's critical dimensions. The fluid is removed from these catchers with a four head peristaltic pump.

The droplet generator, catcher and droplet deflection electrode assembly were packaged to work as a complete printhead on the 3DP Alpha machine. The complex and lightweight printhead support structure was cast in aluminum from a 3DP ceramic shell. This aided in building a printhead chassis that was rigid, low in mass, and precise.

A fluid system to support the needs of a multijet printhead was also constructed. The system automatically recirculates unprinted fluid back to a pressurized reservoir. This system also provides the printhead with a constant pressure irrespective of pressure spikes created from the velocity and acceleration of the printhead.

This work documents the design of an electrostatic multijet printhead and a useful methodology for designing future printheads to meet the ever-growing needs of Three Dimensional Printing. This design methodology is applicable to changes in droplet flight path, deflection requirements, drop size, drop velocity, and flow rate. Calculations relating to droplet deflection are also encompassed in a Microsoft Excel spreadsheet showing droplet flight trajectory for an arbitrary printhead geometry.

10.2 Printhead Development Progress

The multijet printhead is currently printing large parts in short periods of time on the 3DP Alpha machine. It has been a grueling development period to get the entire system to run reliably. Unfortunately many seemingly trivial details in the development of the multijet printhead took several time consuming iterations before converging on a workable solution. Extremely large parts made of both metal and ceramic that would have been extremely (40 hour) long runs with one jet have been printed easily with eight jets. The longest print period thus far without intervention is eight hours during a ceramic part build. To date, the development work has been successful; however, there are still more enhancements to be made in fluids, droplet generators, and electronics.

10.3 Future Work

In the short term there will be a redesign of the fluid system to accommodate many different fluids. This new system will have separate modules which will slide into a larger frame structure. The pressurized bladders will be disposable and each compact system will run and recirculate on as little as 1000cc. It will also be easier to remove, disassemble, and clean each system after use. This new system will accommodate the ever-increasing need to try different material systems.

In conjunction with new fluid systems, a different droplet generator capable of jetting two different fluids at once is being developed. This change would require the insertion of a plug into the longitudinal fluid channel in the Domino droplet generator and a second fluid fitting added as shown in Figure 10-1. This modification to the existing droplet generator in conjunction with the four separate catchers currently in use on the Alpha machine would make it virtually effortless to jet different fluids simultaneously.

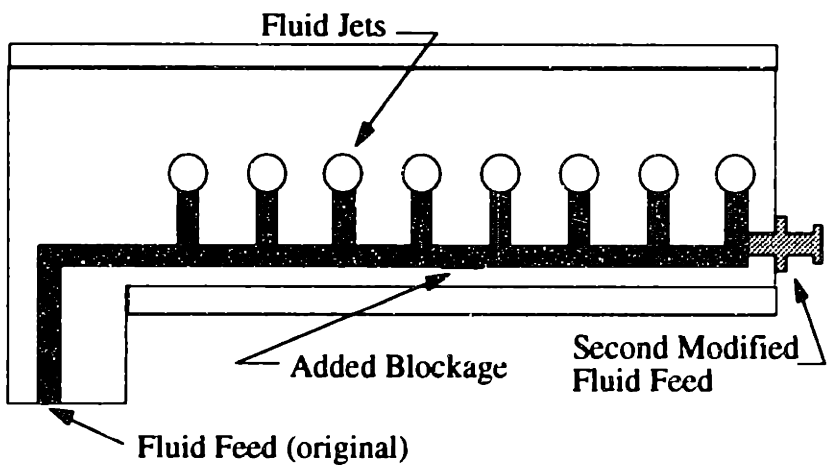

Figure 10-2: A proposed method for achieving multiple fluid operation using a Domino droplet generator.

Multiple fluid printing will eventually be accompanied by some minor changes in the current deflection electrode design. This new design will incorporate a plated integral edge connector. This connector would replace the current system, which uses stainless steel pins plated into the ABS block. This would greatly simplify the electrode construction. The electrode mounting hinge will also undergo some redesign. An alternate design would be easier to remove for maintenance and cleaning. Some work is currently being done on the concept of using two steel balls for location, while allowing the assembly to swing into place during startup and shutdown.

A longer term project in printhead design is reducing the flight path of the droplets from breakoff to the print plane. This would increase the accuracy of the machine by reducing the effects of aerodynamic drag. This printhead would be a hybrid design similar to a single sided printhead, but configured like a two sided deflection cell as previously described. Currently the lead drop merges before hitting the powder bed. A shorter printhead would possibly help prevent this.

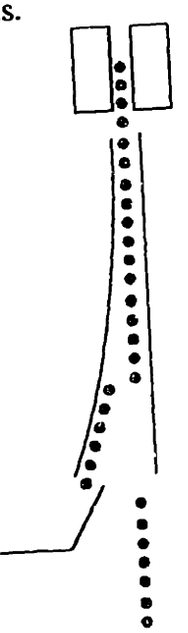

Figure 10-3: Possible positioning electrode improvements used to shorten the flight path.

This design is very similar to the current design, but in order to increase the deflection the droplets fly close to the deflection cell wall, increasing their deflected acceleration, allowing the printhead to have a shorter flight path. Alignment and flooding will be serious issues that must be addressed for this design to be successful.

References

Abel, Godard, "Characterization of Droplet Flight Path and Mass Flux in Droplet-Based Manufacturing", MIT masters thesis, May 1994.

Brancazio, David, "Development of a Robust Electrically Deflecting Printhead for Three Dimensional Printing," MIT, Master's Thesis, May 1991.

Bredt, Jim,"Binder Stability and Powder\Binder Interaction in Three Dimensional Printing", MIT PhD thesis January 1995.

Bredt, Jim, "Physics of Our Printhead," Three Dimensional Printing group literature, April 1993.

Clausing, Don, "Total Quality Development, the Development of Competitive New Products", 1993, MIT.

"Domino JetArray ink jet printer operator's manual" Issue 3.0, Domino Amjet, March 1993.

Fillmore, G.L., W.L. Buehner, and D.L. West. 1977. "Drop Charging and Deflection in an Electrostatic Ink Jet Printer." IBM J. Res. Develop. (January 1977): 37-47.

Horowitz, P. and Hill, Winfred, The Art of Electronics, Cambridge University Press, NY 1989.

Lienhard, John H. 1987. A Heat Transfer Textbook. Prentice Hall Inc., Englewood Cliffs, N.J.

Milner, Jill, "Time of Flight Controller and Stream Position Compensation System for Three Dimensional Printing Process," MIT, Master's Thesis, May 1993.

Modern Plastics Encylopedia, Mc Graw-Hill Inc., New York, October 1983.

Ohanian, Hans C., Physics, WW Norton & Company, New York, 1985.

Pimbley, W.T. and Lee, H.C. 1977. "Satellite Droplet Formation in a Liquid Jet." IBM J. Res. Develop. (January 1977): pp21-30.

Suh, N., Chryssolouris, G., Gutoxski, T., Sachs, E., Cook, N. 1990, "Manufacturing Engineering: Part I Macro-View of Manufacturing", MIT, pp 6-1 to 6-6.

White, Frank M., Fluid Mechanics, McGraw-Hill, New York 1979.

Williams, Paul, "Thrre Dimensional Printing: A new Process to Fabricate Prototypes Directly from CAD Models," M.I.T. Master's Thesis, May 1990.

Appendix A: Machine Drawings

Printhead machine parts List:

Droplet Deflection Electrodes

Connector pins

Lexan Bar

Delrin Inserts

Casting Print

Catcher

Web Spacer plate

Fast axis shims

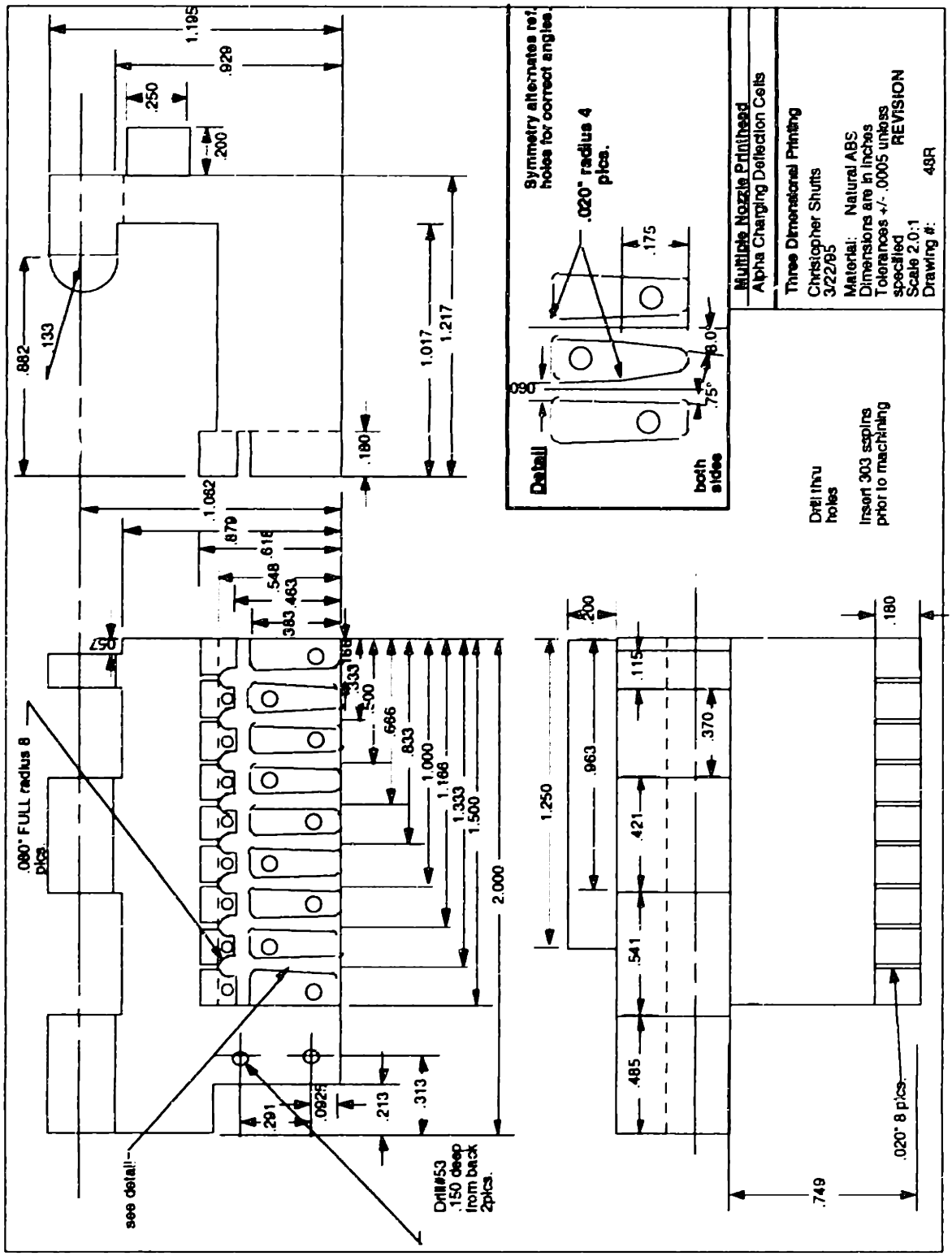
Multiple Nozzle Printhead
Alpha Charging Deflection Cells
Three Dimensional Printing
Christopher Shutts
3/22/95
Material: Natural ABS
Dimensions are in inches
Tolerances +/- .0005 unless specified
Scale 2.0:1
Drawing #: 48R
REVISION
Symmetry alternates ref. holes for correct angles.
.020" radius 4 plcs.
Deball
both sides
Drill thru holes
Insert 303 saplns prior to machining
.080" FULL radius 8 plcs.
see detail
Drill #53 .150 deep from back 2plcs.
.020" 8 plcs.

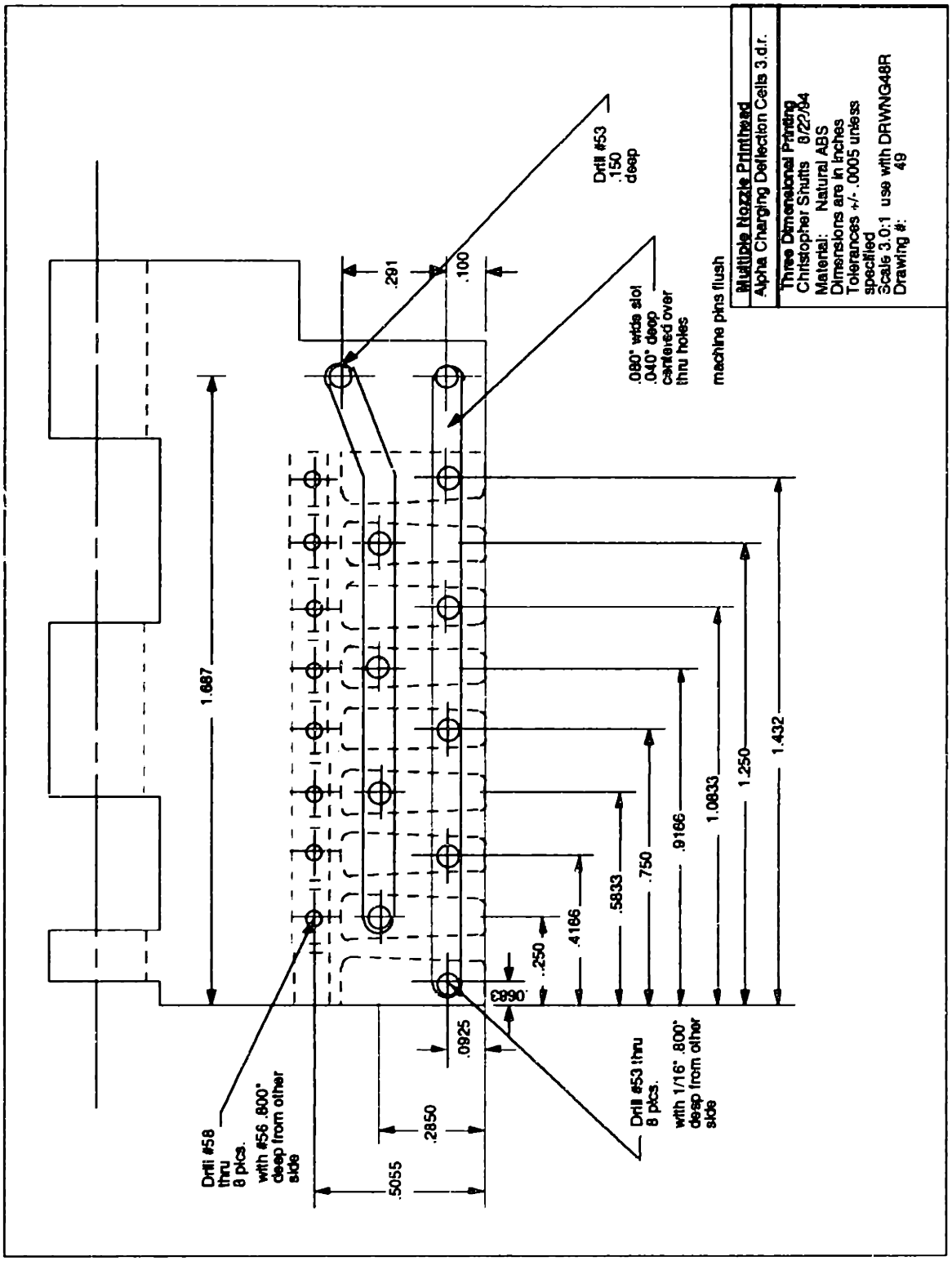
Multiple Nozzle Printhead
Alpha Charging Deflection Cells 3.d.r.
Three Dimensional Printing
Christopher Shutts 8/22/94
Material: Natural ABS
Dimensions are in inches
Tolerances +/- .0005 unless specified
Scale 3.0:1 use with DRWNG48R
Drawing #: 49
machine pins flush
Drill #53 .150 deep
.080" wide slot .040" deep centered over thru holes
.291
.100
1.687
1.432
1.250
1.0833
.9166
.750
.5833
.4166
.250
.2890
.0925
.2850
.5055
Drill #58 thru 8 pcs. with #56 .800" deep from other side
Drill #53 thru 8 pcs. with 1/16" .800" deep from other side

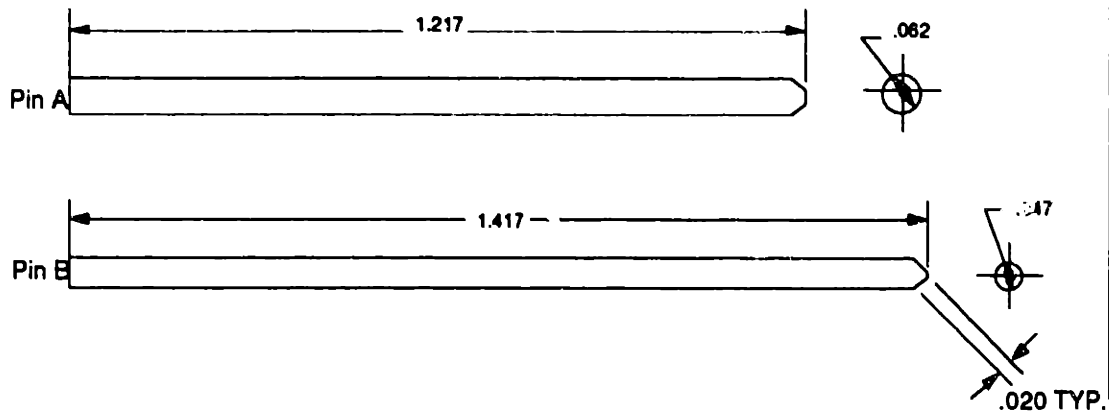

Detail A:

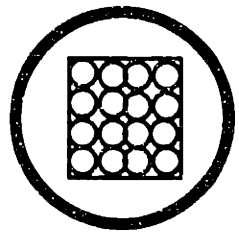

Hold 16 pins in square collet for surface grinder.

Notes:

1. Pin A (9 req'd) is used for deflection cell connection.
   Material Part # S1-84 Berg Precision.
   Pin B (8 req'd) is used for charge cell connection
   Material Part # S1-2 Berg Precision.

2. Pins A must be inserted into ABS electrode prior to machining of HV bus in assembly.

3. Pins must be surface ground oppsite chamfer prior to insertion see Detail A.

4. Refer to Drawing 48R and 49R. Wet sand 400 grit pin surface in ABS block prior to Plating.

Multiple Nozzle Printhead
Electrode Pin Connections

Three Dimensional Printing
Christopher Shutts
3/24/95

Material: 303 SS
Dimensions are in Inches
Tolerance as +/- .010 unless specified
Scale 4:1
Drawing #: 134

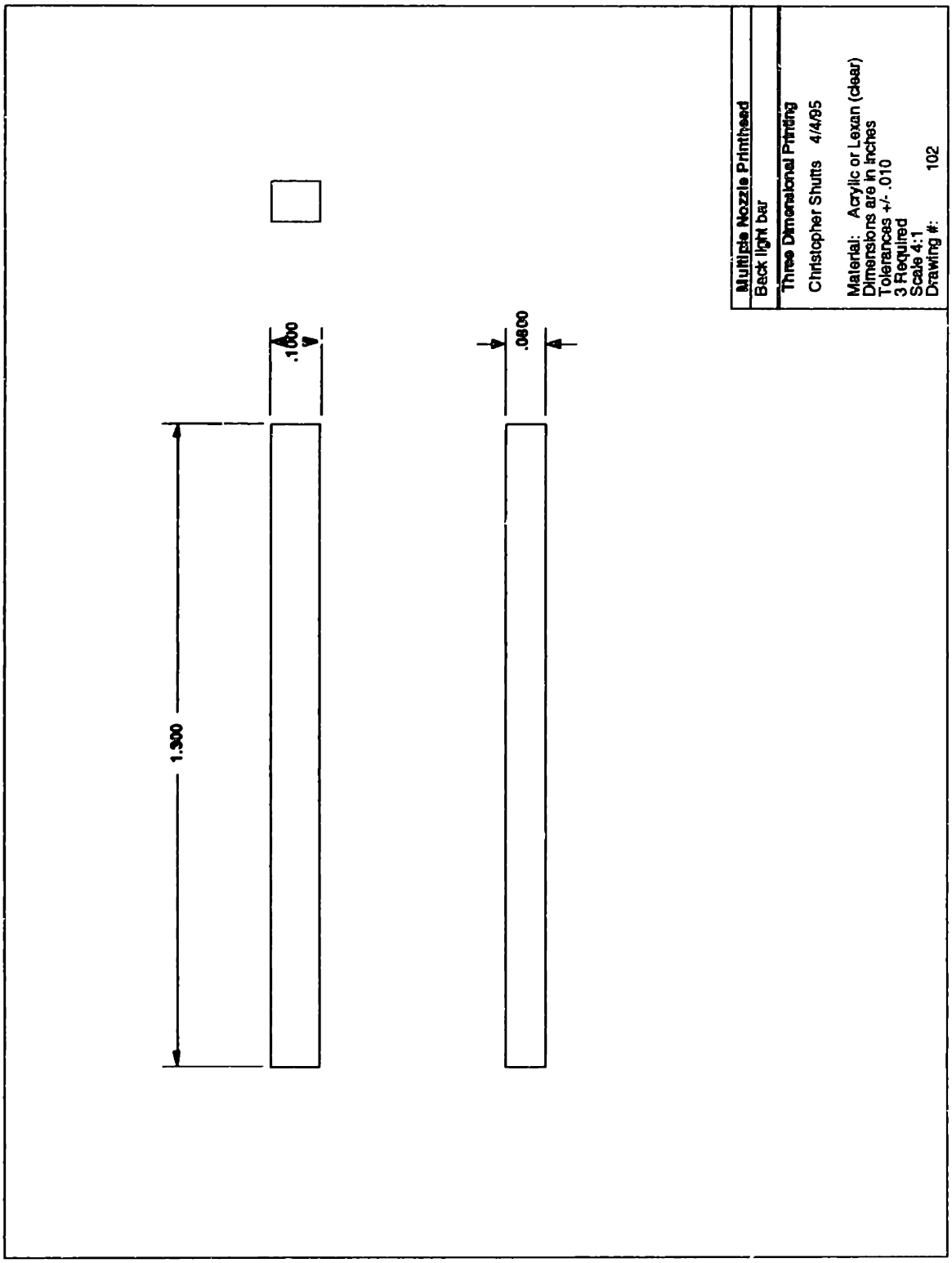
Multijet Nozzle Printhead
Back light bar
Three Dimensional Printing
Christopher Shutts 4/4/95
Material: Acrylic or Lexan (clear)
Dimensions are in inches
Tolerances +/- .010
3 Required
Scale 4:1
Drawing #: 102
1.500
.1000
.0800

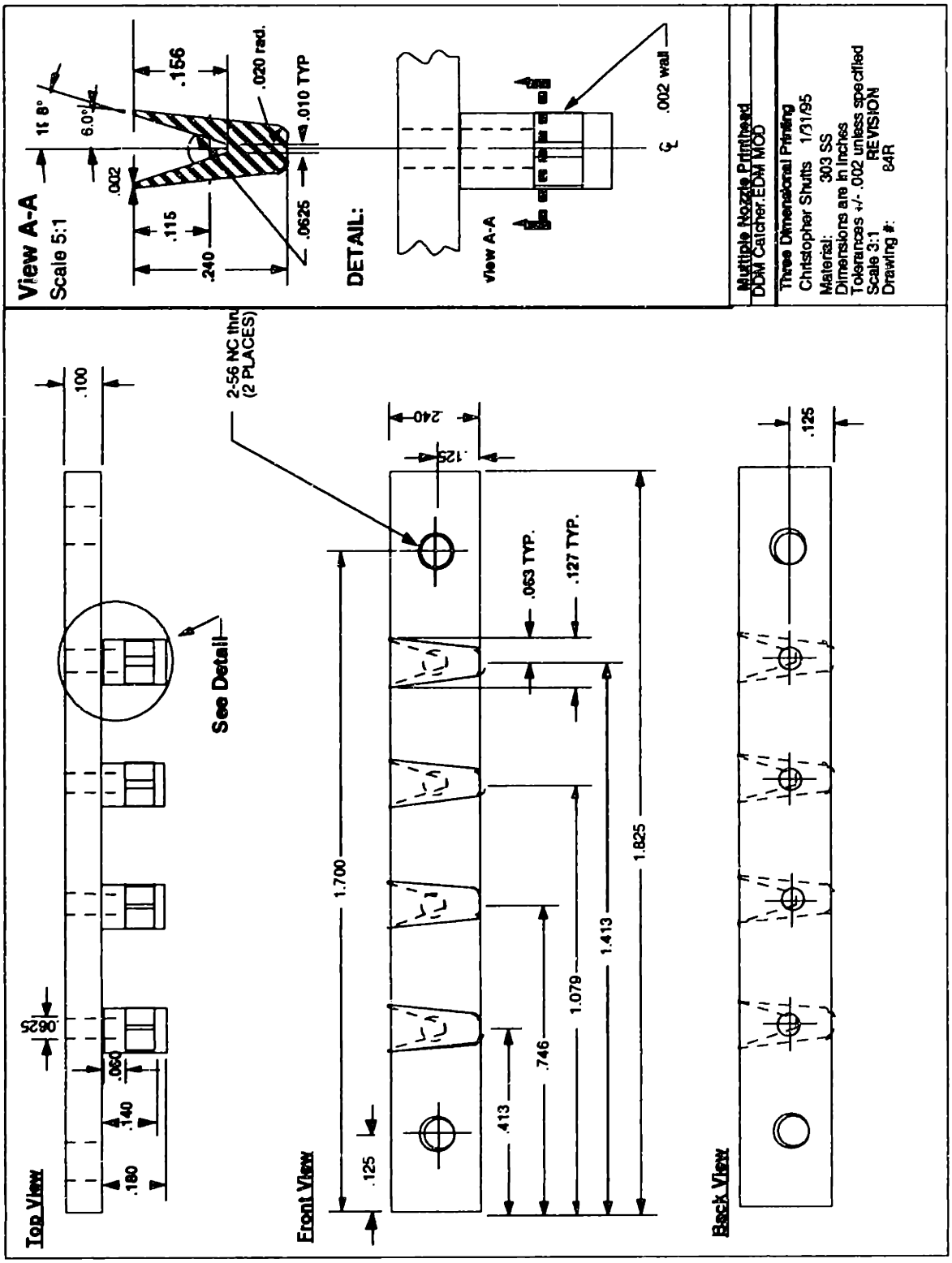
Multiple Nozzle Printhead
DDM Catcher.EDM MOD
Three Dimensional Printing
Christopher Shutts 1/31/95
Material: 303 SS
Dimensions are in inches
Tolerances +/- .002 unless specified
Scale 3:1
Drawing #: REVISION 84R
View A-A
Scale 5:1
15° 8°
6.0°
.002
.156
.020 rad.
.010 TYP
.115
.240
.0625
DETAIL:
View A-A
.002 wall
Top View
.100
.0825
.060
.140
.180
See Detail
2-56 NC thd
(2 PLACES)
Front View
.240
.125
.063 TYP.
.127 TYP.
1.700
.125
.413
.746
1.079
1.413
1.825
Back View
.125

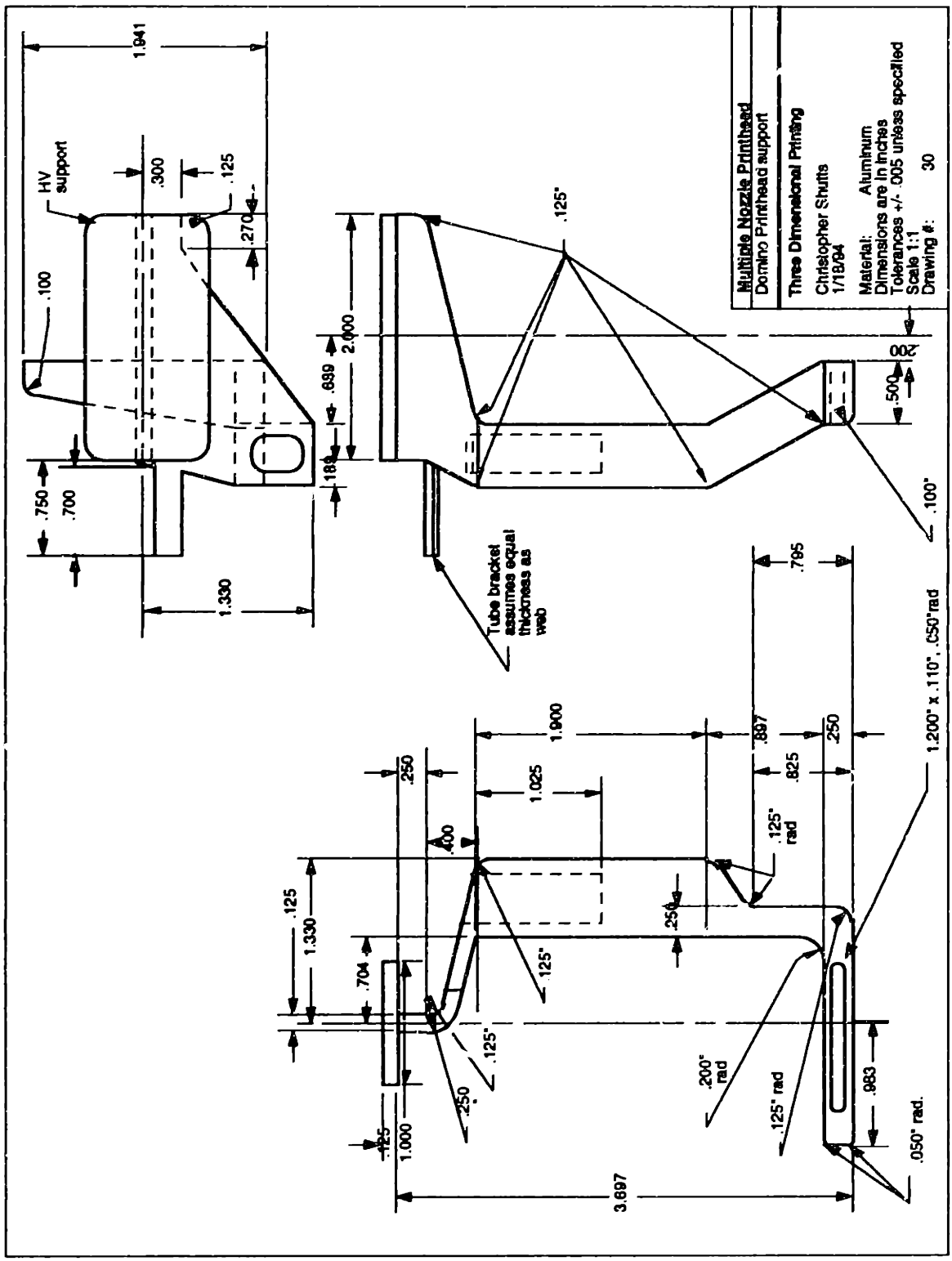
Multiple Nozzle Printhead
Domino Printhead support
Three Dimensional Printing
Christopher Shutts
1/18/94
Material: Aluminum
Dimensions are in inches
Tolerances +/- .005 unless specified
Scale 1:1
Drawing #: 30
HV support
1.941
.300
.125
.270
.100
.750
.700
1.330
.689
2.000
.125"
.500
.100"
Tube bracket assumes equal thickness as web
.795
1.900
.807
.250
1.025
.825
.400
.125" rad
.125
1.330
.704
.125"
.250"
.200" rad
.125" rad
.983
.050" rad.
1.000
3.697
1.200" x .110", .050"rad

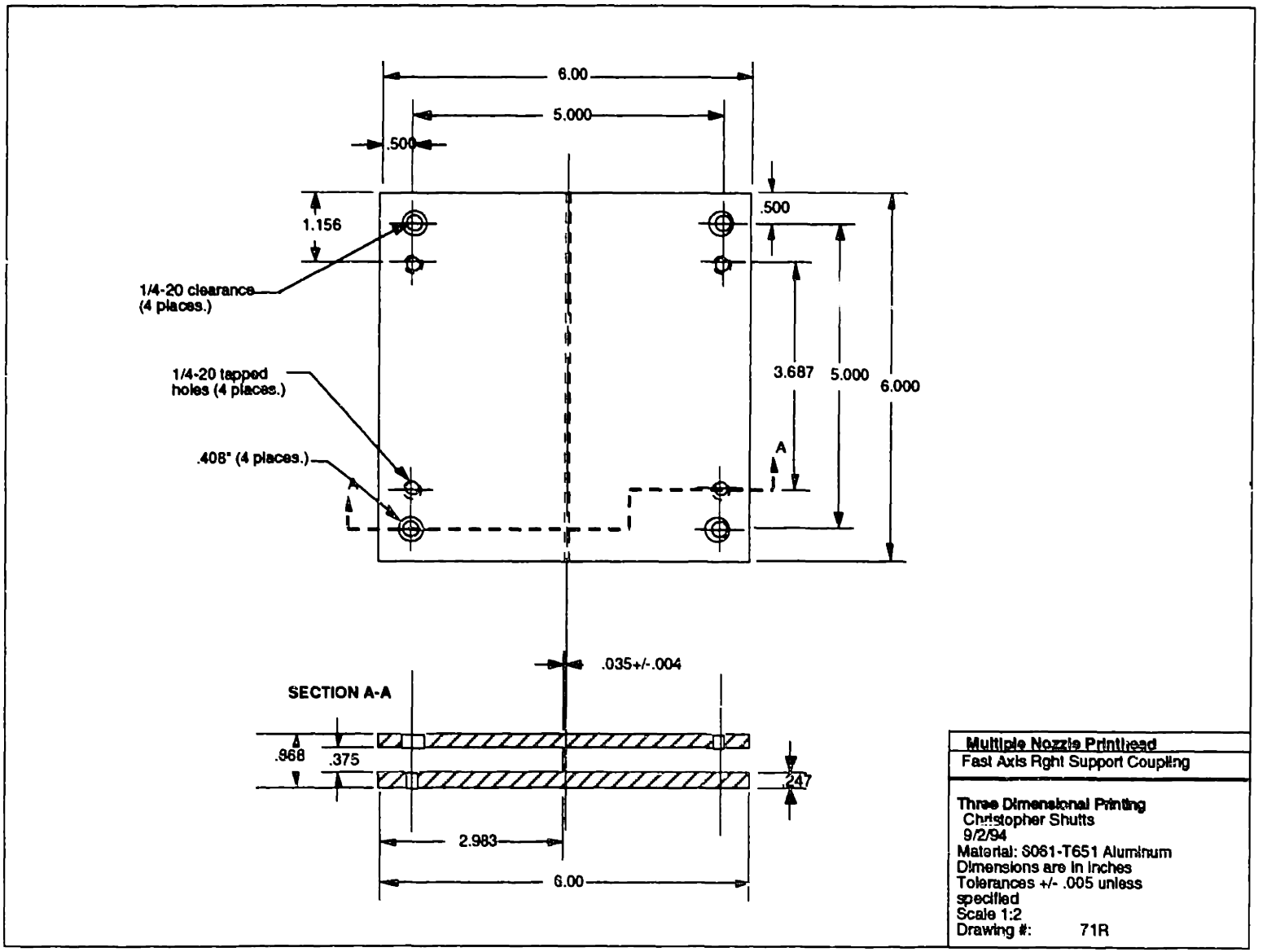
6.00
5.000
.500
.500
1.156
1/4-20 clearance
(4 places.)
1/4-20 tapped
holes (4 places.)
.408" (4 places.)
3.687
5.000
6.000
A
.035+/-.004
SECTION A-A
.868
.375
.247
2.983
6.00
Multiple Nozzle Printhead
Fast Axis Right Support Coupling
Three Dimensional Printing
Christopher Shutts
9/2/94
Material: S061-T651 Aluminum
Dimensions are in inches
Tolerances +/- .005 unless
specified
Scale 1:2
Drawing #: 71R

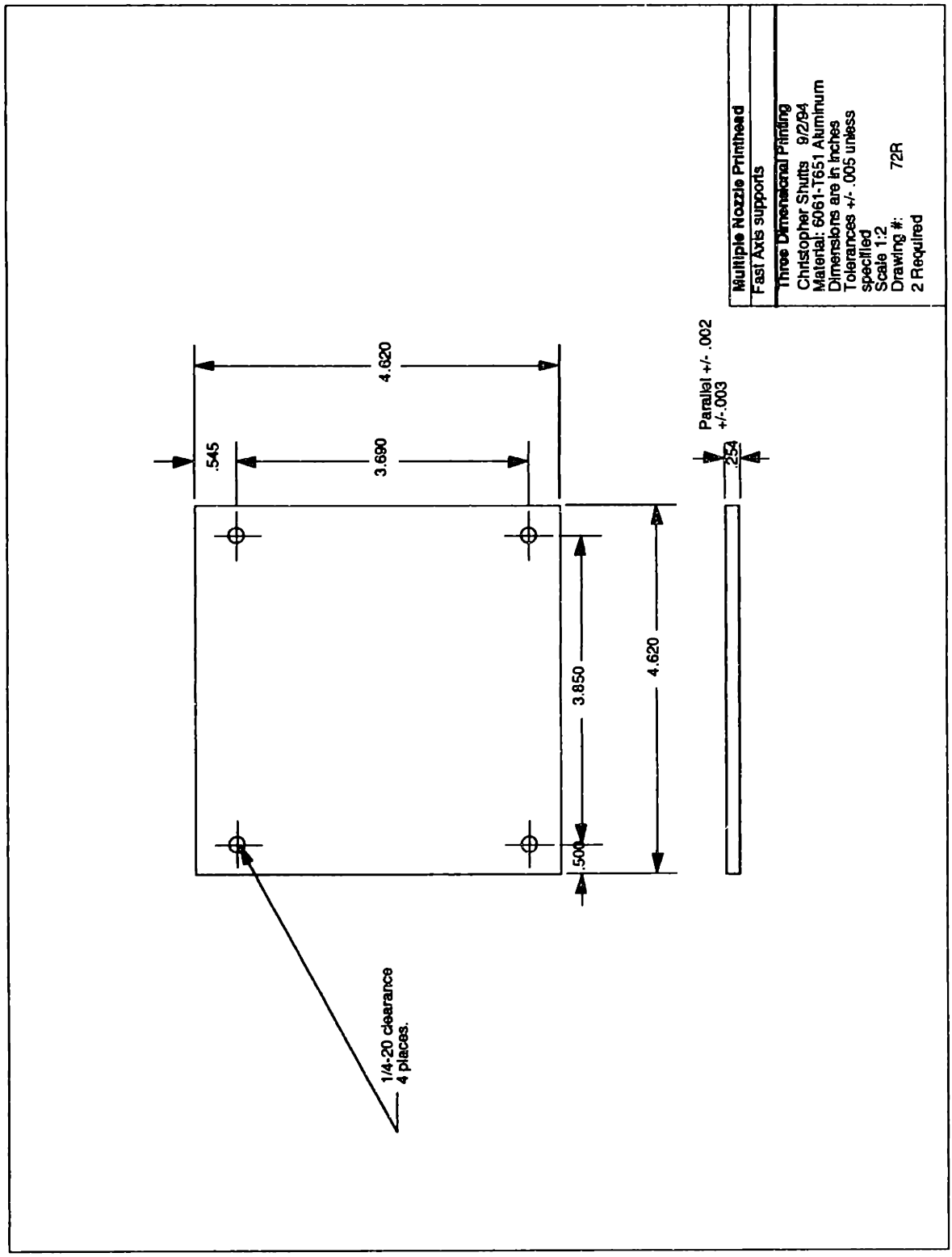
Multiple Nozzle Printhead
Fast Axis supports
Three Dimensional Printing
Christopher Shutts 8/2/94
Material: 6061-T651 Aluminum
Dimensions are in inches
Tolerances +/- .005 unless specified
Scale 1:2
Drawing #: 72R
2 Required
4.620
.545
3.690
Parallel +/- .002
+/-.003
.254
3.850
4.620
.500
1/4-20 clearance
4 places.

Appendix B: Wiring Diagrams

Drawings:

Printhead flood detector
Description of operation:
The sensing circuit uses via a 5v regulator the DC voltage from the HV power supply for power. The optoisolator on the printhead is the actual current sensing device. When approximately 25 microamps flows through the diodes in the optoisolator the transistors on the output saturate (.0000025amps*200k=5v) causing one or both of the inputs to the NAND gate to go low. This illuminates the red LED on the carriage and sends the active high signal back to the control box. The control box latches the signal until reset, and sends the signal to the IIfx. The second optoisolator is used to prevent ground looping with the computer.

Recirculation Contoller with float switches
Recirculation Controller weight measurement
Led Strobe
Description of operation:
The area in the dashed box creates a 50-100ns (gate propagation delay) pulse which triggers the VP01 MOSFET. The MOSFET pulses the LEDs at the piezo frequency.

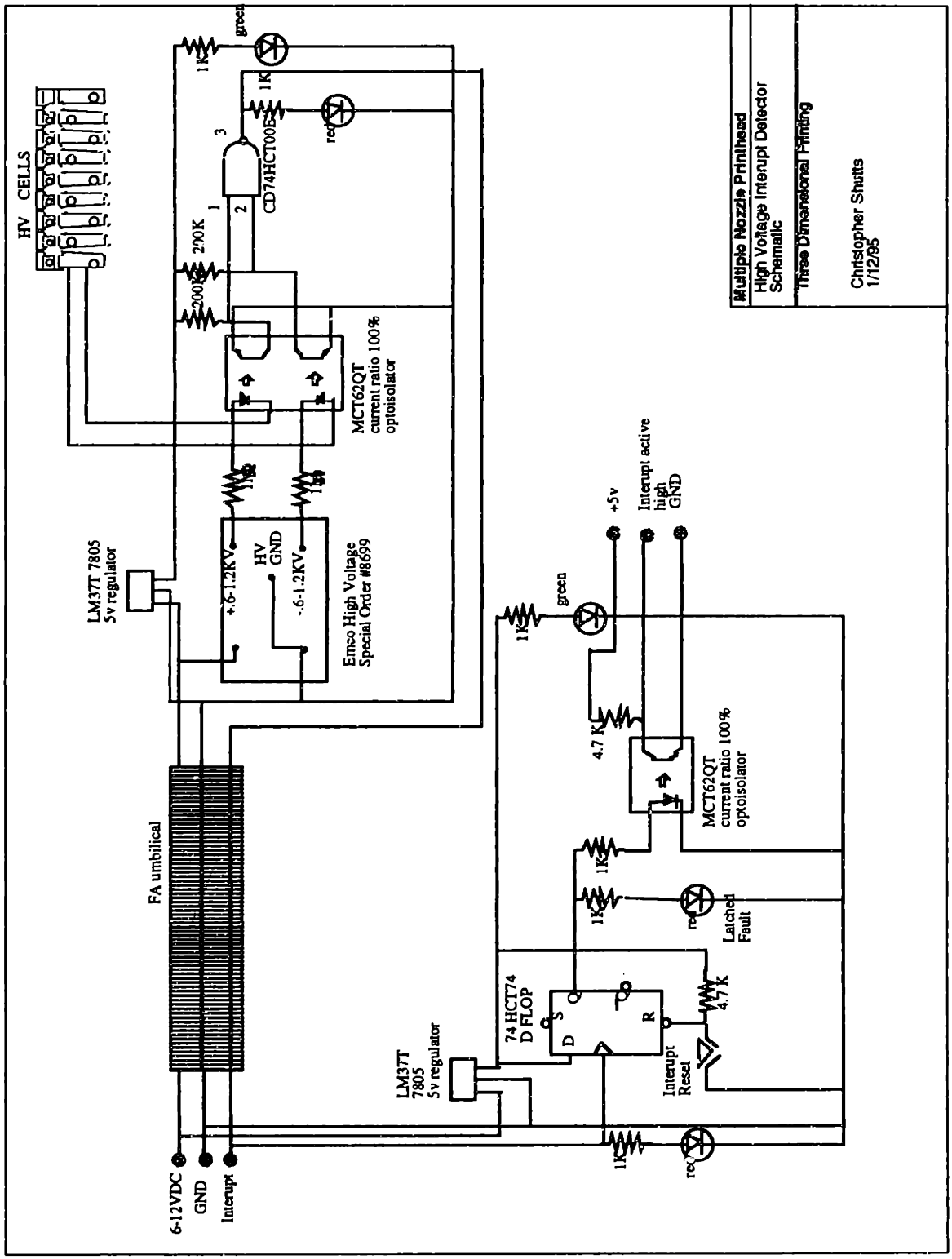
Multiple Nozzle Printhead
High Voltage Interupt Detector Schematic
Three Dimensional Printing
Christopher Shutts
1/12/95
HV CELLS
LM377 7805
5v regulator
+.6-1.2KV
HV GND
-.6-1.2KV
Emco High Voltage
Special Order #8699
MCT62QT
current ratio 100%
optoisolator
200K
200K
1K
green
red
CD74HCT00E
FA umbilical
6-12VDC
GND
Interupt
+5v
Interupt active
high
GND
4.7 K
74 HCT74
D FLOP
S
D
R
Latched
Fault
Interupt
Reset
LM377
7805
5v regulator

Recirculation Control Circuits

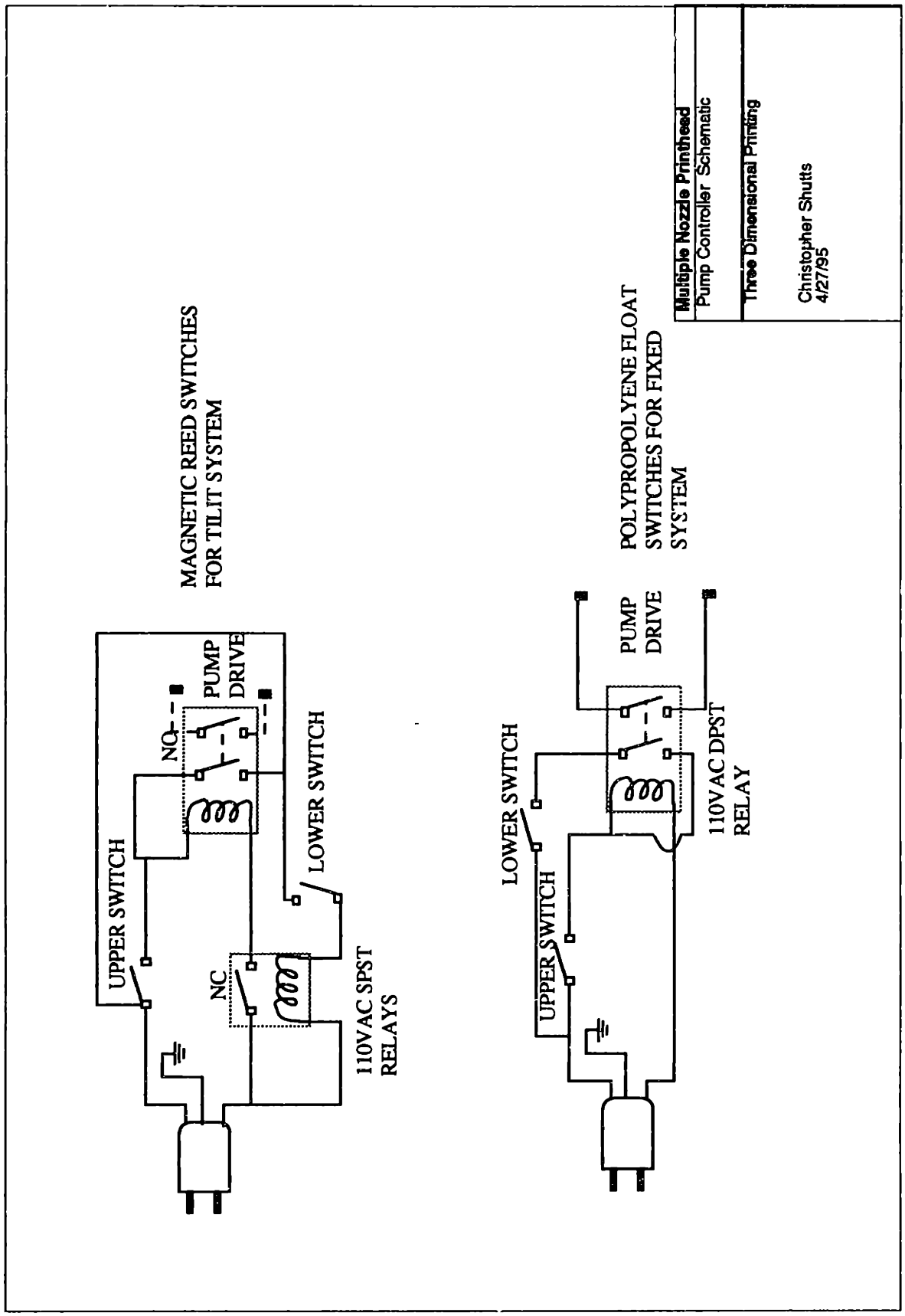

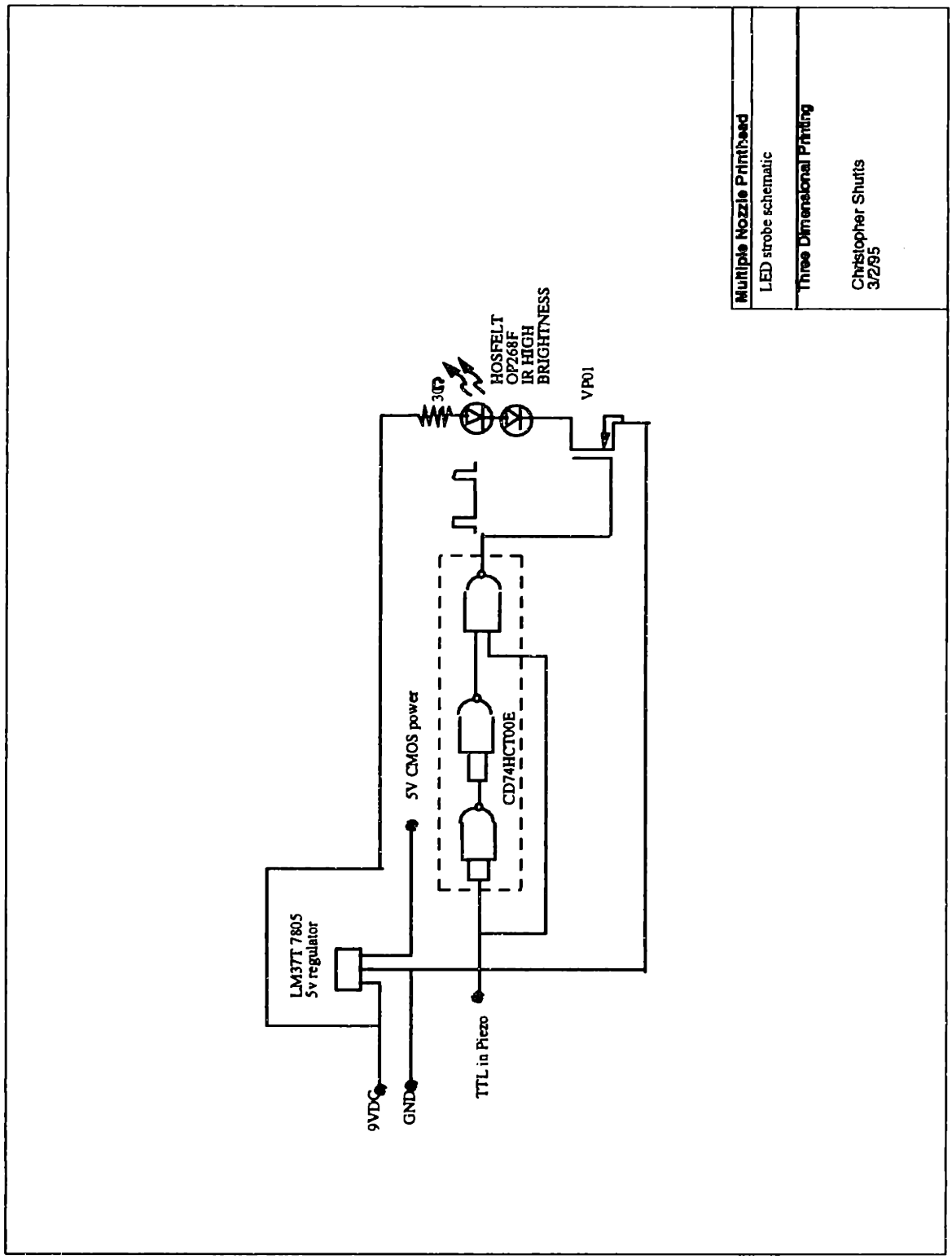
Multiple Nozzle Printhead
LED strobe schematic
Three Dimensional Printing
Christopher Shufts
3/2/95
HOSFELT
OP268F
IR HIGH
BRIGHTNESS
30Ω
VPD1
5V CMOS power
CD74HCT00E
LM37T 7805
5v regulator
9VDC
GND
TTL in Piezo

Appendix C: Off-center Droplet Charging

The droplet charging amount for a parallel plate capacitor and an off-center jet in a parallel capacitor were derived using the method of images. The theory is based on the assumption that a point of charge is affected by a plate at a fixed potential similar to a mirror image of a point equally charged positioned on the other side of the plate. This method is based on the fact that a grounded conducting plane affects the electric field near a charged body in the same way as a mirror image of

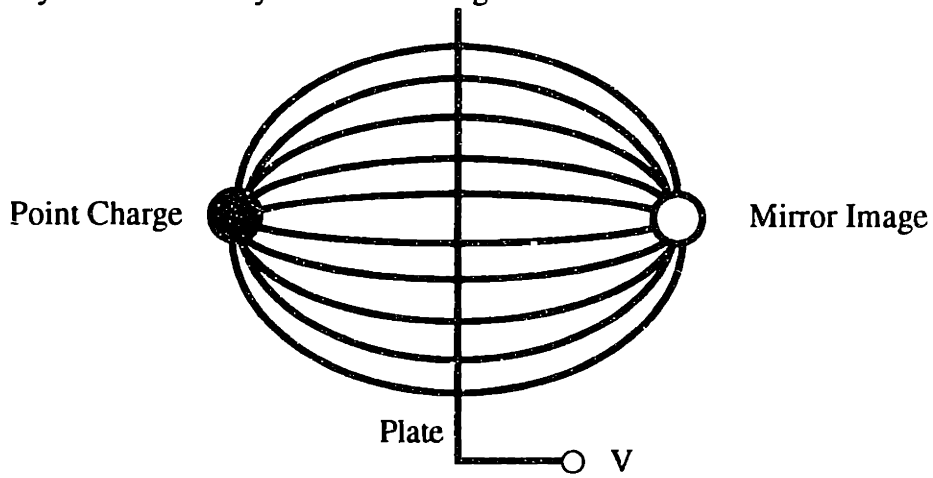

Figure C1: The Theory behind The Method of Images.

the body with an opposite charge. At the surface of the plane the electric field will always be perpendicular to the wall [Bredt, 1995].

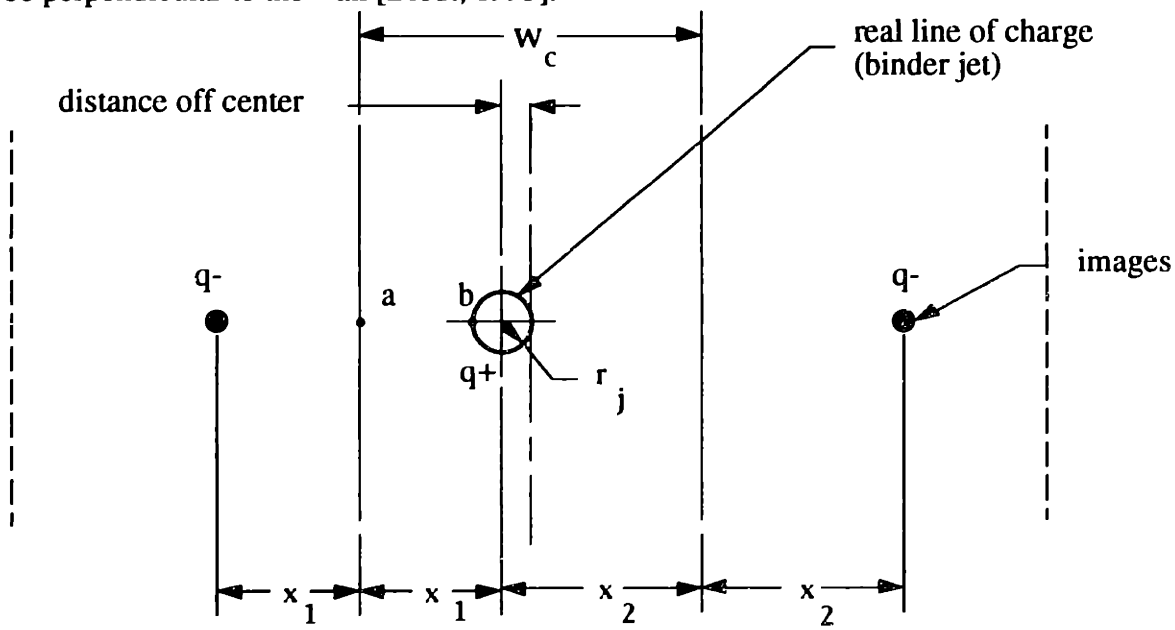

Figure C2: Images of Line Charge for a Parallel Plate Charge Cell

In Figure C2 one can see the jet represented as an infinite line of charge (into the page) off center in the charge cell. The cell walls act as two mirrors creating an infinite number of images all at distance w_c.

By integrating the electric field from point b on the edge of the jet to point a on the cell wall the potential difference between the charge cell and the wall can be found. This expression shows the first few terms of this potential.

$$V = \frac{q'}{2\pi\varepsilon_o}\left[\int_{x_1}^{r}\frac{dr}{r} + \int_{x_1}^{2x_1-r}\frac{dr}{r} - \int_{2x_2+x_1}^{2x_2+r}\frac{dr}{r} + \int_{2x_2+x_1}^{2x_2+2x_1-r}\frac{dr}{r} - \ldots\right] \qquad (C.1)$$

Evaluating this integral leads to the following expression.

$$V = \frac{q'}{2\pi\varepsilon_o}\ln\left(\frac{r}{x_1}\right) + \ln\left(\frac{2x_1 r}{x_1}\right) + \ln\left(\frac{2x_1-r}{2x_2+x_1}\right) + \ln\left(\frac{2x_2+2x_1-r}{2x_2+x_1}\right) - \ldots \qquad (C.2)$$

Unfortunatly this equation concerges after many terms. An iteration program was developed to solve equation C.2 for 50 terms in the integral. The jet capacitance is at a minimum when the jet is perfectly centered and increases exponentially as the jet approaches on wall of the charging cell.

The derivation has two key assumptions that are worth noting. The method of images assumes a line of charge, when in reality the jet is a series of droplets. Secondly, as the jet approaches a cell wall (x1 or x2=0) the piont of drolet charge fails to coincide with the geometric center of the droplet. Modeling both of these effects would be extremely difficult.

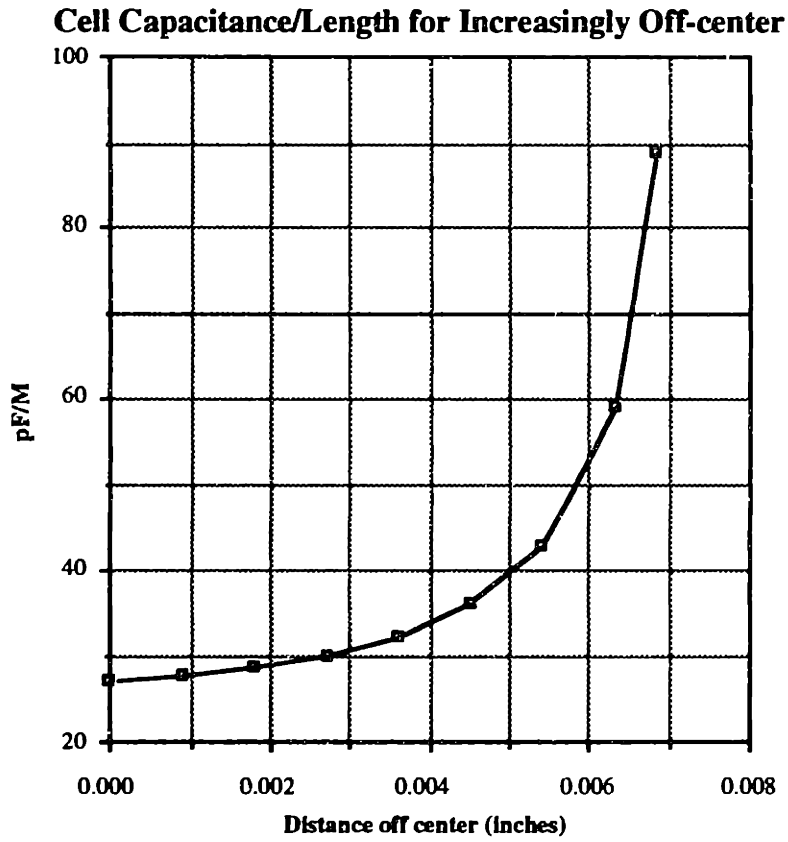

Figure: C3: Affect of jet misalignment in the charging cell on capacitance.
Charging cell width =.018". Droplet size=.003"

The effects of an off centered jet are small until the jet is out of position by approximately .003-4" in an .018" chargeing cell.

Appendix D: Additional Parts and Vendors

Part /Material	Vendor	Phone/Conact
ABS/Delrin/Teflon	Altec Plastics South Boston	269-1400
Droplet generator orifice plates pivot pin-spring	Domino Amjet Gurnee, IL	708 244-2501 Tom Schwarz
Toxot Drop Gen.	Imaje Inc.	404 438-2194
Diaphragm Pump (purchase)	Gelber Industries	610-497-7720
Diaphragm Pump (specs.) 3218	Shurflo	1 800-854-
Diaphragm pump minature	KNF Neuberger	609-890-8600
Hypotubing Annealed	New England Small Tube	603- 429-1600
SS connector pins	Berg Precision	516 596-1700
Chrome Plating Greenleaf	General Superplating	315-446-2264 Scott
Bright IR LED	Hosfelt Electronics	1800 524 6464
OP amps(Piezo & Charge signals)	APEX or Burr Brown	1800421-1865
Casting	Mass Foundry	864-2000
Filer-last chance	Porex	1800 2410195
Filter-replaceable syringe Nucleapore filter elements	Harrington Industrial	909 597-8641
Filters, Tygon Tubing, Peristaltic pumps, plastic fittings	Cole Parmer	18003234340
Float switches	McMaster Carr	
Micro End Mills	MSC	1 800645 7270
Delrin Rod, stainless bolts	Small Parts	1 305667 8222

Part /Material	Vendor	Phone/Conact
Metric stainless bolts,pins	Metric Tool and Screw	245 4950
Belows Pump	Gorman Rupp	419 886-3001
Connectors	DigiKey	
High flex Ribbon	Gore Inc.	
Leur Lock Fittings	Value Plastics	303 223-8306
Charge cell slitting saws	Harbor Tool	329-4432
10" Polyp. Filter housings	AAlanco	508757 2900
Stainless fittings	Boston Pipe and Fitting	497-5000
pressure vessels	Wessels	313 875 5000
plastic balls	United States Plastics	800-537-9724
DC-DC HV power supply	EMCO	209 223 3626
Double Throw 110vac relay	Physics Stookroom	
Small Bladders	Vynal Products	209 221-1283

Appendix E: Time of flight data and jet position data: Run length 48hrs. 50 μm jets, silica binder.

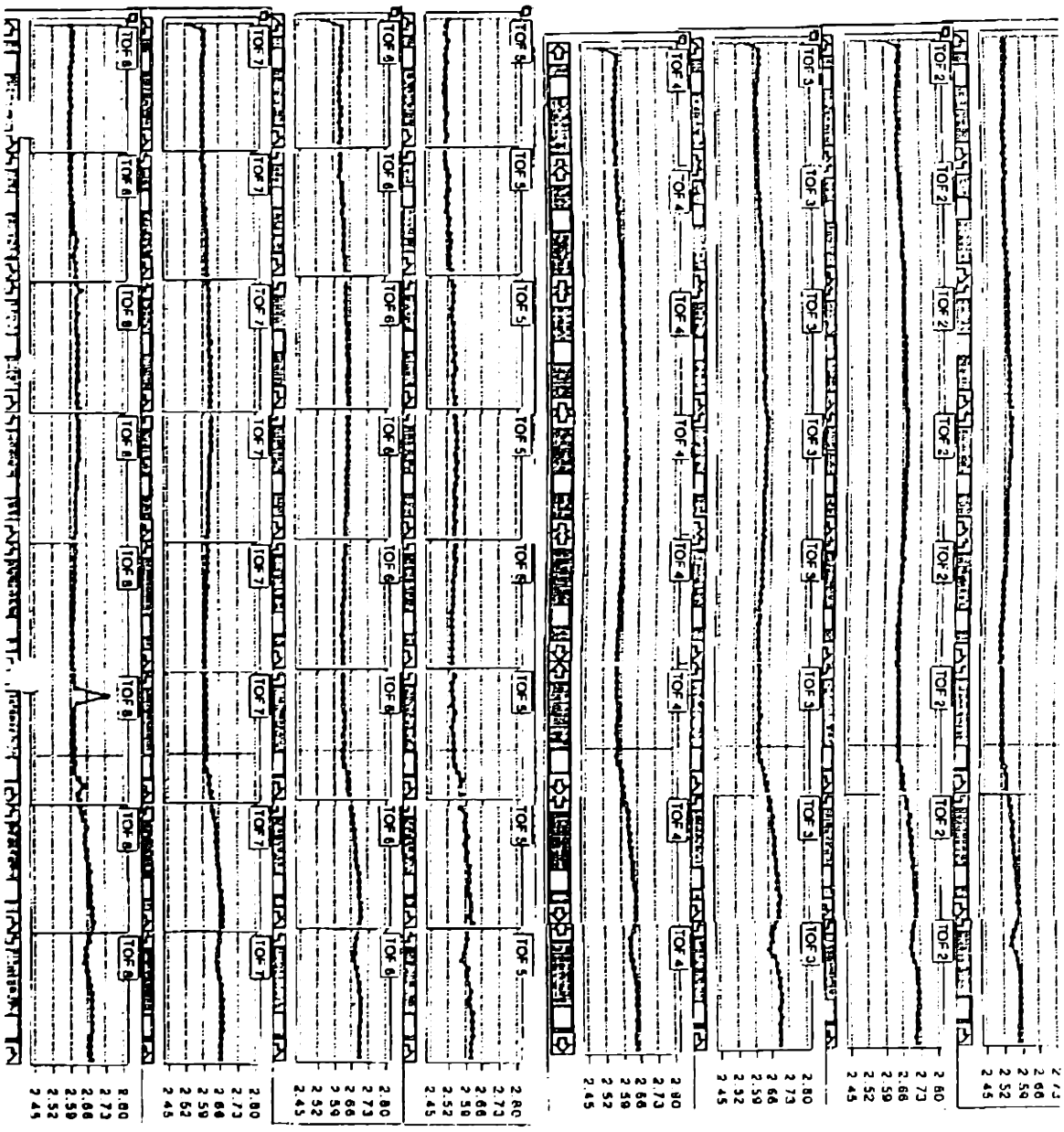

Figure E-1: TOF data for the eight jet head(measured in ms).

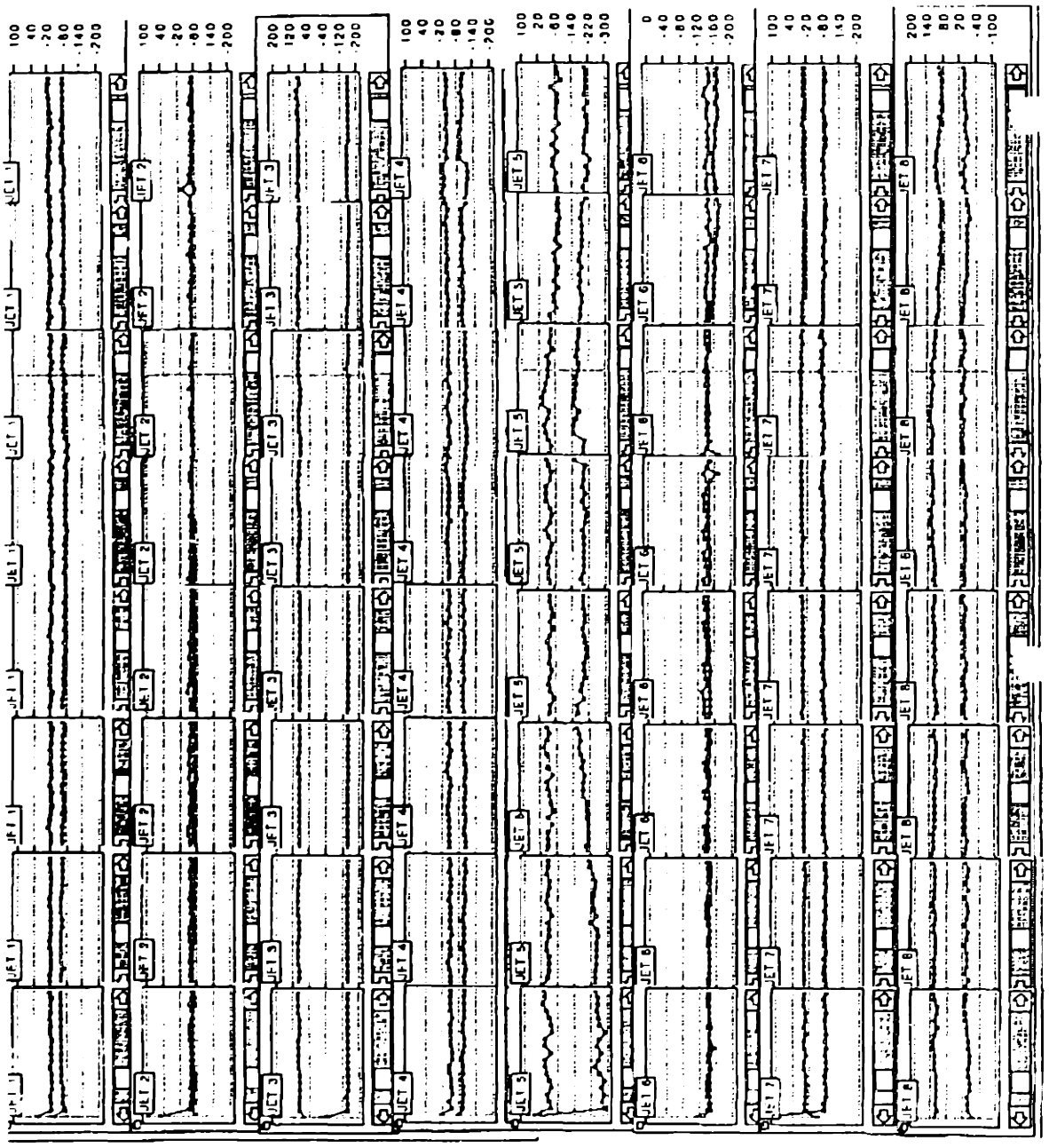

Figure E-2: Static jet wander for eight jets (measured in microns).

Appendix F: Binder mixing and composition

This section details the actual procedure for proper binder mixing. It is important to filter at the appropriate steps as well as the order in which ingredients are added. The 'recipe' is the product of some very solid work by Jim Bredt. The only compositional change has been the addition of the antifoam agent.

Mixing as per Jim Bredt's reccommendations:

385.9 cc = 385.9 g Distilled Water
23.4 cc = 24.6 g Propylene Glycol [CAS# 4254-15-3]
= 1-2 Propanediol
35.0 cc = 36.8 g Polypropylene Glycol (PPG) MW 425 [CAS# 25322-69-4
= Polypropylene oxide (PPO)
21.7 cc = 24.4 g Triethanolamine (TEA) [CAS# 102-71-6]
= 2-2'-2" Nitrilotriethanol
12.6 cc = 12.2 g Diethylene Glycol Monobutyl Ether [CAS# 112-34-5]
= Butyl Carbitol
= 2-(2-Butoxyethoxy)ethanol
(solid) **1.0 g Polyethylene Glycol** (PEG) MW 20,000 [CAS# 25322-68-3]
= Polyethylene oxide (PEO)
= Carbowax
= Polyoxyethylene
(solid) **0.5 g Thymol Blue** [CAS# 76-61-9]

Mix these components thoroughly to dissolve the solids. The PEG is the slowest to dissolve: it comes in solid flakes which sink.

Then add:

525.0 cc = 735.0 g Nyacol 9950 (prefiltered to 5 μm) [CAS# 7631-86-9]

Some Important Notes:

When mixing with AntiFoam 1500, Add 20 drops to the 24.6g Propylene Glycol. If this is not done prior to adding the glycol, the antifoam surfactant will never disolve into the binder.

Filter the silica to 5 μm a few times prior to adding it to the mixture of the other ingredients. Filter the entire batch with a 10" 222oring 1 μm filter.

Appendix G: Sample Printhead Design Spread Sheet Simulation

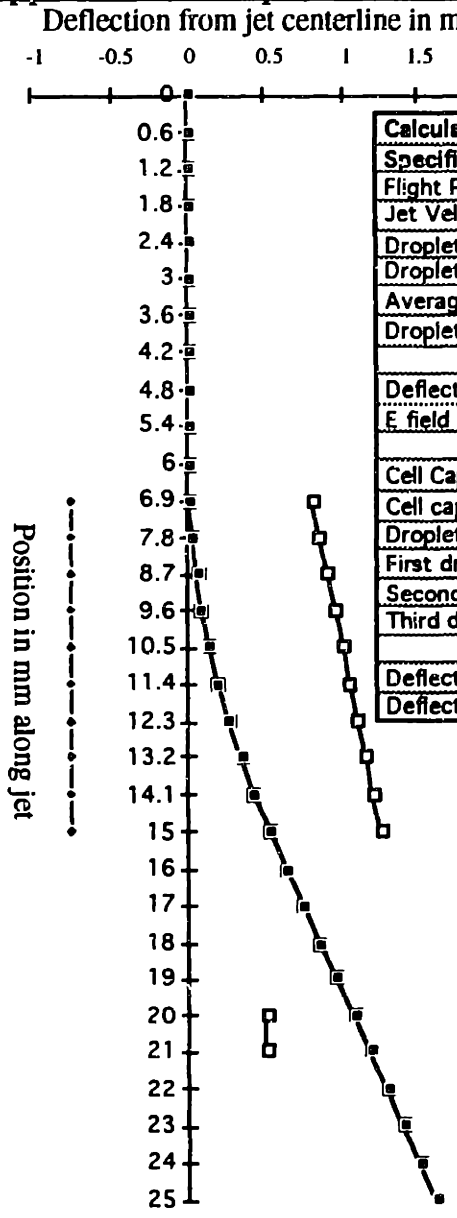

Calculated	Values	Units
Specifications		
Flight Path from orifice-powder bed	25	mm
Jet Velocity	14.724973	m/s
Droplet Diameter	75.052152	microns
Droplet mass	2.656E-10	kg
Average Droplet Acceleration in D.cell	2644.2702	m/s2
Droplet Spacing	0.2300777	mm
Deflection cell E field	1333333.3	V/m
E field as percent of maximum	44.444444	%
Cell Capacitance per length	1.992E-11	F/m
Cell capacitance per length with induce	1.895E-11	F/m
Droplet Charge	6.104E-13	Coulombs
First droplet induced affect	3.3542308	%
Second droplet induced affect	1.3721853	%
Third droplet induced affect	0.121972	%
Deflection at catcher	1.0661159	mm
Deflection at powder bed	1.6149099	mm

Jet Dynamics		
Flowrate	cc/min	0.85
Frequency	kHz	64
Orifice Diameter	microns	35
Fluid Density	g/cc	1.2
Charging parameters		
Charge Voltage	volts	140
Charge Cell Width	mm	0.46
Charge Cell length	mm	2
C.cell diatance from orifice	mm	1
Distance between C.cell and D.cell	mm	3

Deflection parameters			
Deflection cell voltage		volts	2000
Deflection cell Length		mm	9
Width of deflection cell at	0	mm	1.5
Width of deflection cell at	0.9	mm	1.55
Width of deflection cell at	1.8	mm	1.6
Width of deflection cell at	2.7	mm	1.65
Width of deflection cell at	3.6	mm	1.7
Width of deflection cell at	4.5	mm	1.75
Width of deflection cell at	5.4	mm	1.8
Width of deflection cell at	6.3	mm	1.85
Width of deflection cell at	7.2	mm	1.9
Width of deflection cell at	8.1	mm	1.95
Width of deflection cell at	9	mm	2
Distance to catcher from D.cell		mm	5
Distance from jet C.Line to catcher edge		mm	0.5
Distance to Powder bed from D.cell		mm	10